Unlocking Ampacity and Maximising Photovoltaic Penetration through the Phase Balancing of Low Voltage Distribution Network Feeders

A thesis submitted to the University of Manchester for the

degree of Doctor of Philosophy in the Faculty of Engineering and Physical Sciences.

2015

Martin Christopher Caton

School of Electrical and Electronic Engineering

Table of Contents

Word count: *34833*

List of Figures

List of Tables

Nomenclature

Symbol	Description
$\boldsymbol{a}$	Cable ampacity row vector.
$\check{\beta}$	The minimum of the maximum feeder bus voltages.
$\hat{\beta}$	The maximum of the maximum feeder bus voltages.
c	The number of phase connection matrix possibilities.
$\boldsymbol{C}$	The switch configuration matrix.
$\dot{\boldsymbol{C}}$	The capacitance matrix.
f	Feeder bus address.
g_v	Symbols used to represent an unbalanced power flow solver.
h	The feeder Hot Spot scaler.
I	Conductor current.
$\boldsymbol{i}$	Row vector containing the sum of phase and neutral conductor currents.
$\boldsymbol{I}$	The identity matrix.
I_T	Total hot spot current.
$\boldsymbol{j}_L$	The optimum quality measurement row vector (modulus unbalance correction method).
$\boldsymbol{j}_s$	The optimum quality measurement row vector (cumulative sum method).
k	Discrete time sampling instant.
l	Phase Switcher address integer.
L_T	Total feeder cable losses
$\boldsymbol{M}$	The phase mapping matrix.
N	The number of iterations.
N_{pv}	The number of PV installations on a feeder.
n_r	The number of buses on the reference branch
n	The number of feeder buses.
n_s	The number of PSs in a network.
n_{pv}	The number of PV installations for a given realisation of $\boldsymbol{P}_b$
p	The total number of possible realisations of a given network.
$\boldsymbol{P}_b$	The Phase Connection Matrix.
$\boldsymbol{p}_b$	The phase connection segment vector.
$\boldsymbol{P}_s$	The segment phase connection matrix.

1

Symbol	Description
$\boldsymbol{P}_b^*$	The calculated phase connection matrix that relates to a specific feeder switch position and PS placement.
$\dot{p}$	The measured average real phase power
$^d\boldsymbol{P}_b$	The dwelling Phase Connection Matrix.
$^s\boldsymbol{P}_b$	The street lamp Phase Connection Matrix.
$\boldsymbol{p}_r$	The phase reference column vector.
$^I\boldsymbol{P}_b$	The phase connection matrix for the straight through configuration.
p_r	The phase reference scaler
$\boldsymbol{p}$	The stacked segment connection matrix column vector.
$\boldsymbol{P}_b^{max}$	The phase connection matrix that specifies which buses on the reference branch can accommodate PV installations.
$\boldsymbol{q}_L$	The quality measurement row vector.
$\boldsymbol{q}$	The aggregate phase allocation vector.
$\boldsymbol{R}$	The resistance matrix.
s	Is the number of allowable phase switcher switch positions.
ΔT	Designated time window.
V	Bus voltage.
$\boldsymbol{v}$	The bus voltage row vector.
v^*	The maximum feeder bus voltage.
$\boldsymbol{v}_{n_{pv}}$	The maximum feeder bus voltage row vector for a specific feeder PV penetration.
$\boldsymbol{v}_{np\cdot}$	A row vector of maximum bus voltages each with a unique PV penetration allocation.
$\hat{v}$	The maximum feeder bus voltage.
x_{pv}	The number of additional PV installations required on a feeder.
x_f	The total number of possible feeder switch positions.
X	Feeder switch position n_s-tuple object.
$\boldsymbol{X}$	The switch configuration matrix.
X^I	The straight through feeder switch position.
X^*	The extended feeder switch position $2n_s$-tuple object used when PSs placements are not fixed.
X^F	The feeder switch position n_s-tuple object used when PSs are fixed.
$\boldsymbol{X}_0$	The switch configuration matrix of the PS located nearest to the reference

Symbol	Description
	transformer.
X	The reactance matrix.
$\check{X}$	The optimal feeder switch position.
X_i	The switch configuration matrix corresponding to the ith PS in the network.
Z	The variable of interest.

Acronymns

ADMD	After Diversity Maximum Demand
AU/ph	Average Unbalance per Phase
bus voltage	phase to neutral voltage
CCA	Climate Change Act
DECC	Department of Energy & Climate Change
DG	Distributed Generation
DN	Distribution Network
DNO	Distribution Network Operator
DSM	Demand Side Management
DTR	Dynamic Thermal Rating
ESQCR	Electricity Safety, Quality and Continuity Regulations
EV	Electric Vehicle
FIT	Feed in Tariff
ITS	Incremental PV Allocation Through Simulation
LCNF	Low carbon network Fund
LV	Low Voltage
MV	Medium Voltage
OV	over-voltage
PS	Phase Switcher
PT	Peak Time
PV	Photo Voltaic
TSO	Transmission Service Operator
UG	underground
UR	Uniform Randomised Assessment
UR10	Uniform Randomised assessment with 10 Iterations per PV penetration
UR100	Uniform Randomised assessment with 100 Iterations per PV penetration level

The University of Manchester

Martin Christopher Caton B.Eng (Hons) Manc

Submitted for the degree of Doctor of Philosophy

Unlocking Ampacity and Maximising Photovoltaic Penetration through the Phase

Balancing of Low Voltage Distribution Network Feeders

January 2015

Abstract

In recent years there has been a large increase in the connection of photovoltaic generators to the low voltage distribution network in urban residential areas. In the future, it is predicted that this trend will continue and be accompanied with a rise in the uptake and connection of electric vehicles and heat pumps. Recently, monitoring trials have found widespread current unbalance in the feeders that transmit electrical energy to and from these urban residential areas. This unbalance is likely to be accentuated by the gradual and piecemeal uptake of the aforementioned devices. The combined impact of the changes and present day unbalance is likely to be more frequent thermal and voltage constraint violations unless new strategies are adopted to manage the flow of electrical energy.

Here, a novel device named the 'phase switcher' that has no customer compliance requirements is proposed as a new tool for distribution network operators to manage the thermal and voltage constraints of cables. The phase switcher is shown to unlock cable ampacity and maximise voltage headroom and it achieves this through phase balancing in real time. A centralised local feeder controller is simulated to employ dynamic and scheduled phase switcher control algorithms on a real network model, and it's ability to unlock cable ampacity and reduce cable losses is quantified. Also, a small model based controller algorithm is presented and shown to perform almost as well as others despite having a very limited sensing and communication system requirement. Phase switchers are also quantified for their ability to increase feeder voltage headroom when employed to improve the balance of photovoltaic distributed generators across phases. To this end, an exhaustive offline photovoltaic capacity prediction technique is documented which shows that when phase switchers are placed explicitly to a known photovoltaic installation scenario, an almost linear relationship exists between the penetration level and maximum node voltage when PSs or phase conductor rejointing is considered as an option for implementation. Finally, a fast feeder assessment algorithm is detailed that is found to be better and more robust at estimating extreme maximum and minimum photovoltaic penetration level scenarios that cause over-voltage.

All the work is presented within a new general mathematical framework that facilitates formulation of the problem and calculation of device phase connections for networks containing phase switchers.

Declaration

No portion of the work referred to in the thesis has been submitted in support of an application for another degree or qualification of this or any other university or other institute of learning.

Copyright

Acknowledgements

I would like to extend my sincere gratitude to those that have assisted and supported me throughout the course of this research, in particular:

- Dr Ognjen Marjanovic, my supervisor – for his counsel and attention to detail.
- Ken Lennon of Scottish Power – for invaluable insights into the practical operation of the Distribution Network.
- Electricity North West – for information on their Low Voltage Distribution Network.
- All of my colleagues at the Control Systems Centre at the University of Manchester.
- The University of Manchester.
- Colleagues in the Electrical Energy and Power Systems Research Group at the University of Manchester.
- The IET – for facilitating countless networking opportunities.
- My fellow volunteers of the IET Manchester Power Technical Group committee – for their wise counsel.

Finally, the most important element that made this work possible was the patience and understanding of my wife and children.

Thank you, Lucy, Fraser and Sebastian.

Statement

A patent application for the "Phase Switcher" which forms the basis for the majority of the work documented in this thesis is currently being progressed. The access to this thesis will be restricted until the outcome of the patent application is known and it is the authors intent that publications will follow.

1 Introduction

1.1 Background

Significant changes to the UK power system will take place over the next thirty seven years which will change the way that electricity is generated and consumed. In the UK, changes are being shaped by politicians and implemented through the regulation of generators, TSOs (Transmission Service Operators) and DNOs (Distribution Network Operators). The CCA (Climate Change Act) 2008 [1] was introduced by the UK government, it sets a target which mandates an 80% cut in greenhouse gas emissions by 2050 on 1990 levels. Moreover, it sets out a requirement for five yearly UK Climate Change Risk Assessments, the first of which, published in 2012, projects a reduction in energy demand in winter and an increase in summer due to higher climatic temperatures [2]. The emissions target was derived from the International Panel on Climate Change's report 2007 which followed the Kyoto Protocol from December 1997. The IPCC report aimed to cut greenhouse gas emissions by at least 5 per cent of those recorded in 1990, by 2012.

In the medium term, the 2009 Renewable Energy Directive [3] has been formulated. It sets a UK target of 15% energy consumption to be generated by renewable sources by 2020, as a marker of progress the 2009 figure was 3%. This lead to the UK Government releasing The Renewable Energy Roadmap [4] in 2011, which sets out a programme of actions aimed at enabling the level of renewable energy consumed in the UK to reach the target specified by [3]. Some key actions are concerned with:

- A targeted increase of energy generated by wind turbines.
- An increase in the use of air source heat pumps by permitting development rights on domestic properties.
- Providing new investment on the infrastructure for vehicle recharging.

The Feed-in Tariff (FIT) scheme has resulted in a higher installed capacity of DG in the UK low voltage (LV) distribution network. It was introduced by the UK government in April 2010 and has lead to an increase of 19,959% in 3.25 years [5] which is shown in Fig. 1. Analysis in 2012 of the DG technology mix in the UK revealed that

photovoltaic (PV) technology is the normal, as it accounted for 90% of the installed capacity.   The complete DG technology mix recorded in the FIT energy trends statistics [5] is shown in Fig. 2.   The cumulative numbers of PV installations are split out into capacity categories in Fig. 3 [5] which shows that installations up to 4kW accounted for 86% of all installations.
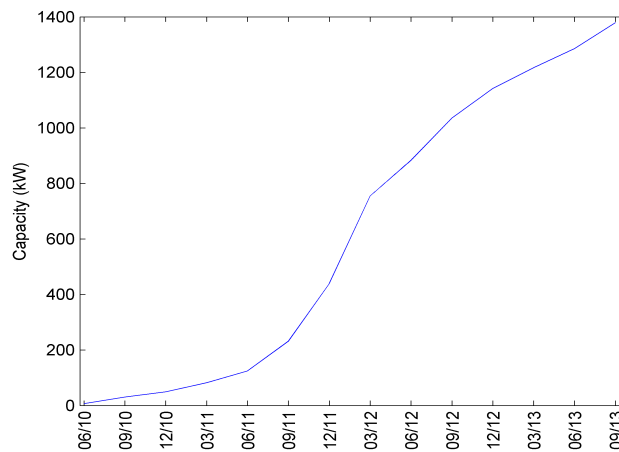
Fig. 1 FIT Statistics – KW of Domestic Generation [5]
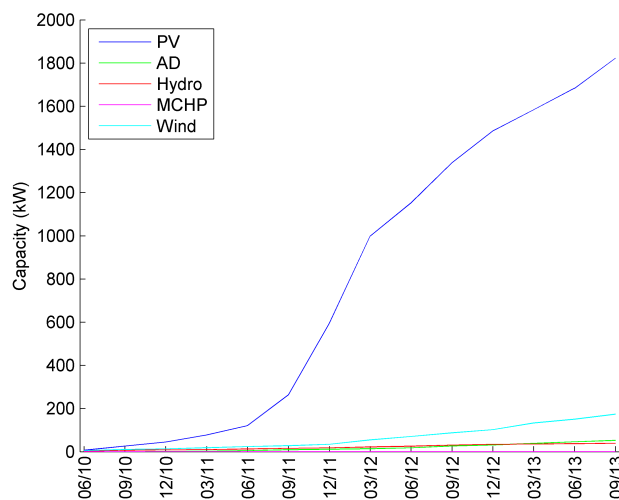
Fig. 2: FIT Technology Mix [5]
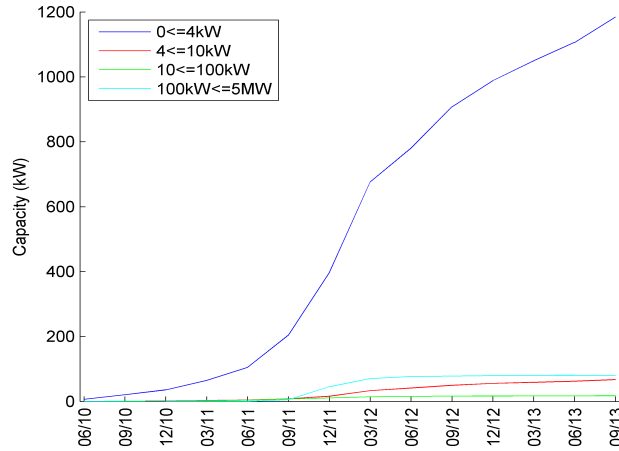
Fig. 3 Cumulative FIT PV Capacity for installations up to 5MW [5]

The roll out of smart meters in the UK is obligatory to suppliers and includes the replacement of all existing meters by the deadline of the end of 2019 [6]. In May 2013 DECC (Department of Energy & Climate Change) issued a Written Ministerial Statement to the UK Secretary of State [7] which put the deadline back by 12 months to the end of 2020. Smart Meters should provide new real time visibility on the state of the power system [6] in the LV distribution network.

The Electricity Safety, Quality and Continuity Regulations (ESQCR) 2002 [8] delegate responsibility of keeping phase to neutral voltages in LV networks within +10%, -6% of 230V to DNO's. BS EN 50160:2010 [9] defines a phase to neutral overvoltage (OV) in the LV network to be when a 10 minute r.m.s. voltage measurement exceeds 253V.

It is clear that the future power system will be different due to the aforementioned policies, legislation, schemes and specifications. The CCA [1], Renewable Energy Directive [3] and ultimately, the Renewable Energy Roadmap [4], will lead to wind power making up a much larger proportion of generation. This increase will lead to peaks and troughs in available energy which will be dependant on the wind. The renewable Energy Roadmap [4] will lead to an increase in the use of heat source pumps and electric vehicles, which is likely to cause an increase in electric power flowing in the LV distribution network. There will be a continued increase in; PV DG due to the FIT

[10] and, potentially electric vehicles [11]. The LV network is changing, single phase DG is being incorperated [10] and the use of electric vehicles and heating are expected to rise increasing the system load [12].

Taking all these factors into consideration, an area that will be greatly impacted by the changes is anticipated to be the LV sector, where businesses (industrial and commercial) and individuals will generate and consume more electrical power. This part of the network presents challenges primarily due to its size, for example, for; a typical medium sized power system with five generating units (power stations), there will be 310,000 elements (consisting of secondary transformers, joints and cabling) [13]. Due to the combination of changes forecast and its sheer size, it is the area of the power system that presents the greatest challenge. It implicitly follows that this is the part of the system that would most benefit from an automatic control strategy as, due to economics arising from scale, manual control is impractical and reinforcement is undesirable.

The UK power system design incorporates assumptions relating to the behaviour of consumers and the location of active loads and generators. One assumption that influenced design was that power would always flow downstream in radial feeders from large-scale generators to all loads. This has lead to the installation of tapered radial feeder networks in the LV distribution network. A tapered feeder is one where the cross-sectional area of the conductors within the cable is greater nearer to the secondary distribution network transformer. If the network shown in Fig. 4 were tapered, the cross-sectional area of L1 would be greater than that of L2 and L3. This is an example of good economic design for a power system focused on central generation and remote loading. However, this design is not as well suited to the installation of DG at remote loads connected via a tapered radial LV feeders due to increases in nodal voltages it causes which is explained in the following subsections.

4
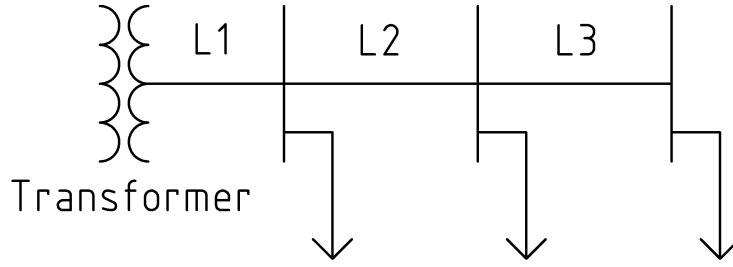
Fig. 4: Simple LV Feeder

1.2 LV Feeders

LV Feeders are the networks of cables that connect customers to the power system, they are specified and installed by DNOs using an amapacity rating which is calculated using the nominal voltage and an After Diversity Maximum Demand (ADMD) value. ADMD is the apparent power requirement of the feeder that considers a diversity factor [14] which accounts for the lack of synchronism in the operation of loads. Domestic customers in the UK normally have single phase connections and are either loads and/or DG. PV is the normal type of DG installed and due to some of the challenges associated with its unique characteristics, it is the DG type that is the focus for this thesis.

To emphasise the difference between domestic loads and PV DG, a single and 71 aggregated load profile is provided in Fig. 5 on the same plot as a trace from a single PV DG which were created using [15] and [16] respectively. The plot clearly shows that an individual load has periods of very low and high power use and that the aggregated or affect of 71 loads is more constant and less spiky. Also, the aggregated load is low during the day and reaches a peak in the early evening, reflecting when many people return home from work and cook meals at home. In contrast, the PV profiles output is at its peak in the afternoon and when it is also considered that PV has a complete lack of diversity, i.e. it is in almost perfect synchronism on a local level, the issue voltage rise on LV feeders is uncovered.
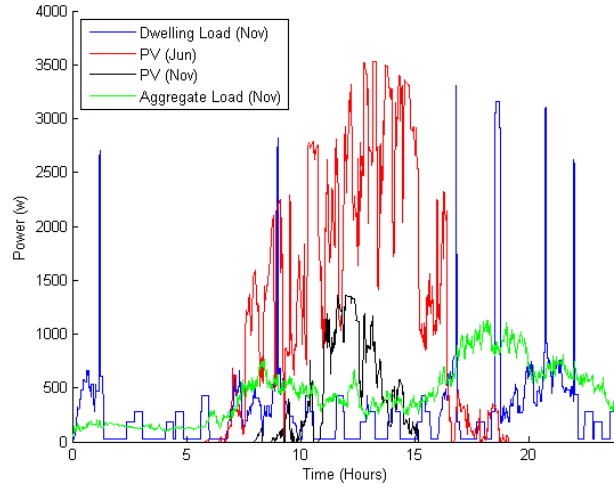
*Fig. 5: Synthetic Profiles for a Single: Dwelling Load, PV Loads
and an Aggregated whole feeder Load*

1.3   Research Scope

The scope outlined for the research presented in this thesis is detailed below:

Current electrical power systems are in urgent need of modernisation in order to address many of the pressing issues that are faced in the world today. These issues include global warming, depletion of fossil fuels, growing global population and an ever increasing reliance on the reliable supply of electrical energy. Smart Grid technology is seen by many as the most appropriate solution to tackle these issues from the perspective of electrical power supply and utilisation.

The main aim of Smart Grid technology is to modernise current electrical power networks using state-of-the-art communication and control methodologies, often combined with new or modified hardware, in order to deliver environmentally friendly, efficient, reliable, resilient and responsive power systems for the future. In other words, Smart Grid is an electricity network that can intelligently integrate the actions of all users connected to it – generators, consumers and those that do both – in order to efficiently deliver sustainable, economic and secure electricity supplies.

This project will focus on the investigation of the impact that the smart grid technologies will have on the operation of the electrical power transmission system. In order

to achieve this objective, the project will firstly focus on the dynamic modelling of smart grids at the distribution and consumer voltage level. The existing control and communication technologies, currently used in industry, will then be implemented and evaluated using representative, lower-power equivalent network systems and their equivalent software-based simulators that incorporate some aspects of smart grid technology. The project will then focus on proposing improvements to the existing control and communication systems in order to facilitate effective exploitation of the smart grid technology in the current electrical power networks.

1.4   Research Aims and Objectives

The research objectives that were identified through the literature review provided in chapter 2 and scope documented in section 1.4 are listed below:

1. Development of a cost effective feeder balancing scheme that incorporates the use of a cost effective switching devices for UK LV networks.

2. Development of a high fidelity simulator capable of quantifying the impact of a switching scheme in real time application in terms of:
   a) Voltage
   b) cable current
   c) Losses

3. Development of a mathematical nomenclature and framework that is capable of describing the phase connections of devices connected to a feeder and calculating how they may be changed when phase switching occurs.

4. Calculation of the actual optimum state of system balance that the switching scheme allows to enable the quality of the scheme to be fully evaluated.

5. Investigate the impact of the switching scheme on PV assessments using methods that have been developed to date.

1.5   Thesis Overview

This section outlines the structure of the thesis and details the contents of each of it's chapters.

Chapter 2 provides a review of relevant literature that relate to the research object-
ives and the work documented throughout this thesis.

An introduction of the novel Phase Switcher (PS) device is provided in chapter 3
along with the supporting nomenclature and terminology that is required to express
device phase connections of an LV feeder and calculate how PS can manipulate them.

The LV network modelling methodology is detailed in chapter 4 which is followed
by a description of the steps taken to to validate it using real world system measure-
ments.

Chapter 5 outlines the methodology used to identify thermal weak points in feeders
and subsequently place PSs to unlock cable current within them. Whilst, chapter 6
contains the results from simulations that test the ability of various control algorithms
to unlock cable current when PSs are placed at locations identified in chapter 5.

How PSs can be used to create voltage headroom is shown in chapter 7 where simu-
lation results show how successful it is for a variety of PV penetration scenarios. Also
in chapter 7, a new feeder assessment methodology is detailed that is efficient at find-
ing minimum and maximum PV penetration scenarios for an LV feeder.

Finally, chapter 8 details the key research conclusions that summarise the impact of
PS on unlocking cable current and maximising PV penetration. Also, it identifies what
the new PV assessment method achieves and identifies the significance and potential
application opportunities for offline and online application of the PS theory.

2 Literature Review

This chapter contains a review of literature used to inform the research documented in this thesis. It links the objectives detailed in chapter 1 with relevant academic and industrial studies. The review highlights changes that are predicted in the LV distribution network network alongside some of its present day characteristics. The following characteristics and changes are considered: current unbalance, PV induced OV, impact of EVs, cable current, thermal cable overload, phase balancing and load balancing. Finally, the research opening for this thesis is identified which mitigates some of the future challenges that the LV distribution network faces in certain circumstances.

2.1 Distributed Generation (DG)

DNO's find it difficult to plan where and when to invest in infrastructure to accommodate new DG connections. Some uncertainties that they encounter relate to the planning and construction process, whilst others relate to technical issues such as the network's voltage and thermal limitations. An excellent literature review on techniques developed by researchers in recent years to address these uncertainties is provided in [17] which was produced to encourage the implementation of such methods. The majority of the methods detailed involve ultimately finding an optimum solution to the combinatoric problem that connecting DG presents, when the objective is for example: to minimise losses or minimise short/long term costs whilst satisfying voltage and thermal constraints. In many cases it is not possible to find the global optimum due to the scale of the problem, so solutions often involve finding one or several local optima. The techniques documented in [17] relate to various distribution network voltage levels and those that have been applied to the LV network are critically reviewed later in this section.

In chapter 1, PV was highlighted as the normal type of DG technology connected to the LV network in the UK and the recent trend is one of growth [10]. Automatic consent is granted for customers connecting DG in accordance with the G83 engineering recommendations [18] for connections rated at 16A or below and the DNO is notified of such installations within 28 days of commissioning. Installations that exceed the

16A threshold require an application to the DNO. Therefore, DNO's do not have control over new PV connections that are rated below 16A, but they are notified where they have been installed 28 days (at the latest) after they were commissioned. Information that distribution networks operators possess varies dependant on the UK region due local historical practices and processes. In addition, significant gaps from the ideal data set often exist. Monitoring of voltages and currents in LV networks is scarce but is being introduced as part of small industrial trials like those detailed in [19] and [20]. The combination of automatic DG consent, distribution network responsibility for voltage levels [8], gaps in network data and an absence of monitoring, presents DNOs with little information or control over high voltages induced by DG in the LV network. Therefore, voltage quality issues are generally only highlighted at LV level through customer complaints, leaving distribution networks with the challenge to plan where and when to reinforce the network in order to maintain compliant voltage levels. At the same time, they have no influence over the location of new DG plant within it.

The location of PV in an LV network has a significant impact on the occurrence of OV and those areas are difficult to identify. Some techniques have been developed to address this difficulty in order to quantify distribution networks for their PV capacity. For instance, one DNO has created a draft policy that provides guidance on when more intensive studies of PV penetration should be carried out for a particular network, this is currently undergoing validation as part of the Low Carbon Networks Fund (LCNF) trial [21]. The intensive studies include LV feeder assessments that aim to estimate permissible levels of PV penetration levels that do not trigger OV conditions. The intention is that this can be used to inform proactive maintenance and asset management.

Meanwhile, academic literature largely focuses on the combinatoric problem that automatic consent creates due to the high numbers of possible permutations of PV, even on small feeders. In [22] Thomson et al. examine the technical impact on voltage of higher penetrations of PV and Micro Combined Heat and Power generators and make recommendations about how to mitigate OV issues. An 11KV UK network was used as a test case and PV connections were allocated to dwellings according to their roof orientation to the south, therefore, reducing the combinatoric problem. Commer-

cial software packages are noted as being ill suited to the complexities of the modelling required and Thomson et al. therefore, develop a modified forward/backward sweep algorithm documented by Shirmohammadi [23] and Kersting [24] that accounts for Dy11 distribution transformers. Thomson et al. assumed that generators were rated between 1KW and 2 KW, which was reasonable in 2007 but not today because the actual DG mix installed in the UK to date shows 4KW to be the normal rating of installation. In [25] Navarro et al. use Opendss [26] to create three phase network models using real network data to calculate the impact of PV installations on different penetration levels of PV. They combat the combinatoric problem by evaluating specific permutations of PV allocation determined through their novel monte-carlo based technique, which results in a range where the minimum and maximum PV penetration levels that do not result in OV is found. Navarro et al. also perform sensitivity analysis on OV to data granularity using a 5min resolution which concludes that hourly and half hourly data underestimates the occurrence of OV which may be detected using BS EN 50160:2010 [9].

2.2   Cable Current and Domestic Loading

A 10% to 20% market penetration of electric vehicles has been shown to lead to an 18% to 36% increase in the daily distribution network peak demand during winter months [12]. Furthermore, such a rise would lead to breaches in cable current and increase instances of cable thermal overload.

Neher and McGrath documented a widely used method for rating cables in [27] which was encompassed by IEEE [28] and BS/IEC standards [29]. Application of the standards relate directly to a cables construction, which, for those manufactured for the UK today are defined by BS 7870 [30]. The operational thermal capacity of underground power cables is evaluated today by applying IEC 60287 [31] which provides a standard cable model relating phase conductor temperature to a cable current rating in steady state. The impact of cable heating on underground LV cables is certified by cable manufacturers in the UK by applying BS 7870 [32] which specifies a series of laboratory tests. The heating cycle laboratory tests within the standard apply to thermal properties and require cables to be mounted under water and in the air while a

balanced electrical current is passed through the phase conductors in order to heat them. The conductor temperature is observed using thermocouple sensors, these measurements are verified by taking electrical resistance readings of phase conductors during the test. Heating cycles are restricted in time to eight hour durations, where, two hours are allocated to maintain conductor temperature to between 5°C and 10°C above the rated temperature, and three hours to natural cooling. However, the tests do not assess unbalanced operation or capture the transient of conductor temperature when it heats or cools. Ultimately, the relationship that is established is between a cables construction and its maximum operating phase current carrying capacity, this is often referred to as cable ampacity.

The standards that define cable current assume phase conductors are balanced and that instantaneous changes in conductor current cause instantaneous changes in conductor temperature. In recent years research has focussed on developing techniques that map the transient relationship between current and temperature in real time. In [33] an equivalent circuit is derived for the transient thermal behaviour of cables in unfilled troughs which is validated through finite element analysis simulations, the circuit is shown to be valid within a specified range. Meanwhile, Shaker et al. [34] use fuzzy computation to predict weather related uncertainties that impact on the DTR (dynamic thermal rating) of overhead lines such as ambient temperature, wind speed and wind direction. The DTR is particularly useful when applied to overhead lines that connect wind farms to the distribution network (DN). Consider a windy period, at this time wind farms transmit additional current to local power lines which induces conductor heating, but at the same time the conductors are cooled by the wind which enables them to transmit more current than in less windy conditions. Jupe et al. developed a DTR scheme through off line simulation of a power system using historical environmental data in [35] and later applied it to a real network, reference [36] details the learning points and experiences from real world application to a 132KV line connecting an offshore wind farm. The technique applied by Jupe et al. involves the interpolation and correction of IEC standards and environmental conditions, meaning that the dynamic relationship between current and temperature is not explicitly tackled, rather an approximation is made that relates current, temperature and environmental condi-

tions. DTR works well on overhead lines due to their exposure to constantly changing environmental conditions, which is monitored by appropriately sited weather stations at critical spans. A hot topic for researchers now is the identification of critical spans that may benefit from DTR. In [37] Matus et al. tackle this problem via a heuristic based technique. Moreover, the heuristic was derived from historical-simulated weather data which was used to compute thermal capacities in each span of a 325km line in Chile to identify the hot-spots. [38]

Historically, technology applied to power systems has cascaded down voltage levels over time as costs reduce due to maturing manufacturing processes of enabling components. A good recent example of this is the use of secondary on load tap changing transformers at MV/LV substations, one was used as part of a combined strategy to control voltage in [39]. DTR however, is not transferable to LV networks in the same way, one reason is that most urban areas in the UK have underground networks [40], meaning they are protected from the environmental conditions which DTR exploits. In any case, the costs associated with: identifying critical spans that may benefit, local tuning of models and the installation and maintenance of weather stations, eliminate the feasibility today of this technology at LV level due to excessive costs.

Other strategies have been developed which focus on making better use of assets through techniques such as curtailment and demand side management (DSM). In [41] Navarro et al. show through simulation of an LV feeder how a load shifting strategy reduces the peak demand by shifting passive washing loads. Therefore, the cable current requirement of cables and transformers feeding loads is reduced, unlocking the potential to defer reinforcement. The high costs associated with the reinforcement required to accommodate higher loads have attracted research to be conducted to consider social factors as well as technical ones. For example, [42] presents the first stages of a socio-technical methodology to identify circuits that are likely to require reinforcement in a 33KV network in the UK. In [43] statistical measures are used to to predict utilization levels of components and assess the scale of potential reinforcement requirements due to breaching thermal and voltage constraints. Other DSM techniques conjectured are summarised into convenient groups by Zhang et al. in [44] which include:

load priority techniques [45], control of appliances [46], differential tariffs [47] and conservation voltage reduction [48]. O'Connell et al. directly tackle the problem of increased loading induced by higher penetrations of electric vehicles (EVs) connecting to the LV distribution network in [49] where they develop an EV management scheme which uses a three phase unbalanced load flow model from [50] to monitor voltage and thermal network constraints. Meanwhile, the objective function is focussed on minimising the cost of charging EV's to customers who are all assumed to have advanced metering infrastructure that facilitate time of day tariffs. A rolling optimisation is used to manage uncertainties relating to customer behaviour. The study concludes by stating that controlled charging schemes for EV's can be used to defer network reinforcement and that balanced system modelling at LV level does not accurately represent the actual system state.

2.3   Current Unbalance

DNO monitoring trials conducted in the UK such as [20], [51], [52] and [19] have uncovered unbalanced phase currents on LV feeders in the urban LV distribution network. Unbalance of this nature has also been recorded in countries outside the UK, for example in [53] where it is referred to as load imbalance. A complete consensus does not yet exist in industry or academia on vocabulary associated with current unbalance. Either imbalance or unbalance is used to describe a lack of balance across phases of voltage or current in a three phase power system. Siti et al. [54] define phase and load balance/unbalance to describe the state of a power system at MV (Medium Voltage) and LV level respectively.

2.3.1   Phase Balancing

Phase balancing involves changing the configuration of primary feeders in the distribution network to minimise neutral currents. This can be achieved either through the manipulation of sectionalising and/or tie switches, or manually reconfiguring phase connections. Phase balancing has been extensively researched and the earliest reference found that explicitly develops an algorithm for remote control of switches, which also addresses fault isolation and service restoration, was conducted by Castro et al. in 1980 [55]. The problem of determining the optimum setting for the switches is one of combinatorics which is outlined by Civanlar et al. [56] as conceptually straightforward

but computationally inefficient. Published research focuses on finding the optimal balanced configuration at MV level whilst minimising labour, cost, customer interruptions and power system losses. A typical example of what has been published can be found in [57] and [58] which correspond with studies conducted in Taiwan (2008), and Iran (2012) respectively. Although there have been significant advances in computational power over the past 33 years, the problem outlined by Civanlar et al. [56] persists today, partly due to the large number of possible permutations for reconfiguration.

Chia-Hung et al. [57] tackle the combinatorics problem by devising a strategy for reconfiguring phases which incorporates some heuristic rules derived from the experience of distribution network engineers to identify locations for phase reconfiguration. Furthermore, the algorithm aims to minimise cost, neutral current, labour and customer interruptions. Hooshmand and Soltani [58] take a different approach and use bacterial foraging oriented by particle swarm optimisation integrated into a fuzzy multi objective function to reduce neutral current, re-phasing cost, voltage drop and line losses. The techniques developed by Chia-Hung et al. [57] and Hooshmand and Soltani [58] both directly combat the combinatoric problem that phase balancing presents, therefore showing it to be a persistent issue.

2.3.2 Load Balancing

Load balancing is the reconfiguration of LV feeders to correct unbalances caused by active loads. A literature review was conducted which uncovered nine conference papers and one journal paper on the subject authored by two separate research groups. The sparsity of the research in this area reflects anticipated difficulties associated with intervention at LV level, primarily due to the great number of its constituent elements as summarised by Willis and Philipson [13]. Published research has been based on the concept of changing the phase connection of single phase loads via a switching matrix or phase connection switcher, which present day technology could support, see [54] and [59]. Published research from the groups commenced in 2005 and focused on the South African and Iranian distribution networks respectively. Owing to the small number of papers on load balancing, all publications have been included in the critical analysis provided in this section.

2.3.2.1   M.W. Siti et al, Tshwane University of Technology

The studies documented in [59] and [60] formulate an optimisation problem which is solved using the following numerical solvers: Dynamic Leapfrog and Gauss-Newton. The results from both the solvers is compared and the concept of automatic load balancing is introduced, and discussed in terms of cost, solution speed and optimisation.

A specific case study is used in [59] and [60] where 15 single phase household loads are connected through phase switching devices to an LV feeder. The numerical methods are necessary to find a sub/local optimal solution due to the large number of combinations which total 14.3 million. The relationship between switchers and combinations is shown in (1). The objective function is defined in the study as the difference between the sum of the squares of phase currents. Therefore, the mathematical model assumes each load is of the constant current type, which effectively ignores cable impedances and the associated changes in nodal voltage that they cause. Ultimately, the dependence on voltage of constant power and impedance loads, which in turn cause phase and neutral conductor currents is ignored. The study simplifies the problem by assuming that each household load is single phase with a unity power factor and, that each phase current angle is perfectly aligned to 0º, -120º and 120º respectively. A snapshot of load current data from each of the five groupings of aggregated loads is used to show the impact of each method. Therefore, the study does not consider switching or measurement frequency, rather, it implies an assumption that switching frequency is infinite and can respond immediately with no delay to instantaneous measurements of network currents. The study aims to reduce system losses, but measures the quality of the solution by evaluating neutral current which is calculated by finding the sum of the phase currents.

The fundamental problem that [59] and [60] set out to solve is the combinatoric one caused by the number of combinations of possible switching matrix settings. The relationship between the number of combinations represented by p and number of switchers represented by n_s is as follows:

$$p = 3^{n_s} + 1 \qquad (1)$$

To emphasise the enormity of the quantity of possible combinations even for modest numbers of switchers, the figure below is provided that plots the number of switchers against the number of combinations.
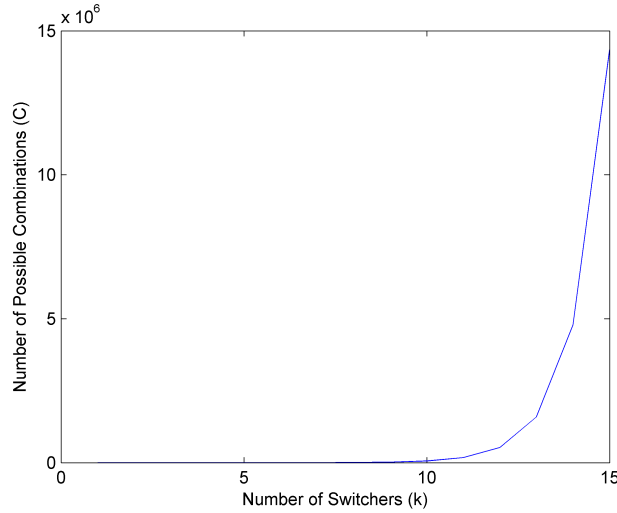
Fig. 6 The Combinatoric Problem Shown Graphically (1)

Fig. 6 shows clearly that the number of combinations increases rapidly with the number of switchers as for 1, 5, 10 and 15 switchers there are 4, 244, 59thousand and 14.3million combinations respectively. The numerical solvers are used to find sub/local optimal solutions for the practical implementation of real time automatic control. In that regime the absolute optimum could only be found by testing all combinations, which is impractical when the number of switchers exceed 10.

The papers [59] and [60] record a significant reduction in neutral current when the Dynamic Leapfrog and Gauss Newton methods were applied. Of the two methods tested, the Dynamic Leapfrog was found to provide the most optimal result, although it took longer to execute than Gauss Newton.

In [61], [62], [54] and [63] Siti et al. compare the impact of using their new Heuristic algorithm with a Neural Network to find sub optimal switching sequences. The journal paper [54] presents an additional scenario to the two conference papers [62]

and [63], but is otherwise very similar, therefore, the journal paper is the sole focus in this literature review.

[54] considers two scenarios where 15 and 45 radially connected single phase loads are fitted with switchers on the South African distribution network. One characteristic of the approach adopted is that for both methods compared, it is assumed that a perfectly balanced MV network is connected to the secondary transformer(s) supplying the loads. Results are presented that show the Heuristic approach to be significantly more effective and robust than that of the Neural Network when evaluated by examining the differences between phase currents as shown in (2).

The heuristic algorithm in [54] uses predetermined rules that result in a reduction in the number of possible permutations, enabling all those that remain to be tested. A subroutine is used to group the loads into sets of 5 and 15 for the respective 15 and 45 load scenarios, which has the impact of reducing the number of permutations from 14.34×10^{6} and 2.9543×10^{21} to 28 in both cases. This subroutine does not guarantee the optimum groupings of loads, rather, it makes an approximation. The paper does not contain a discussion that evaluates the quality of this measure. Moreover, this approach implies that all loads are active in the network, which does not necessarily reflect reality. The switch setting is chosen by finding the minimum result from all 28 remaining permutations when compared to a theoretical 'perfectly balanced' phase current I_{ideal} through the application of (3).

The results from the Neural Network and Heuristic controllers in [54] are evaluated for both methods according to the total maximum difference between two phase currents for the switch setting chosen by the method (2). However, evaluating results in this way only approximates the impact of the methods on the network. This is because it is assumed that all loads are of the constant current type, meaning that actual phase and neutral currents are not calculated. Fundamentally, the paper does not attempt to accurately model the system due to the absence of constant impedance/power loads and cables. Moreover, an attempt to show the benefit of either method in terms of the

objectives outlined, which are to reduce system real power losses and relieve system overloads, is not included.

[54] then uses 3 snapshots of data measured from the real network on the 15 load LV network, and one snapshot of data for the 45 load network. The real measurements were synchronised when recorded. The paper finds that the Heuristic method is more robust than that of the Neural Network and records both methods as achieving better current balancing than is recorded in the measurement data. Therefore, what is shown is that the methods can take current measurement data from a network and predict a sub/local optimal switching sequence to balance phase currents. The quality of the settings is not evaluated. What the paper does not show is the expected impact that either method would have upon implementation. To undertake this analysis, accurate modelling of the network with time series data is required.

$$\Delta I_{max} = max\ \left\{ \left\| I_{ph1} \right| - \left| I_{ph2} \right\|, \left\| I_{ph2} \right| - \left| I_{ph3} \right\|, \left\| I_{ph3} \right| - \left| I_{ph1} \right\| \right\} \tag{2}$$

$$arg\ min \left| \sum_{j=1}^{5} I_j - I_{ideal} \right|, where\ \ I_j \in \boldsymbol{I}_{load}. \tag{3}$$

In [64] Siti et al. use a larger network to test a fuzzy controller to find switch sequences on an assumed network. The data used originated from a measurement study in a South African City [65] that measured the load power over a month. Data from the superset was randomly selected to form five hypothetical test feeders that each consisted of 150 loads, a figure which was also informed by [65].

The average total phase load is used to measure the success of the state of fuzzy controller by calculating AU/ph (Average Unbalance per Phase) (4). The controller is only designed to invoke when AU/ph drops below 10KW. Results are measured by comparing the initial average power values from (4) with that obtained when the fuzzy controller is used. Finally [64] concludes that unbalanced conditions are improved through the use of the fuzzy controller. The use of power instead of current in this

study assumes that all loads are constant power loads and it does not attempt to calculate the impact on phase and neutral conductor currents.

$$AUlph = \frac{\left|L_{ph1} - L_{ph2}\right| + \left|L_{ph2} - L_{ph3}\right| + \left|L_{ph3} - L_{ph1}\right|}{3}$$

(4)

2.3.2.2 Raminfard et al.

All the three papers [66], [67] and [68] from Raminfard et al. focus on improving the LFOP optimisation algorithm used by Siti et al. in [59] to the combinatoric problem. The complete algorithm presented is referred to as the "Modified Leap Frog Algorithm for Constrained Optimization" which adds a compensator subroutine to the LFOPC which was first presented by Snyman in [69]. The compensator sub routine chooses loads based on the maximum and minimum phase current values, then moves them to other phases whilst monitoring the ratio shown in (5). If the sub routine ratio (5) is improved by a predetermined level during execution, it returns new switching sequences that improve network optimisation, If this is not the case, it simply returns those computed by the LFOP algorithm.

In [66] the MOLFOP method is compared to the Neural Network and Heuristic methods which was presented by Siti et al. In [54], it is found to achieve similar results to the Heuristic method which is shown as achieving the best performance. However, when all cases were compared, the Siti et al. Heuristic algorithm achieved better ΔI_{max} when computed using (2).

Loads with variable power factors are used in [67] and the method from [66] is extended to accommodate it. The measurement that is used to assess the quality of the balancing achieved is β (5) and neutral current as a percentage of the minimum norm current as defined in the paper.

MOLFOP optimisation is performed on hourly time series data in [68] which assumes that the load will remain constant for an hour. Therefore, the results presented

are impacted as they would not be achieved in reality owing to the load frequency being faster than once every hour (28mHz) which is assumed.

$$\beta = \sqrt{\frac{I_M - I_m}{I_M + I_m}} \qquad\qquad (5)$$

2.3.3 PV Balancing

PV Balancing is the balancing of single phase PV DG in the LV distribution network through the control of switchers as described in section 2.3.2. The literature review did not uncover any publications on this topic to date.

2.4 Conclusion

This literature review has highlighted relevant publications and projects in the areas of: DNO connected DG, DG in LV networks, domestic loading and its impact on cable current and current unbalance. The two significant challenges that face LV networks relate to the voltage and thermal constraints that are anticipated to be put under pressure due to increases in the take up of DG and EVs in particular. The well documented solution of DTR for transmission lines that connect DG at voltage levels above LV have been reviewed and found to be unsuitable for implementation in LV networks. Therefore, current balancing was explored and academic literature confirmed that it can be effective in reducing neutral and phase conductor currents. The objective of Load Balancing has been to reduce losses by correcting system unbalances. Published research focused on the combinatoric optimisation problem which is presented when switchers are considered to connect individual loads. Fundamental assumptions such as: constant current loading and infinite switching frequency have so far masked the quantification of improvements that load balancing achieves. Practical implementation of the schemes conjectured in publications are thought to be costly, largely due to requirements associated with the installation of PSs at every load and the required communications infrastructure. Finally, the concept of PV balancing was introduced as the literature review did not uncover any publications on this topic to date.

2.5 Research Gaps

The research that were highlighted during this literature review and relate to the scope are highlighted in this section.

UK LCNF monitoring trials uncovered significant phase current unbalance in underground (UG) urban LV feeders, which indicate unequal connections of active single phase loads and DG to phases. Some of this neutral current can be considered as locked cable current that could be released through current balancing. The advantages of load balancing has previously been indicated in [54] but PV balancing has not, as yet, been assessed. Implementation of either type of balancing would be costly in the UK if the switching device in [54] were used, due to expansive UG networks meaning substantial excavation requirements for installation. Therefore, the economic case for its implementation in the UK is weak, however, innovations to the switching device could be made and a new type of device conjectured to make implementation more feasible for the present day by reducing the points of required intervention. Therefore, modification will focus on a new switching device that can be installed in series along the feeder rather than at every dwelling location, this innovation will enable one device to manipulate many single phase connections to improve device balance as outlined in the objectives in section 1.4. To understand more accurately it's impact on voltage, losses and cable current when PV, dwelling loads and street lamps operate, a high fidelity model will be developed that does not assume constant current loads as some published research highlighted earlier in this literature review did. The device itself may prove more costly per unit than the one previously conjectured in [54] due to its components having higher ratings (short circuit currents and breakaway forces) but the economic case for implementation when compared to previous schemes reviewed will be significantly strengthened.

3 Introduction to Phase Switchers

This chapter introduces the novel device termed the PS that simultaneously reconfigures the phase connections of multiple dwelling loads and distributed generators on low voltage distribution feeders. It is shown later in this thesis how such phase connection reconfiguration allows a substantial increase in both the current carrying capacity of cables and the penetration of PV distributed generation. A mathematical framework as well as the terminology associated with PS is also presented in this chapter. Finally, the process used to model an example feeder is provided and followed by a commentary on the procedure used to validate it. An additional discussion regarding the appropriate choice of sampling time employed by the proposed control algorithms is also detailed.

3.1   Nomenclature and Key Terminology

LV feeders in the distribution network provide single and multiphase connections for dwellings and devices to the wider power system. Dwellings are residential houses or flats that behave as loads, small embedded generators or a combination of the two, whilst the term devices covers everything else which could include street lamps and CCTV cameras for example. All the results reported in this thesis are obtained for the case of an example UG radial LV feeder. This is a reasonable because UG radial LV feeders are the most common network configuration found in the UK [40]. Nevertheless, it is shown in Section 3.1.9 how PSs could be readily employed in the interconnected networks. Conventional power flow on radial LV feeders was established before the introduction of small embedded generators and lead to the 'upstream' and 'downstream' definitions which describe the relative position of devices and objects with respect to each other where upstream is towards and downstream away from the medium to low voltage transformer. Cables define the path of a feeder and they are interconnected through joints which provide dwellings with their phase connections effectively making joints buses.

3.1.1 The Unconstrained Phase Switcher

The PS is a device capable of switching phase connections of individual LV feeder conductors in the distribution network by adopting one of the six possible unique switch positions, it shown in the following figure:
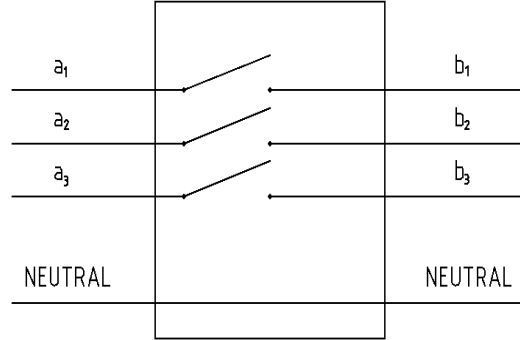
Fig. 7: The Unconstrained LV Phase Switcher

The PS can be installed at any point on an LV feeder other than a service joint location, it changes the phase connection of all downstream loads and/or generators in radial networks. The work presented here focuses on radial LV feeders. Nevertheless, it is shown in section 3.1.9 that PSs can be readily applied to interconnected networks where an additional constraint is imposed in order to ensure that the interconnected substations have consistent phase connections.

Referring to Fig. 7, unconstrained PS operation allows the six switch positions as defined in the following table:

Switch Position Integer	Phase Conductor Connections
1	*(a1 to b1) and (a2 to b2) and (a3 to b3)*
2	*(a1 to b1) and (a2 to b3) and (a3 to b2)*
3	*(a1 to b3) and (a2 to b1) and (a3 to b2)*
4	*(a1 to b2) and (a2 to b1) and (a3 to b3)*
5	*(a1 to b3) and (a2 to b2) and (a3 to b1)*
6	*(a1 to b2) and (a2 to b3) and (a3 to b1)*

Table 1 Switch Positions of the Unconstrained PS

3.1.2 The Constrained Phase Switcher

The constrained PS only allows switch positions that obey phase rotation which make it suitable for application on feeders that provide connections to three phase

loads, the following diagram highlights provides an intuitive insight into it's function-
ality:
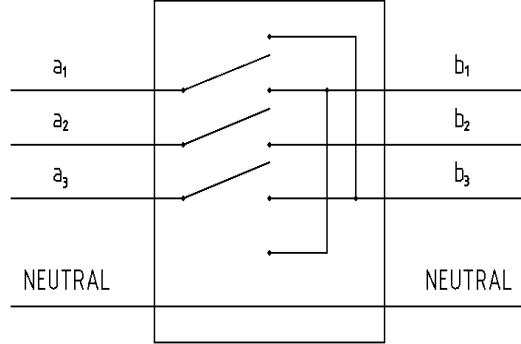
Fig. 8: The Constrained LV PS

This PS is is identical to the unconstrained PS but has a constrained operation
which allows only three switch positions which are defined as an integer and as a phys-
ical position with reference to Fig. 8 up, centre or down in the following table:

Switch Position Integer / Physical Position	Phase Conductor Connections
1 / Up	*(a1 to b3) and (a2 to b1) and (a3 to b2)*
2 / Centre	*(a1 to b1) and (a2 to b2) and (a3 to b3)*
3 / Down	*(a1 to b2) and (a2 to b3) and (a3 to b1)*

Table 2 Switch Positions of the Constrained PS

3.1.3 LV Feeder Phase Connections

The default phase connection information for a given network can be represented
using the phase connection matrix, denoted as P_b, whose elements provide either
the number of connected devices of a specific type, such as loads or small embedded
generators, or the total power consumed or injected at a particular bus. For the sake of
simplicity, when the generic term "devices" is used no distinction is being made
between the aforementioned specific types, this matrix has 3 rows and n_b columns,
where n_b is the number of buses.
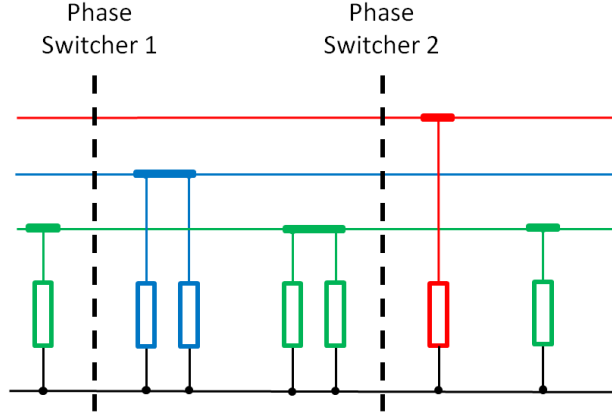
Fig. 9: Example Five Bus LV Feeder Network with One Branch

An example of a simple LV feeder network with 5 buses is provided in Fig. 9 and its corresponding phase connection matrix P_b is given as follows:

$$P_b = \begin{bmatrix} 0 & 0 & 0 & 1 & 0 \\ 0 & 2 & 0 & 0 & 0 \\ 1 & 0 & 2 & 0 & 1 \end{bmatrix} \tag{6}$$

The introduction of n_s PSs into a network effectively partitions that network into (n_s+1) segments, each of which contains anywhere between 0 and n_b buses. In the case of the particular example illustrated in (7), the P_b matrix is partitioned into three block elements corresponding to three matrix segments:

$$\begin{bmatrix} 0 & 0 & 0 & 1 & 0 \\ 0 & 2 & 0 & 0 & 0 \\ 1 & 0 & 2 & 0 & 1 \end{bmatrix} \implies P_{b_1} = \begin{bmatrix} 0 \\ 0 \\ 1 \end{bmatrix}, \quad P_{b_2} = \begin{bmatrix} 0 & 0 \\ 2 & 0 \\ 0 & 2 \end{bmatrix}, \quad P_{b_3} = \begin{bmatrix} 1 & 0 \\ 0 & 0 \\ 0 & 1 \end{bmatrix} \tag{7}$$

Phase Switcher 1   Phase Switcher 2

P_b features on the left hand side of equation (7) where the right hand side is partitioned block elements which can be represented as segment column vectors as shown below:

$$p_{b_1} = \begin{bmatrix} 0 \\ 0 \\ 1 \end{bmatrix}, \qquad p_{b_2} = \begin{bmatrix} 0 \\ 2 \\ 2 \end{bmatrix}, \qquad p_{b_3} = \begin{bmatrix} 1 \\ 0 \\ 1 \end{bmatrix} \qquad (8)$$

Each of these vectors correspond to a particular network segment created by the PSs when they are located as shown in Fig. 9, the vectors are found by combining all the devices in a segment as demonstrated in (7).

A new segment phase connection matrix P_s can be established with 3 rows and $n_s + 1$ columns, where n_s is the number of PSs and p_z is the aggregate segment load vector from (7) for the zth segment (9):

$$P_s = \begin{bmatrix} p_1 & p_2 & \cdots & p_{n_s+1} \end{bmatrix} \qquad (9)$$

3.1.4 Network References – Branches and Transformers

Unless a given LV feeder has a single branch, loads will be connected to the power system by a network of parallel branches. An example 9 bus 1 branch LV feeder is provided in Fig. 9 and an example 7 bus 2 branch LV feeder is shown in the following figure:
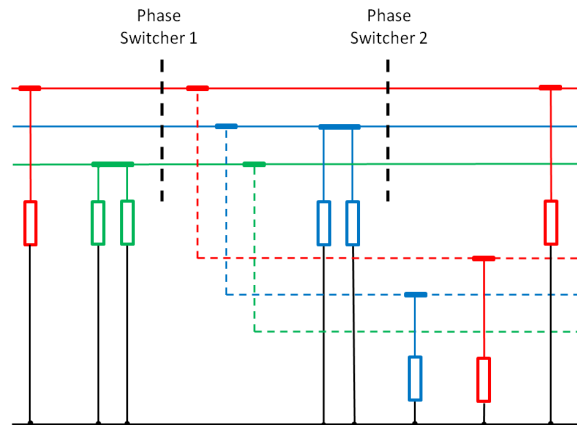
Fig. 10 Example 9 Bus LV Feeder Network with 2 Branches

In order to produce a phase allocation matrix with a consistent number of rows and columns, regardless of the number of branches, a reference branch must be designated.

27

This is done by designating a particular branch as the "reference branch", which imposes the new assumption that all dwellings which are connected to a branch other than the reference branch, are assumed to be connected directly to the reference branch at the junction where the two branches are joined. The reference branch in Fig. 10 is identified by the solid lines that represent the phase conductors, the resultant phase allocation matrix for this example feeder is represented as follows:

$$\boldsymbol{P}_b = \begin{bmatrix} 1 & 0 & 1 & 0 & 1 \\ 0 & 0 & 1 & 2 & 0 \\ 0 & 2 & 0 & 0 & 0 \end{bmatrix} \tag{10}$$

Note that the devices connected to a non-reference branch are highlighted with dashed lines in Fig. 10 and constitute the 2nd column of the Pb matrix shown in (10). Also, the underlying assumption of this methodology is that PSs can only be installed upon the reference branch. This assumption could be lifted if it was determined that PSs should be installed on more than one branch, but this would increase the number of rows in the $\boldsymbol{P}_b$ matrix and impact upon the mathematical nomenclature detailed which would require extending to support it.

A consequence of designating a reference branch is that PSs can only be placed upon it, a convention that can be appreciated on inspection of the particular example shown in Fig. 10. When the reference branch is designated as that represented by the solid lines in Fig. 10, the resultant three associated segment column vectors for it are as follows:

$$\boldsymbol{p}_{b_1} = \begin{bmatrix} 1 \\ 0 \\ 2 \end{bmatrix}, \quad \boldsymbol{p}_{b_2} = \begin{bmatrix} 1 \\ 3 \\ 0 \end{bmatrix}, \quad \boldsymbol{p}_{b_3} = \begin{bmatrix} 1 \\ 0 \\ 0 \end{bmatrix} \tag{11}$$

In order to assign PSs with addresses and also to design PS control algorithms that manage specific problems in particular feeder segments, a transformer is designated as the reference.

The PS address in a network is taken from the upstream bus integer and denoted as l_i, where i is the number of PSs between it and the reference transformer plus 1 as shown in the following figure:
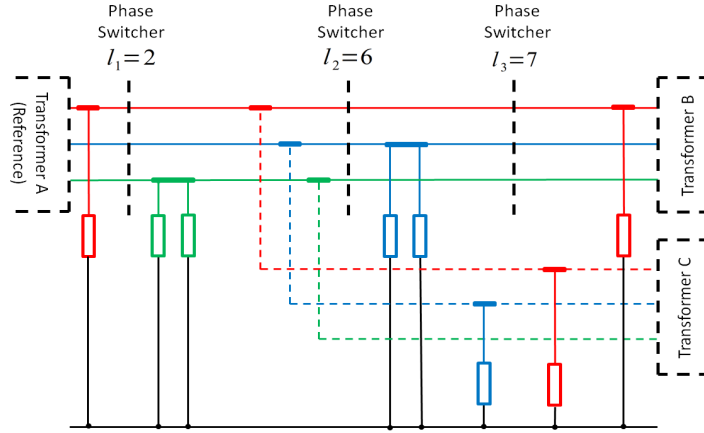
Fig. 11 Example 2 Branch Network with 3 PSs and 3 Interconnected Transformers (the reference branch is represented has red blue and green solid lines)

Whereas, details how to mathematically represent a problem for control algorithm design is provided in section 3.1.9.

3.1.5 Phase Switcher Placement

"PS placement" is a term used throughout this thesis to describe the process of allocating locations for PSs to particular places on a given feeder. Using the mathematical framework presented, PSs can be represented as being installed between any two adjacent buses of the reference branch.

3.1.6 Switch Configuration Matrices

A switch configuration matrix, denoted as C, describes how the phase connections of two adjacent segments are interconnected. This matrix has six realisations and for each, there are two alternative definitions that are dependent on which of it's terminals are taken to be the reference.

Assuming the reference terminal is that connected upstream for a particular PS, which is the definition followed in this thesis, then the PS arrangement and the corresponding configuration matrix are given for each of the six possible realisations are shown in the following table:
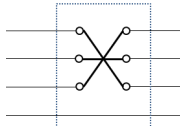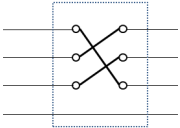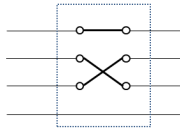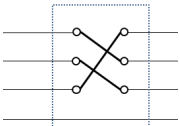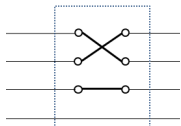
Switch Positions that **Do** Maintain Phase Rotation		Switch Positions that **Do Not** Maintain Phase Rotation	
Phase Connections	*Switch Configuration Matrix*	*Phase Connections*	*Switch Configuration Matrix*
	$C_A = \begin{bmatrix} 1 & 0 & 0 \\ 0 & 1 & 0 \\ 0 & 0 & 1 \end{bmatrix}$		$C_D = \begin{bmatrix} 0 & 0 & 1 \\ 0 & 1 & 0 \\ 1 & 0 & 0 \end{bmatrix}$
	$C_B = \begin{bmatrix} 0 & 0 & 1 \\ 1 & 0 & 0 \\ 0 & 1 & 0 \end{bmatrix}$		$C_E = \begin{bmatrix} 1 & 0 & 0 \\ 0 & 0 & 1 \\ 0 & 1 & 0 \end{bmatrix}$
	$C_C = \begin{bmatrix} 0 & 1 & 0 \\ 0 & 0 & 1 \\ 1 & 0 & 0 \end{bmatrix}$		$C_F = \begin{bmatrix} 0 & 1 & 0 \\ 1 & 0 & 0 \\ 0 & 0 & 1 \end{bmatrix}$

Table 3: All possible PS switch positions showing the equivalence of phase connections and Phase Configuration Matrices

Note that C_A, C_B and C_C respect the phase rotation assumption whilst C_D, C_E and C_F do not.

If the reference segment is assumed to be located downstream from the PS then the resulting switch configuration matrices are simply the transposes of the those shown in Table 3.

3.1.7 Phase Switcher Cascading and some Resultant Properties

Two non-adjacent segments in any network are interconnected via several PSs. Individual configuration matrices of these PSs can be combined, by simple multiplication, in order to provide the equivalent single PS configuration that describes how the phases of any two non adjacent segments are interconnected. Generally, for a network

that employs n_s PSs, there are n_s+1 segments and the corresponding number of pairs of non-adjacent segments is given by that shown in (12):

$$\sum_{i=1}^{n_s-1} i \tag{12}$$

Throughout this thesis, the special case where there are no PSs impacting on device phase connections or, when all PSs are set to C_A, the term 'straight through config-uration' is used. An example of cascading two phase PSs is shown in Fig. 12 where a colour scheme is used to help illustrate the effect. In this example both PSs have identical switch positions but the combined impact on non adjacent segments is the equivalent to the single switch position C_C.
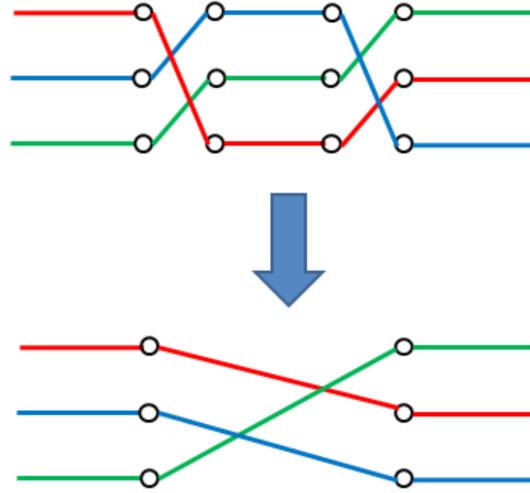
Fig. 12 Cascading Phase Switchers

This can also be demonstrated algebraically by multiplying the corresponding switch configuration matrices:

$$C_B \cdot C_B = \begin{bmatrix} 0 & 0 & 1 \\ 1 & 0 & 0 \\ 0 & 1 & 0 \end{bmatrix} \cdot \begin{bmatrix} 0 & 0 & 1 \\ 1 & 0 & 0 \\ 0 & 1 & 0 \end{bmatrix} = \begin{bmatrix} 0 & 1 & 0 \\ 0 & 0 & 1 \\ 1 & 0 & 0 \end{bmatrix} = C_c \tag{13}$$

In general case, the resultant equivalent switch configuration from combining two phase PSs is given in Table 4.

	C_A	C_B	C_C	C_D	C_E	C_F
C_A	C_A	C_B	C_C	C_D	C_E	C_F
C_B	C_B	C_C	C_A	C_E	C_F	C_D
C_C	C_C	C_A	C_B	C_F	C_D	C_E
C_D	C_D	C_F	C_E	C_A	C_C	C_B
C_E	C_E	C_D	C_F	C_B	C_A	C_C
C_F	C_F	C_E	C_D	C_C	C_B	C_A

Table 4 Equivalent single phase switch position when two are combined

Note that the combining of two phase PSs is commutative if both PSs satisfy phase rotation assumption, otherwise it is non-commutative:

$$C_D \cdot C_B = C_F \neq C_E = C_b \cdot C_D \tag{14}$$

Another two interesting observations from Table 4 relate specifically to switch positions that do not respect the phase rotation assumption. Firstly, the result of combining two phase PSs with any switch position that does not respect phase rotation results in a switch position that does respect phase rotation. For example, see (15) below:

$$C_D \cdot C_E = C_c \tag{15}$$

Also, if combining two phase PSs with identical switch positions that do not respect phase rotation the result is the straight through configuration:

$$C_D \cdot C_D = C_B \cdot C_B = C_F \cdot C_F = C_A = I \tag{16}$$

Results reported in this thesis were obtained under the assumption of phase rotation. This significantly reduces the number of possible combinations that need to be evaluated and, therefore, reduces the computational burden of the controller, especially if complex networks with large number of individual PSs are considered. However, the

methodologies reported in this thesis can be readily extended to the cases where phase rotation assumption can be removed.

Three PS realisations that respect phase rotation also possess some useful properties. Firstly, as mentioned before, their multiplication is commutative as shown in (17), (18) and (19) below:

$$C_A \cdot C_B = C_B \cdot C_A \tag{17}$$

$$C_A \cdot C_C = C_C \cdot C_A \tag{18}$$

$$C_B \cdot C_C = C_C \cdot C_B \tag{19}$$

Another very important property is that:

$$C_B = C_c^{-1} \tag{20}$$

The implication of this is that:

$$C_B \cdot C_C = C_B \cdot C_B^{-1} = I = C_A \tag{21}$$

Similarly:

$$C_C \cdot C_B = C_C \cdot C_C^{-1} = I = C_A \tag{22}$$

Physical interpretation of this result is that C_B provides phase shift of 120 degrees in one direction whilst C_C provides phase shift of 120 degrees in another direction. Therefore, when these two operators are combined, the resultant phase shift is equal to 0 degrees, which is also realised by implementing C_A.

Also, note that:

$$C_C \cdot C_C \cdot C_C = C_B \cdot C_C = I = C_A \tag{23}$$

$$\boldsymbol{C}_B \cdot \boldsymbol{C}_B \cdot \boldsymbol{C}_B = \boldsymbol{C}_C \cdot \boldsymbol{C}_B = \boldsymbol{I} = \boldsymbol{C}_A \tag{24}$$

This property can be explained from physical interpretation in that if 3 consecutive rotations of 120 degrees are applied, then this results in a full-circle rotation of 360 degrees which is equivalent to 0 degrees.

Due to the fact that matrix multiplication is associative, equivalent single switch positions can be obtained for any finite number of interconnected phase PSs, as exemplified below:

$$\boldsymbol{C}_C \cdot \boldsymbol{C}_A \cdot \boldsymbol{C}_B \cdot \boldsymbol{C}_B = (\boldsymbol{C}_C \cdot \boldsymbol{C}_A) \cdot (\boldsymbol{C}_B \cdot \boldsymbol{C}_B) = \boldsymbol{C}_C \cdot \boldsymbol{C}_C = \boldsymbol{C}_B \tag{25}$$

3.1.8 Feeder Switch Position

The term "feeder switch position" is used throughout this thesis to describe a unique combination of PS switch positions for a specific PS placement realisation. To illustrate this point, the example network from Fig. 9 is shown below in two unique feeder switch positions:
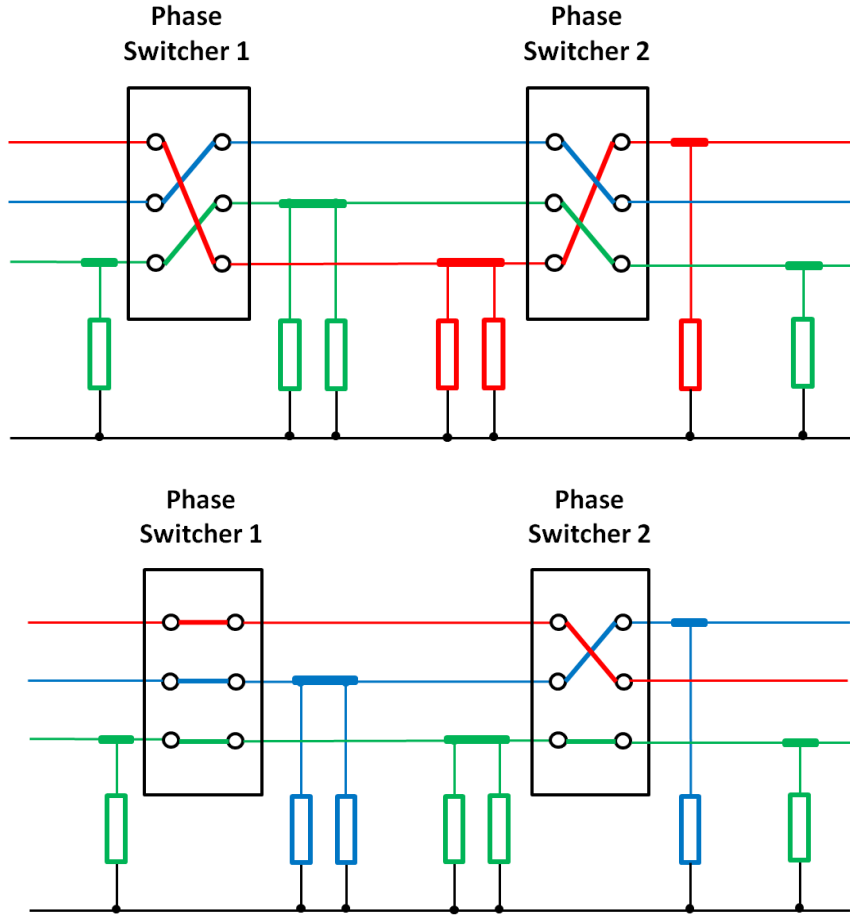
Fig. 13 Two Unique Feeder Switch Positions of the Example Network shown in Fig. 9

The number of feeder switch positions expressed as x_f, can be calculated from the number of allowable switch positions denoted by s and the quantity of PSs deployed represented by n_s on the feeder by applying the following equation:

$$x_f = s^{n_s} \qquad (26)$$

Where s is three for the constrained PS and six for the unconstrained PS.

Taking a particular example of a network with 2 constrained PSs, the resulting number of possible switch position combinations is equal to 9 which are shown in Table 5.

Ca,Ca	Cb,Ca	Cc,Ca
Ca,Cb	Cb,Cb	Cc,Cb
Ca,Cc	Cb,Cc	Cc,Cc

Table 5 All possible PS Combinations of 2 constrained PSs

Observing Table 5 it is clear that each feeder switch position is characterised by two switch configuration matrices ordered in a manner that reflects the physical location of the corresponding PSs on the LV feeder. In general, for the case of n_s PSs installed at fixed locations on the network, the particular feeder switch positions are described by the n_s-tuple object X structured as follows:

$$X\left(\boldsymbol{X}_{1,} \boldsymbol{X}_2 ..., \boldsymbol{X}_k\right)$$ (27)

Where $\boldsymbol{X}_j$ is the switch configuration matrix corresponding to the jth PS installed on the network. As already mentioned, the convention used in this thesis is that the order of the PSs is imposed according to their proximity to the reference substation end of the feeder.

Note that the "straight through" configuration is the default state of a feeder without PSs which can be represented as the following, rather simple, feeder switch position:

$$X\left(\boldsymbol{I}, \boldsymbol{I} ..., \boldsymbol{I}\right)$$ (28)

The straight through configuration is denoted as X^1 for the remainder of the thesis and is one of x_f possible realisations. The set containing all the permitted feeder switch positions is denoted as:

$$\left\{X_i\right\}_{i=1}^{x_f}$$ (29)

In order to fully characterise a given feeder switch position it would be necessary to also specify the locations at which the PSs are installed. Such additional information can be incorporated into the extended $2n_s$-tuple object denoted as X^*:

$$X^*(\boldsymbol{X}_1, l_1, \boldsymbol{X}_2, l_2, \dots, \boldsymbol{X}_k, l_k) \tag{30}$$

The additional n_s elements of X^* refer to specific locations where the PSs are installed.

3.1.9 Calculating the Phase Allocation Matrix for a Feeder with Phase Switchers

The calculation of phase allocations for any load connected to a substation via n_s PSs can be mathematically computed by cross-multiplying the intermediate switch configuration matrices. For the particular case where switch positions are constrained to the three that respect phase rotation, the cross-multiplication of n_s matrices will result in a single phase configuration matrix that is one of the three that respect phase rotation. Therefore, for any radial network of any topology, and with any number of PSs, all of which are assumed to respect phase rotation, loads in each segment can be thought of as connected directly to the substation via a single phase PS that respects phase rotation.

The resultant phase allocation matrix $\boldsymbol{P}_b^*$ for any feeder switch position can be found by computing n_s+1 partitioned block elements $\boldsymbol{P}_{b,n_s}$ that reflect each segment as follows:

$$\boldsymbol{P}_{b,n_s}^* = \left[\prod_{j=0}^{n_s} \boldsymbol{X}_j \right] \boldsymbol{P}_{b,n_s} \tag{31}$$

Where $\boldsymbol{X}_0$ is the switch configuration matrix of the PS located nearest to the transformer designated as the reference. However, when a PS is not located next to the secondary transformer which is assumed in this thesis, $\boldsymbol{X}_0$ is equal to the identity matrix $\boldsymbol{I}$. The phase allocation matrix can then be simply constructed from the resultant partitioned block elements as shown below:

$$\boldsymbol{P}_b^* = \begin{bmatrix} \boldsymbol{P}_{b,1}^* & \boldsymbol{P}_{b,2}^* & \cdots & \boldsymbol{P}_{b,(n_s+1)}^* \end{bmatrix} \tag{32}$$

Where $n_s + 1$ is the number of segments.

A phase mapping matrix can be constructed which is denoted as M and is constructed as follows:

$$M = [\begin{matrix} I & X_1 & X_1 \cdot X_2 & ... & \prod_{i=1}^{n_s} X_i \end{matrix}] \tag{33}$$

Where X denotes the configuration matrix that corresponds to the ith phase PS in the network. This matrix has 3 rows and $3(n_s + 1)$ columns where n_s is the number of PSs and $(n_s + 1)$ is the number of segments. Therefore, the phase mapping matrix is composed of block elements each of which refers the phase connection information of the aggregate segment loads to the reference segment. Since it is assumed that there is no PS between the substation and the first segment, which is also the reference segment, the first block element in the phase mapping matrix is the identity 3-by-3 matrix.

In this thesis it is determined that the cable constituting the thermal hot spot of the feeder is located in the segment next to the substation. However, the methodology reported in the thesis can be readily generalised to the cases where cables located in other segments are considered to be the thermal hot spot. In the case of a radial network for which the thermal hot spot is not in the first but in the jth segment away from the substation, the corresponding phase mapping matrix is given as:

$$M = [\begin{matrix} 0^{3 \times 3(j-1)} & I^{3 \times 3} & X_j & X_j \cdot X_{j+1} & ... & \prod_{i=j}^{n_s} X_i \end{matrix}] \tag{34}$$

Where N is the number of segments and is equal to $n_s + 1$. Note that the first $j - 1$ block elements of the phase mapping matrix are equal to zero to reflect the fact that the realisations of the PSs located upstream from the reference segment do not affect the phase currents in the reference segment.

In order to explicitly provide information related to the number of PSs in a given network and their particular switch positions, the phase mapping matrix can be denoted as $M(X_1, X_2, X_3, ..., X_{n_s})$. Therefore, $M(C_A, C_A, C_A)$ is an example of the phase mapping matrix for a network that is comprised of 3 PSs, all of which are in the straight through configuration.

In this thesis a simulated radial network is used to demonstrate the benefits of employing PSs. However, PSs can also be applied to interconnected networks. For such networks the product of the switch configuration matrices of the PSs that are placed on a path connecting adjacent substations must be equal to the identity matrix (straight through configuration) to ensure that the phase connections between transformers match, otherwise a line to line fault would be encountered. This can be represented as a constraint that applies to interconnected networks as follows:

$$\prod_{i=1}^{n_s} X_i = I \tag{35}$$

Where n_s denotes the number of PSs that interconnect adjacent substations.

Constraint (35) reduces the number of permitted switch positions to a third, assuming phase rotation is respected. The following figure gives the example of when 2 PSs are deployed:
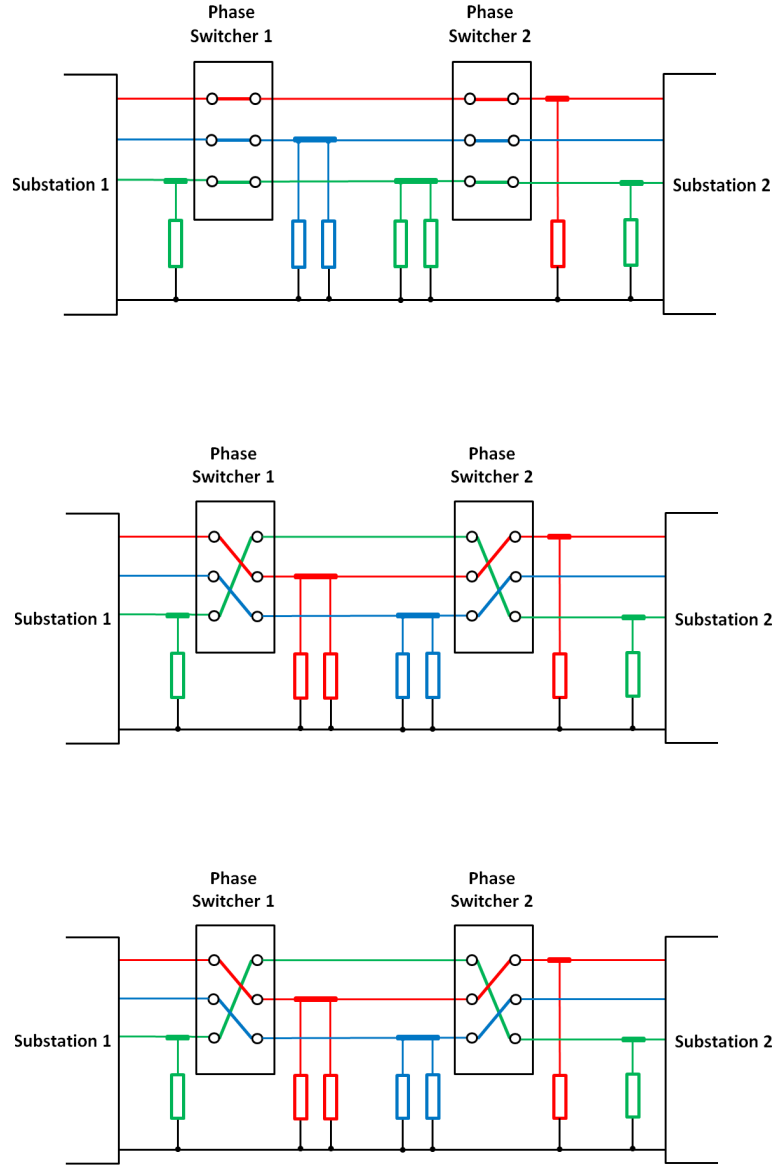
Fig. 14 Valid feeder switch positions that maintain constraint (35)

Constraint (35) reduces the number of possible combinations from 9 to 3, which are: $M(C_A, C_A)$, $M(C_B, C_C)$ and $M(C_C, C_B)$.

4 Network Modelling

This section details the methodology used to model the example feeder and how it was validated using data from the real network. The example feeder used in this thesis to show the impact that PSs have on unlocking cable current and maximising PV penetration is shown below.
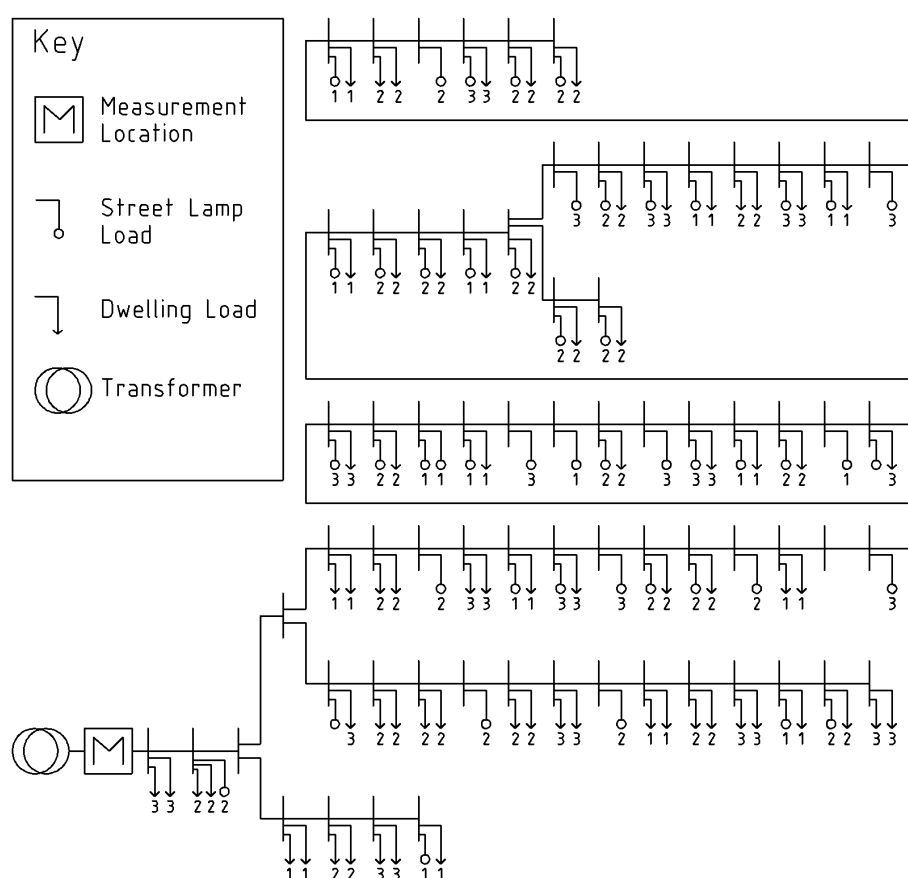
Fig. 15 Example LV Feeder

This network is the subject of a DNO monitoring trial [70] which enabled the model of it to be validated by comparing the data it generated in simulation with real measured values. The real values consist of five minute mean measurements for phase and neutral conductor currents, and phase to ground voltages taken at the location highlighted in Fig. 15.

This section discusses modelling decisions that were made and goes on to detail how the real measured data was used to validate the model.

4.0.1 Power Flow Analyser

OpenDSS [26] was selected as the power flow analyser as it is capable of unbalanced three phase power flow which is required to simulate the impact of PSs. OpenDSS is a state of the art power flow analyser with a convenient com interface to MATLAB which is a powerful data analysis tools. Moreover, OpenDSS is open source and can be driven over the com interface by Python which itself is open source therefore, there is no commercial obstacle to researchers who may wish to extend this research by applying the same methodology.

4.0.1.1 The Simulation Process Using MATLAB and OpenDSS

The process that was used to simulate PSs when employed on the example feeder is provided in this section. The flow chart shown in Fig. 16 details the process that was repeated for every discrete time interval where, functions carried out by MATLAB and OpenDSS are highlighted with numbered blue and red arrows respectively that are executed chronologically and fully defined in Table 6.
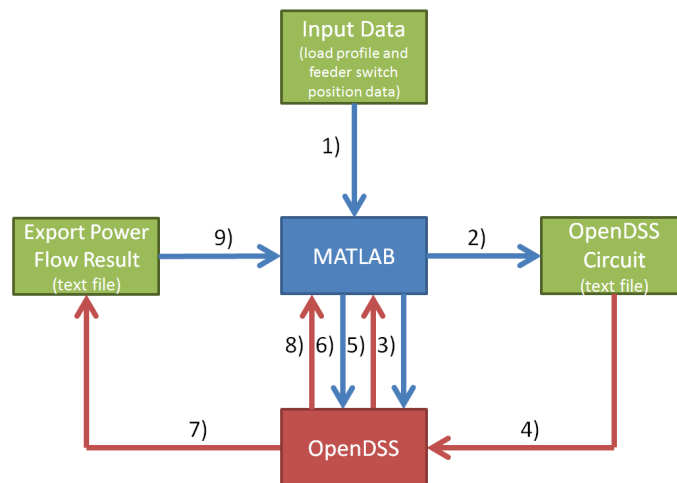
Fig. 16 MATLAB and OpenDSS Power Flow Snapshot Simulation

ID	Definition
1)	MATLAB loads the input data for the discrete time sample into the workspace.
2)	MATLAB creates a text file containing the OpenDSS script describing the example feeder at the discrete time sample which incorporates the following input data: • Feeder switch position (used to set the line connections at PS locations). • Load profile data.
3)	Matlab instructs OpenDSS via com interface to compile and solve the circuit defined in the text file in snapshot mode.
4)	OpenDSS solves the circuit defined in text file in snapshot mode.
5)	OpenDSS confirms solution as complete to MATLAB via com interface.
6)	MATLAB instructs OpenDSS via com interface to export circuit solution data to a text file.
7)	OpenDSS exports data to a text file.
8)	OpenDSS confirms data export as complete to MATLAB via com interface.
9)	MATLAB imports data to workspace.
10)	Repeat from 1) until all time samples have been evaluated.

Table 6: MATLAB and OpenDSS Power Flow Snapshot Simulation

4.0.2 Loads

Each load in the example feeder model was configured as a constant power load with a pf of 0.97 to match the measured local aggregate from [20]. Unique load profiles were generated using [15] for each dwelling in the example feeder and used as inputs for power flow simulations documented in this thesis. Two example load profiles which were generated from [15] are provided in the following figure:
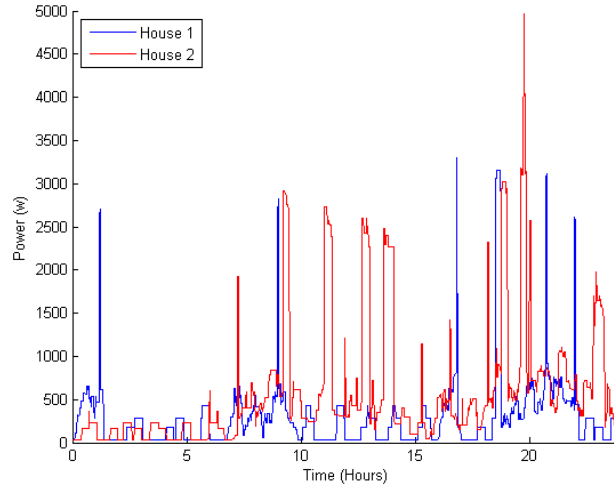
Fig. 17 Two unique synthetic load profiles created for an occupancy level of three persons using [15]

The most common type of dwelling in the network was found to be the two bedroom house, and as data on the occupancy level of each dwelling was not available, it was assumed that each dwelling was occupied by three people. To provide the reader with an indication of the impact of this assumption, the example feeder was surveyed using google street view where it was found to actually consist of: two, three, four bedroom houses and, one and two bedroom flats.

4.0.3 Photo Voltaic Generators

PV was modelled as a negative constant power load with a unity pf driven by synthetic PV profiles obtained from [16] for the month of the year relevant to the simulation. The same PV profile was used for each dwelling considered to have an active PV installation to replicate it's synchronous local behaviour. The power rating 3.8kW was assumed for all dwellings with active PV installations as this is the maximum value permitted without consent in the G83 engineering recommendations [18].

4.0.4 Cables

The resistance $\boldsymbol{R}$, inductive reactance $\boldsymbol{X}$ and capacitance $\dot{\boldsymbol{C}}$ matrices were used to specify the cable parameters in OpenDSS and were constructed as follows:

$$\boldsymbol{R} = \begin{bmatrix} R_s & R_m & R_m & R_m \\ R_m & R_s & R_m & R_m \\ R_m & R_m & R_s & R_m \\ R_m & R_m & R_m & R_s \end{bmatrix}, \; \boldsymbol{X} = \begin{bmatrix} X_s & X_m & X_m & X_m \\ X_m & X_s & X_m & X_m \\ X_m & X_m & X_s & X_m \\ X_m & X_m & X_m & X_s \end{bmatrix}, \; \dot{\boldsymbol{C}} = \begin{bmatrix} C_g & C_c & C_c & C_c \\ C_c & C_g & C_c & C_c \\ C_c & C_c & C_g & C_c \\ C_c & C_c & C_c & C_g \end{bmatrix} \quad (36)$$

Since the cable lengths in the example feeder were short, sequence component data that was obtained from a DNO was used to find the matrix elements as shown in (36) through the application of the equation outlined below [38].

$$R_s = \frac{(2R_1 + R_0)}{3}, \; R_m = \frac{(R_0 - R_1)}{3}, \; X_s = \frac{(2X_1 + X_0)}{3}, \; X_m = \frac{(X_0 - X_1)}{3} \quad (37)$$

Where the subscripts $s, m, 1$ and 0 denote the self, mutual, positive sequence and zero sequence components respectively. Conductor to conductor capacitance C_c was modelled by equating it to the positive sequence component whilst, conductor to ground capacitance was assumed to be negligible and set to zero as shown below.

$$C_c = C_1, \; C_g = 0 \quad (38)$$

Approximation of cable properties from sequence component data is inevitable due to the sparsity of data held by DNO's, a fact noted by Thomson and Infield in [22] who also reported the sensitivity of such approximations to network nodal voltages to be insignificant. Most cables detailed in the DNO data obtained for the example feeder have four conductors but of those that had three, the specific electrical properties of the neutral conductor were not included. Therefore, all cables were modelled incorporating the assumption that the phase and neutral conductors have equivalent electrical properties.

Excluding service cables which were not modelled due to the negligible impact of PSs on their neutral currents, the example feeder was found to contain 5 unique cable types, the longest and shortest of which were 262m and 1m respectively and the mean

length was 14.6m. The conductor sizes and the corresponding parameters used to model the cables is provided in the table below:

Conductor Size	Parameters *(Resistance, Reactance, Capacitance)* $\left(\Omega/km,\ \Omega/km,\ nF/km\right)$
70mm^2	$R_s{=}0.6916,\ R_m{=}0.3483,\ X_s{=}0.0908,\ X_m{=}0.0166,$ $C_c{=}0.00011,\ C_s{=}0$
0.6in$^2{\approx}$38.7mm^2	$R_s{=}0.7813,\ R_m{=}0.3246,\ X_s{=}0.0664,\ X_m{=}0.0134,$ $C_c{=}0.00013,\ C_s{=}0$
35mm^2	$R_s{=}0.6393,\ R_m{=}0.4380,\ X_s{=}0.1625,\ X_m{=}0.0194,$ $C_c{=}0.00008,\ C_s{=}0$
0.1in$^2{\approx}$70mm^2	$R_s{=}0.6916,\ R_m{=}0.3483,\ X_s{=}0.0908,\ X_m{=}0.0166,$ $C_c{=}0.00011,\ C_s{=}0$
0.4in$^2{=}$322.58 0.4in$^2{\approx}$300mm^2	$R_s{=}5783,\ R_m{=}0.3903,\ X_s{=}0.1146,\ X_m{=}0.0137,$ $C_c{=}0.00012,\ C_s{=}0$

Table 7: Example feeder cable parameters

4.0.5 Single Phase Voltage Sources

Single phase voltage sources were used to model grid connections at the head of the feeder, this was primarily done for validation as it enabled the real world measurements to be precisely applied as an inputs, this is described in section 4.2.

4.0.6 Phase Connection Data

The DNO GIS data of the example feeder included the phase connection information for 76% of dwellings and street lamps. When $\dot{p}$ is the measured average real phase power of the feeder over 24 hours and j is the phase integer, the remaining 24% were randomly allocated whilst satisfying the following relationships:

$$\frac{\dot{p}_j}{\dot{p}_1+\dot{p}_2+\dot{p}_3} \approx \frac{\sum_{i=1}^{n}{}^{d}\boldsymbol{P}_{b,[j,i]}}{\sum_{i=1}^{n}{}^{d}\boldsymbol{P}_{b,[1,i]}+\sum_{i=1}^{n}{}^{d}\boldsymbol{P}_{b,[2,i]}+\sum_{i=1}^{h}{}^{d}\boldsymbol{P}_{b,[3,i]}} \tag{39}$$

$$\frac{\dot{p}_j}{\dot{p}_1 + \dot{p}_2 + \dot{p}_3} \approx \frac{\displaystyle\sum_{i=1}^{n} {}^{s}\boldsymbol{P}_{b,[j,i]}}{\displaystyle\sum_{i=1}^{n} {}^{s}\boldsymbol{P}_{b,[1,i]} + \sum_{i=1}^{n} {}^{s}\boldsymbol{P}_{b,[2,i]} + \sum_{i=1}^{n} {}^{s}\boldsymbol{P}_{b,[3,i]}} \tag{40}$$

Where n is the number of feeder buses and the phase allocation matrices are represented by ${}^{d}\boldsymbol{P}_b$ and ${}^{s}\boldsymbol{P}_b$ for dwellings and street lamps respectively.

4.1 Simulation Sample Period

The simulation sample period was chosen so that simulations could evaluate the impact of phase PSs on the variables of interest, namely: phase to neutral voltage and cable cable current. This section details how these variables are assessed in the real world and how this resulted in the selection of a 5min simulation sample period.

4.1.1 Phase to neutral Voltage

DNO's are responsible for feeder phase to neutral voltages which is represented here by the variable V and mandated to stay below 253V by the ESQCR [8]. The term OV is used in this thesis to describe the condition when the phase to neutral voltage exceeds 253V as shown below:

$$V_f \geqslant 253 \tag{41}$$

Where f represents the bus address.

BS50160 [9] sets out the requirements of how supply voltage voltage variations should be measured to determine compliance with the ESQCR [8]. The BS states that 95% of 10min mean r.m.s values of U_n in a period of a week should be equal to or less than 253V.

The term "phase to neutral voltage" is abreviated to "bus voltage" for the remainder of this thesis.

4.1.2 Ampacity

BSIEC60287 [71] is the standard that defines the calculation for a cable's current carrying capacity, otherwise known as ampacity, this variable is an expression of the permissible current rating in a cable's phase condyuctor and is represented by the variable I.

4.1.3 Conclusion

A literature review uncovered a recent relevant study conducted by Navarro et al. [25] which examined the sensitivity of data granularity in the detection of OV events, it was found that a 60min period significantly underestimates occurrences by 11% when compared to 5mins.

Of the two aforementioned variables, it is the bus voltage that sets the minimum requirement of 10mins for the simulation sample period in order to detect OV, because the consequence of a longer period would render simulations incapable of detecting OVs. Therefore, owing to the minimum requirement imposed by BS50160 [9], a 5min simulation sample period was chosen as it allows simple conversion to a 10min period to test compliance with the BS, whilst also being substantiated in recently published literature.

4.2 Model Validation

This section first describes some real network data measured and recorded on the example feeder then, how it was used to validate the OpenDSS model.

The real network data was logged as part of the DNO project [20], it consists of 5min mean r.m.s. measurements of voltages and currents taken at the location highlighted in Fig. 15 on Thursday 1st November 2012 and is shown below:
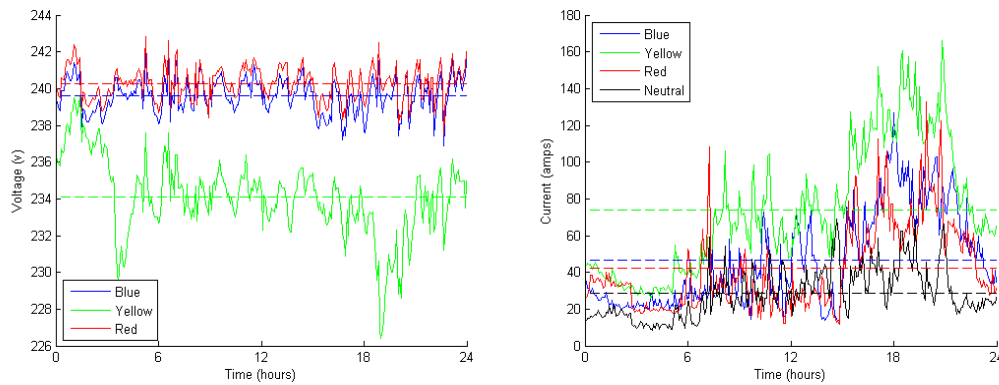
Fig. 18

Left: *Real Feeder bus voltage Data* **Right:** *Real Feeder Current Data*

Dotted lines indicate 24 hour mean values

Validation of the OpenDSS model was performed by comparing data it generated in simulation when load profiles for a weekday in November and the real measured voltage data were used as an inputs. The real voltage data was used to replicate as precisely as possible the conditions in the real network, although it should be noted that the implied underlying assumption here is that any imbalance in the connection of loads to phases has a negligible impact on phase voltages and that voltage unbalance is inherited entirely from the HV network.

Data obtained from the OpenDSS model validation simulation alongside the real measured data is presented in the following figure:
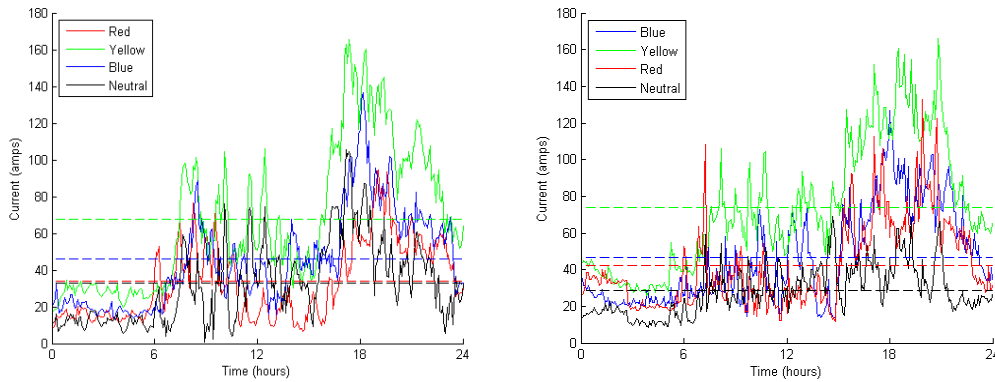
Fig. 19

Left: *OpenDSS Model Simulated Feeder Current Data* **Right:** *Real Feeder Current Data*

Dotted lines indicate 24 hour mean values

The two data sets are not identical and this was expected due to the natural variation, or diversity in the behaviour of people activating loads day to day. The average values of both data sets are represented in the figures by dotted lines and are shown to be similar. The maximum difference in the average values was found on the Red phase which was approximately 5 amps. The synthetic data set assumed that each house was populated by three persons, which in reality is not the case, this variation could account for the small difference in the average current values. Another significant difference can be identified in the neutral currents between 17.00 and 18.00, where, in the simulation there is a spike which is absent from the real data set. Inspection of the phase currents in the simulated data reveals that this is attributed to the low red phase current during this period. Therefore, the variations between the two data sets identified in Fig. 19 can be accounted for by differences between the synthetic and real load profiles, which could be attributed to the natural differences in human behaviour from day to day.

The corresponding real and simulated phase current trends are provided in the following figure:
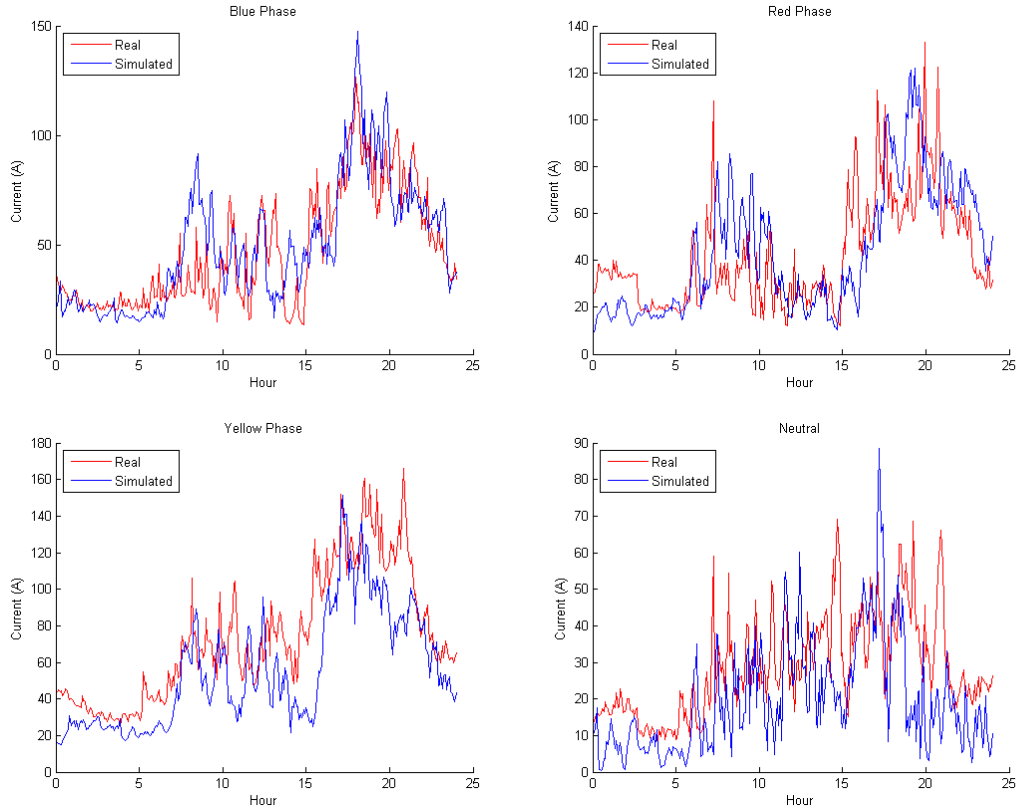
Fig. 20 Real and Simulated Conductor Currents from the Example Network

A comparison of each of the trends shown in Fig. 20 relative to each other is provided in Table 8 where the real data is shown as being very similar to the simulated data. Out of the 6 comparisons, 4 have an error of 2.1% or less, which provides assurance that the balance of loads to phases in the simulated network is close to that of the real network. Also, this provides confidence that the assumption applied of 3 persons per dwelling is reasonable.

	Real Network Data	Simulated Network Data
$I_r > I_y$	6.60%	6.60%
$I_r > I_b$	36.50%	36.40%
$I_y > I_b$	96.5%	68.06%
$I_n > I_b$	16.32%	8.3%
$I_n > I_r$	22.20%	19.10%
$I_n > I_y$	0.69%%	1.74%

Table 8: Real and Simulated Current Data Statistics

The validation was limited to the measurements that were available at the time of writing and would be improved by comparing simulated bus voltages with real data. However, the two current data sets that it has been possible to compare are similar enough for the model to be considered as validated.

5 Unlocking Cable Current Through Phase Reconfiguration - Methodology

This chapter sets out the sensing and communication requirements of a PS system, details how the thermal hot spot of a feeder can be identified, shows some methods used in this thesis to place PSs, and, highlights how simulations documented here differ from the real world activity. Also, an outline of the optimisation problem for minimising cable current and cable losses is provided, which is followed by some novel 'scheduled control algorithms' and 'dynamic control algorithms' that are suitable for implementation on a PS scheme. The scheduled algorithms correct baseline phase current unbalances, whereas the dynamic algorithms correct temporal current unbalances caused by the activation and deactivation of devices over 5min intervals.

5.1 Sensing and Communication Requirements of a Phase Switcher System

All control algorithms documented in this thesis are intended for PS schemes that are deployed on LV feeders, to illustrate the sensing and communication requirement of the system a simple example network adopting a particular switch position is provided below:
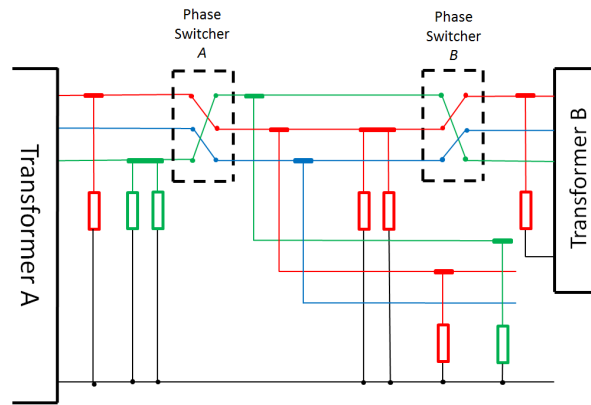
Fig. 21 An Illustrative Example of a PS deployment adopting a particular switch position.

The sensing requirements of the PS system pictured above depends on the control algorithm applied. All of those that are detailed in this thesis require every load as an

input except for the simple model based controller documented in section 5.7. This control algorithm requires phase current measurements at supplying transformers and at each PSs only. The communication requirement applies to the causal dynamic controllers only that are discussed in detail later in this section, they require that all inputs can communicate to a centralised controller.

5.2 Hot Spot Identification

Before applying PSs to unlock the cable current an initial exercise was conducted that involved the identification of the cable within the feeder with the least amount of cable current headroom. This particular cable is referred to as the hot spot, it is that which is likely to experience thermal overload in the event of a fault or increased load. The hot spot represents the region of interest that the controller focuses on to rebalance phase currents and, therefore, unlock cable current headroom. Below the method used for identifying the feeder hot spot is outlined.

Cable current headroom is a cable's rated ampacity multiplied by 3 which is denoted by a, subtracted from the sum of phase and neutral conductor currents that is carried within it which is represented by i as shown below:

$$(a - i) \tag{42}$$

When the cable current ratings and phase currents are arranged into row vectors whose elements correspond to specific cables, the feeder hot spot scaler h identifies the index of the cable classified as the hot spot as shown in the equation below.

$$h = arg\ min\ (a - _{24h}i) \tag{43}$$

Where $_{24h}i$ is a row vector whose elements are the sum of average daily phase and neutral conductor currents for all cables in a feeder, and a is a similar row vector whose elements are the corresponding ampacity ratings multiplied by 3.

5.3 The Placement of Phase Switchers in the Example Feeder

This section documents two metrics that can be used to identify some optimal locations on a feeder for PSs. A commentary is first provided which outlines how to calculate the total number of possible realisations of the network for a given number of PSs. This is followed by a description of the "Modulus Unbalance Correction" and "Cumulative Sum" methods. Finally, a commentary on how the results from both methods were processed to determine the fixed locations of PS placements used in chapters 6 and 7 is detailed.

5.3.1 Quantity of Unique Feeder Realisations Enabled by PS

There is a finite number of unique network realisations, therefore also phase connection matrices $\boldsymbol{P}_b$, for a particular feeder when the reference branch is designated and the number of PSs to be deployed on it is predetermined. The total number phase connection matrices is the number of PS placement possibilities which is found by evaluating the binomial equation, multiplied by the number of feeder switch positions. Therefore, the total number of phase connection matrix possibilities denoted as c is found by applying the equation below.

$$c = x_f \times \frac{n!}{n_s!(n - n_s!)} \tag{44}$$

Where n is the number of buses on the reference branch of the feeder, n_s is the number of PSs and x_f is the number of feeder switch positions as defined in (26).

5.3.2 The Modulus Unbalance Correction Method

Each unique phase connection matrix is denoted as $^j\boldsymbol{P}_b$ where j is an exclusive address integer that spans the range $1 \leq j \leq c$. The modulus unbalanced correction method evaluates the addressed PS matrices to form the quality measurement row vector $\boldsymbol{q}_L$ which contains c elements that are a measure of load balance for the specific PS placement and feeder switch position with the corresponding address j and found by applying the following equation:

$$q_{L_j} = \left| \sum_{i=1}^{n_r} {}^j P_{b,[1,i]} - \sum_{i=1}^{n_r} {}^j P_{b,[2,i]} \right| + \left| \sum_{i=1}^{n_r} {}^j P_{b,[1,i]} - \sum_{i=1}^{n_r} {}^j P_{b,[3,i]} \right| + \left| \sum_{i=1}^{n_r} {}^j P_{b,[2,i]} - \sum_{i=1}^{n_r} {}^j P_{b,[3,i]} \right| \quad (45)$$

Where n_r is the number of buses on the reference branch. The method finds PS placements that achieve optimum load balance that are the minimum arguments of q_L as stored in the elements of vector j_L as shown in the equation below.

$$j_L = arg\ min\ (q_L) \quad (46)$$

Where, all elements of j_L have a unique associated set of optimum PS placements and feeder switch positions.

5.3.3 The Cumulative Sum Method

The Cumulative Sum Method finds PS placements, it's objective function attempts to equally split devices into the feeder segments that PSs create.

The phase connection matrix ${}^I P_b$ where the leading superscript I denotes it as the straight through configuration, is used to calculate the phase reference scalers p_r for each phase as defined in the following equation:

$$p_{r1} = \left(\frac{\sum_{i=1}^{n_r} {}^I P_{b,[1,i]}}{(n_s+1)} \right), \ p_{r2} = \left(\frac{\sum_{i=1}^{n_r} {}^I P_{b,[2,i]}}{(n_s+1)} \right), \ p_{r3} = \left(\frac{\sum_{i=1}^{n_r} {}^I P_{b,[3,i]}}{(n_s+1)} \right) \quad (47)$$

Where n_r is the number of buses on the reference branch of the feeder and n_s is the number of PSs. A new phase reference column vector is next established as follows:

$$p_r = \begin{bmatrix} p_{r1} \\ p_{r2} \\ p_{r3} \end{bmatrix} \quad (48)$$

Then, using the straight through phase connection matrix, c addressed segment phase connection matrices from (9) denoted as ${}^{j}\boldsymbol{P}_{s}$ are found, where j is an exclusive address integer that spans the range $1 \le j \le c$. Each realisation of ${}^{j}\boldsymbol{P}_{s}$ has a unique combination of PS placements and feeder switch positions which are associated with j. Each column of the segment phase connection matrix is denoted as vector $\boldsymbol{p}_{z}$, where z specifies the column of the segment phase connection matrix. Then the equation below is applied to create the $1 \times c$ row vector $\boldsymbol{q}_{s}$ whose elements are measures of load balance for the specific PS placements and feeder switch positions with the corresponding address j.

$$\boldsymbol{q}_{s,[j]} = \left| \sum_{i=1}^{3} \left(\boldsymbol{p}_{r,[i]} - \boldsymbol{p}_{1,[i]} \right) \right| + \left| \sum_{i=1}^{3} \left(\boldsymbol{p}_{r,[i]} - \boldsymbol{p}_{2,[i]} \right) \right| \ldots + \ldots \left| \sum_{i=1}^{3} \left(\boldsymbol{p}_{r,[i]} - \boldsymbol{p}_{n_s+1,[i]} \right) \right| \tag{49}$$

Where n_{s} is the number of PSs and j is an integer over the range $1 \le j \le c$ and c is the total number of phase connection matrix possibilities. Finally, the method measures the feeder load balance using vector $\boldsymbol{j}_{s}$ whose elements are the minimum arguments of $\boldsymbol{q}_{s}$ as shown in the equation below.

$$j_{s} = arg\ min\left(\boldsymbol{q}_{s}\right) \tag{50}$$

Where the indexes of $\boldsymbol{j}_{s}$ have addresses with associated PS placements and feeder switch positions.

5.3.4 The selection of Fixed Optimum Placements

The number of PSs implemented on a scheme has a direct impact on its cost and the benefit that it can realise. Also, as noted in chapter 2, the quantity of switching devices has a significant impact on the complexity of the optimisation problem, this was illustrated in Fig. 6. To ensure that PS schemes are cost effective and benefit from the reduction in complexity that PSs can facilitate, it is desirable that their quantity is minimised. This chapter focuses on the network of today, so to set the number of PSs deployed, it is appropriate that the economics of today should be applied. However, PSs do not currently exist making a cost analysis of their implementation difficult, so their quantity was set by making the judgement that follows. Once the PS device is estab-

lished, two PSs deployed on the example feeder is expected to be cost effective when compared to alternatives such as replacing cables or installing on load tap changing transformers.

Both the methods outlined in section 5.3.2 and 5.3.3 will find many optimum results and their quantity can be reduced by eliminating PS placements that are not the same. A designer can then be provided with the optimum placements that remain, which are significantly reduced in number, and select the most suitable locations whilst taking into account any relevant associated practicalities. The specific two placements were selected that split the feeder into three approximately similar segments, their locations are shown in the figure of the example feeder below.
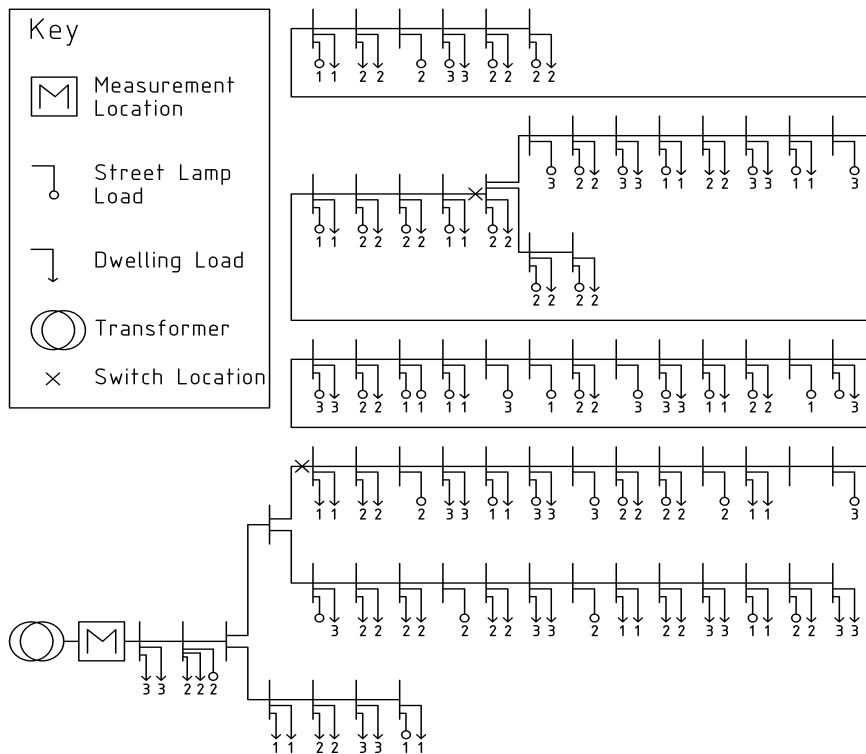
Fig. 22 example feeder Network with Phase Switcher Locations

5.4 Simulation versus Real World

Before the optimisation problem and control algorithms are explained in detail, a fundamental difference between what is simulated in this thesis and the real world re-

quires explanation. The difference is caused by a 'quirk' embedded in the synthetic load profiles [15] which require an occupancy level to be specified for every dwelling, this is an approximation as discussed in chapter 4. However, the difference is not due to the approximation, it is due to changing the month or weekend/weekday parameter in the load profile generator. Each time either of these things is changed, the synthetic profile produced assumes a new occupant behaviour pattern, which, when compared to reality, would be like occupants moving out of a dwelling and new occupants moving in. This is a fundamental difference and has to be understood in order that the results documented in chapter 6 are reviewed in context. The impact of this is seen in the scheduled control algorithm results where different feeder switch positions are sometimes identified for different months or at weekend or on weekdays. It is therefore important to note what the scheduled control algorithm results are used for in this thesis which is outlined as below:

- To show how PS schedules are developed for particular devices (present day dwelling loads and street lamps are used in this thesis).

- To provide a fair benchmark for comparison with the dynamic control algorithms which are not impacted by month or weekend/weekday parameters changes.

- To indicate what impact rejointing phase conductors would have on the present day network.

5.5   The Optimisation Problem

This section introduces general features and notation that relate to an optimisation problem that is modified and utilised by each of the control algorithms considered in section 5.6.

When $\check{X}$ is the optimal feeder switch position setting and k represents the discrete sampling instant, the optimisation problem is described mathematically as follows:

$$\check{X}_k = arg \min_{\{X_{i|k}\}_{i=1}^{x_f}} mean_{\Delta T} \left(Z_{i|k \to k+1} \right) \tag{51}$$

subject to:

$$Z_{i|k \to k+1} = f\left(X_{i|k}, \boldsymbol{P}_{b|k \to k+1} \right) \quad for \quad i = 1, 2, ..., x_f \tag{52}$$

As outlined in (51) the objective function of the optimisation problem is given as the mean value of the variable of interest, denoted here as Z, which in this thesis is assumed to be equal to either the total current in the hot spot of the feeder or to the total losses in the feeder.

The mean of the variable of interest is calculated over the time window designated as ΔT. This time window is either equal to 5mins, 24hours or to peak time (PT) period which takes place each day between 16:30 and 23:00 hours. The lagging subscript of the variable of interest consists of two parts. Firstly, index i that corresponds to a particular feeder switch position. Inclusion of this index highlights the fact that the value of Z is dependent on the feeder switch position realisation. The second part of the lagging subscript highlights the fact that the variable of interest is provided over the time window of length given by ΔT that begins at the current sample instant k and finishes at the future instant $k+1$.

Equation (52) mathematically describes the network model used to evaluate the impact that the ith feeder switch position has on the variable of interest for a given time window of load profiles, which are provided. This function is expressed here in a general form indicating only its input and output variables. This was done intentionally to ensure generality of the discussion and the applicability of the methodology proposed

here to any network model that could be feasibly utilised today either during offline analysis or real-time implementation.

The solution of the optimisation problem is expressed as an n_s-tuple object denoted as $\check{X}$ which describes the optimal feeder switch position that minimises the objective function, which itself is given as the mean value of the variable of interest, as shown in (51).

Generally, it is assumed that the optimisation is solved by performing exhaustive search for all possible feeder switch positions. Due to the small number of used PSs, however, the computational burden associated with the optimisation problem is significantly reduced and deemed to be solvable for most realistic cases either during offline analysis or even in real-time. Such reduction in complexity is even more pronounced if the phase rotation assumption is imposed.

5.6 The Phase Switcher Control Algorithms

This section introduces various control algorithms all of which are based on the optimisation problem described in section 5.5. Firstly, the so-called scheduled control algorithms are considered in subsection 5.6.1. These algorithms are assumed to be executed during offline analysis rather than in real-time. Subsection 5.6.2 considers dynamic control algorithms that are executed repetitively but that rely on a high-fidelity network model which, due to it's extensive communication requirement is economically infeasible for implementation today. Finally, subsection 5.7 details a control algorithm that relies on a very simple model of the network that is computationally and inexpensive. Also, due to the limited feedback it requires, it's sensing and communication needs are modest making it economically feasible for real-time implementation today.

5.6.1 Scheduled Control Algorithms

Scheduled control algorithms address unbalances associated with a particular device type, they can be implemented through the installation of PSs or by rejointing phase conductors. The advantage of implementing them using PSs is increased flexib-

ility, as, schedules can be established for specific device types (PVs and EVs for example) for implementation at predetermined times of day when the unbalances associated with them occur. Also, when unbalances develop over time due to dwellings becoming active/inactive or new dwelling development for example, the schedule can be modified accordingly. Whereas, implementation by rejointing has the advantage of being lower cost, it would be suitable for implementation on a feeder where a specific device type is known to cause an unbalance, and, there is confidence over how in future the network will evolve.

The scheduled control algorithms are intended as offline network analysis tools that assess the benefit of scheduled control on the total current and/or losses in the network. These algorithms are given in non-causal form and can be implemented offline using data collected from the network to find optimal feeder switch positions that balance baseline unbalances. The reason for naming this group of algorithms as scheduled, is that the feeder switch position found by the analysis can be scheduled at a time when the device or devices are peaking.

5.6.1.1 Scheduled Current Control Algorithms

Control algorithms presented in this sub-section aim to minimise the total current in the hot spot of a given network by determining the optimal feeder switch position.

The total current in the hot spot of the feeder is represented by the variable I_T and the control algorithm focuses on the minimisation of its daily average. The inputs required by the algorithm are the load profiles of every load for the 24 hour period over which the minimisation takes place. In other words, the load profiles are required 24hours ahead of time which defines the algorithm as non-causal because the output of the system depends on future inputs. The non-causal characteristic means that application of the algorithm would be implemented via an offline power flow analysis on feeders with consistent and predictable daily load profiles for the particular month and type of day, i.e. weekday or weekend. The algorithm performs the optimisation by evaluating every possible feeder switch position to find $\check{X}$ which represents the one

with the corresponding minimum value of I_T, this is mathematically represented as the following optimisation problem:

$$\check{X}_k = \arg \min_{\{X_i\}_{i=1}^{x_f}} mean_{24h}\left(I_{T,i|k \to k+1}\right) \qquad (53)$$

Subject to:

$$I_{T,i|k \to k+1} = f_I\left(X_{i|k \to k+1}, \boldsymbol{P}_b\right) \qquad for \quad i = 1, 2, ..., x_f \qquad (54)$$

This control algorithm is termed the daily scheduled current control algorithm. It is abbreviated to $_{24h}ICC_{k+1}$ with its leading subscript indicating that the total current is averaged over 24 hours. The lagging subscript indicating that the time window of load profile data considered in the optimisation starts at the current sample instant k and extends to the future sample instant $k+1$, thereby emphasising it's non-caual nature. The Abbreviation ICC stands for "ideal current controller" where the term 'ideal' indicates that the controller utilises a high-fidelity network model and power flow analyser with minimal, if any, inaccuracy.

A closely related controller that focuses on the total current in the hot spot of the network but only during the peak time is described using the following optimisation problem:

$$\check{X}_k = \arg \min_{\{X_i\}_{i=1}^{x_f}} mean_{PT}\left(I_{T,i|k \to k+1}\right) \qquad (55)$$

This optimisation is performed subject to the equality constraint, i.e. network model equation, that is identical to that used in the case of daily scheduled current control algorithm that is provided in (54). Note that the peak time period is assumed to take place daily from 16:30 until 23:00 hours. Once calculated, the optimal feeder switch position is then implemented for a full 24 hours. This controller is termed the peak time scheduled current control algorithm and is abbreviated to $_{PT}ICC_{k+1}$. Similarly to daily scheduled current control algorithm, this controller relies on ideal network model, described by (54) and considers load profiles during the future time window

starting at the current time sample and finishing at the future sample $k+1$. However, the leading subscript PT which stands for "peak time", its abbreviation indicates that this algorithm considers the average of the total current in the hot spot of the network during the peak time rather than 24 hour period.

5.6.1.2 Scheduled Losses Control Algorithms

Control algorithms presented in this subsection are very similar to those introduced in Subsection 5.6.1.1. The only difference is the choice of the key variable which comprises the objective function. Whilst the ICC control algorithms aim to minimise the total current in the hot spot of the network, algorithms considered in this subsection focus on the minimisation of the total real cable losses which is represented using the variable L_T.

Similarly to scheduled current control algorithms, the inputs required by the two cable losses algorithms presented below are the load profiles of every load over the time window period over which the minimisation takes place. Moreover, these algorithms differ only in terms of the over which the losses are considered in the optimisation problem.

Firstly, the control algorithm that focuses on the determination of the optimal feeder switch position that minimises the total cable losses in the network during the 24 hour period and is expressed as the following optimisation problem:

$$\check{X}_k = arg \min_{\{X_i\}_{i=1}^{x_f}} mean_{24h}\left(L_{T,i|k \to k+1}\right) \tag{56}$$

This controller is named the daily scheduled losses control algorithm and is abbreviated to $_{24h}ILC_{k+1}$. Note that ILC stands for "ideal losses controller" and is used for both controllers considered in this subsection to differentiate them from ICC control algorithms that focus on the total current instead.

Alternatively, a controller that determines optimal feeder switch position by considering the losses during peak time period only can be expressed as follows:

$$\check{X}_k = arg \min_{\{X_i\}_{i=1}^{x_f}} mean_{PT} \left(L_{T,i|k \to k+1} \right) \tag{57}$$

This controller is termed peak time scheduled losses control algorithm and is abbreviated to $_{PT}ILC_{k+1}$.

In both cases the model used to calculate the objective function, i.e. the average of the total losses, is identical and is expressed as:

$$L_{T,i|k \to k+1} = f_L \left(X_{i|k \to k+1}, P_{b,} \right) \qquad for \quad i = 1, 2, ..., x_f \tag{58}$$

Note that the function given in (58), which is used to calculate the total losses for a given load profile and feeder switch position, is different to (54). However, they both utilise the same input variables, namely feeder switch position and load profile, and may in reality be based on the same underlying simulation model of the network.

5.6.2 Dynamic Control Algorithms

This subsection introduces control algorithms that rely on the high fidelity model of the network but, unlike scheduled control algorithms, they repetitively execute and are therefore termed "dynamic" controllers. The inputs required for these controllers are the load profiles of every load over the time window period for which the minimisation is performed, which is identical to that of the scheduled control algorithms. However, the things that differentiate the dynamic from the scheduled control algorithms is the time window over which minimisation occurs, it is 5 mins for the dynamic algorithms and >5 mins for the scheduled algorithms. Also, there are causal and non-causal dynamic control algorithms, rather than just non-causal as is the case for the scheduled control algorithms. The non-causal algorithms are used as benchmark comparators against the causal algorithms to establish the improvement that could be made if predictive control techniques were adopted. It should also be noted that of the dynamic algorithms, the causal type only are suitable for real world application.

5.6.2.1 Non-causal ideal current controller

This control algorithm that is executed every 5 minutes to obtain an optimal feeder switch position that minimises the total current in the hot spot of the network can be mathematically represented as follows:

$$\check{X}_k = arg \min_{\{X_i\}_{i=1}^{x_f}} mean_{5m} \left(I_{T,i|k \to k+1} \right) \tag{59}$$

Subject to:

$$I_{T,i|k \to k+1} = f_I \left(X_{i|k \to k+1}, \boldsymbol{P}_b \right) \qquad for \quad i = 1, 2, ..., x_f \tag{60}$$

Notice great similarity of this formulation and that used to describe scheduled current control algorithms. In fact, the only difference between these algorithms is the sampling time, which in this case was chosen to be 5 minutes, though it can be changed with no impact on the underlying methodology employed. This level of similarity with scheduled control algorithms is also observed in the abbreviation of the controller described by (59) and (60) which is $_{5m}ICC_{k+1}$.

From a practical implementation perspective however, the optimisation problem shown so far in this section are not physically realisable in real-time. This is due to the fact that it violates the causality assumption. More specifically, the optimal feeder switch position is assumed to be implemented at the beginning of the time window over which the network model evaluations are performed. This is clearly not physically possible unless the future load profiles are assumed to be known in advance. Hence, the controller described in (59) and (60) is termed non-causal ideal dynamic current controller.

Nevertheless, this non-causal dynamic controller represents a useful benchmark in terms of the achievable performance against which other controllers can be assessed. More specifically, this particular controller delivers the optimal performance because it utilises the high-fidelity model which is identical to the actual controlled system. Use of a high-fidelity model coupled with the relaxation of the causality assumption allows the controller to evaluate impact of each possible PS position combination before it is actually applied.

5.6.2.2 Causal Ideal Current Controller

In order to ensure the causality the control algorithm considered in the previous subsection 5.6.2.1 can be modified by imposing a time delay in the implementation of the optimal feeder switch position. More specifically, by optimising the feeder switch position using the load profiles during the time window spanning from last sampling instant, denoted as $k-1$, to the current instant k and implementing it at the current time step the causality is ensured. Mathematically, the optimisation problem is given as follows:

$$\check{X}_k = arg\ \underset{\{X_i\}_{i=1}^{x_f}}{min}\ mean_{5m}\left(I_{T,i|k-1 \to k}\right) \tag{61}$$

Subject to:

$$I_{T,i|k \to k+1} = f_I\left(X_{i|k-1 \to k}, \boldsymbol{P}_b\right) \qquad for \quad i=1, 2, ..., x_f \tag{62}$$

Notice that this problem is almost identical to that given in (59) and (60). The only difference is the time shift from $k \to k+1$ to $k-1 \to k$ on the right hand side of the equation. This shows that the optimal feeder switch position at time k is determined using data from the past time instant at $k-1$ but implemented at time k. Hence, the optimal feeder switch position is determined from the network's operation over the last 5 minutes. Provided the load profiles do not change too rapidly, such a delay should have minimal impact on the controller's performance. This controller is termed the causal ideal current controller and is abbreviated to $_{5m}ICC_k$.

Whilst this controller is physically realisable due to the fact that it respects causality principle, it is not economically feasible today since it assumes an extensive communication infrastructure to transmit feedback from individual load profiles. Hence, it is unlikely that such a controller could be implemented in real-world applications containing large number of loads whose profiles are not known in advance.

5.7 Causal Simple Model Based Current Controller

This subsection details the algorithm of the proposed dynamic controller that requires only a few inputs. The controller is termed the causal simple model based controller algorithm and is abbreviated to $_{5m}SMCC_k$, it requires phase current measurements at supplying transformers and at each PSs only.

The proposed controller assumes piecewise-constant current loads and assumes the simple network model that is provided below:
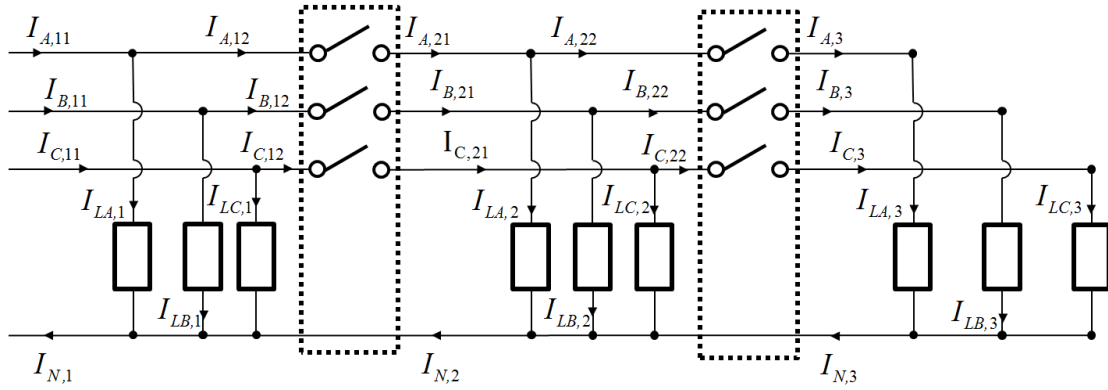
Fig. 23 Assumed Circuit of the Simple Model Based Controller

Estimation of the aggregate segment loads is performed by measuring feeder currents at each PS location and then subtracting them, which can be readily done. Evaluation of the model and subsequent calculation of the objective function is significantly simplified when compared to $_{5m}ICC_k$. In fact, the calculations involved consist solely of matrix multiplication. Such simplification permits real-time implementation of this control scheme.

In order to estimate the aggregate segment loads the proposed controller measures the phase currents at each PS location. Then the phase currents measured at two adjacent PSs are subtracted from each other:

$$I_{LA,j} = I_{A,j1} - I_{A,j2} \quad for \quad j = 1, 2, \dots, n_s \tag{63}$$

$$I_{LB,j} = I_{B,j1} - I_{B,j2} \quad for \quad j = 1, 2, \dots, n_s \tag{64}$$

$$I_{LC,j} = I_{C,jl} - I_{C,j2} \quad \text{for} \quad j = 1, 2, ..., n_s \tag{65}$$

For the last segment on the radial LV network the phase currents are equal to the aggregate segment load currents:

$$I_{LA,j} = I_{A,jl} \quad \text{for} \quad j = n_s + 1 \tag{66}$$

$$I_{LB,j} = I_{B,jl} \quad \text{for} \quad j = n_s + 1 \tag{67}$$

$$I_{LC,j} = I_{C,jl} \quad \text{for} \quad j = n_s + 1 \tag{68}$$

In this case the individual load information is unavailable and therefore $\boldsymbol{P}_s$ matrix, defined in (9) is constructed instead of $\boldsymbol{P}_b$. This matrix is populated with the estimated load currents shown in Fig. 23 as follows:

$$\boldsymbol{P}_s = \begin{bmatrix} I_{LA,1} & I_{LA,2} & I_{LA,3} & \cdots & I_{LA,n_s+1} \\ I_{LB,1} & I_{LB,2} & I_{LB,3} & \cdots & I_{LB,n_s+1} \\ I_{LC,1} & I_{LC,2} & I_{LC,3} & \cdots & I_{LC,n_s+1} \end{bmatrix} \tag{69}$$

This matrix, therefore, provides the aggregate segment current load profile on the feeder and can be used to compute the total phase current in any segment of the network. In order to facilitate matrix operation and structurally simple calculation of the total phase currents the individual columns of matrix $\boldsymbol{P}_s$ are stacked on top of each other so that the resulting column vector has $3(n_s+1)$ rows/elements and is denoted as $\boldsymbol{p}$. Mathematically, this procedure is represented by (70) and (71):

$$\boldsymbol{P}_s = \begin{bmatrix} \boldsymbol{p}_1 & \boldsymbol{p}_2 & \cdots & \boldsymbol{p}_{n_s+1} \end{bmatrix} \tag{70}$$

$$\boldsymbol{p} = \begin{bmatrix} \boldsymbol{p}_1 \\ \boldsymbol{p}_2 \\ \vdots \\ \boldsymbol{p}_{n_s+1} \end{bmatrix} \tag{71}$$

Calculation of the total phase current for a given reference segment is performed by using vector $\boldsymbol{p}$ and multiplying it with the so-called phase mapping matrix, denoted as $\boldsymbol{M}$, which itself is composed of the individual PS switch configuration matrices.

Assuming that the reference segment is the one located next to the substation then the phase mapping matrix is constructed as follows:

$$\boldsymbol{M} = [\boldsymbol{I} \quad \boldsymbol{X}_1 \quad \boldsymbol{X}_2 \cdot \boldsymbol{X}_3 \quad \dots \quad \prod_{i=1}^{n_s} \boldsymbol{X}_i] \tag{72}$$

Where $\boldsymbol{X}_i$ denotes the switch configuration matrix that corresponds to i^{th} PS in the network. This matrix has 3 rows and $3(n_s+1)$ columns where n_s is the number of PSs and n_s+1 is the number of segments. Therefore, the phase mapping matrix is composed of n_s+1 block elements each of which refers the phase connection information of the aggregate segment loads to the reference segment. Since it is assumed that there is no PS between the substation and the first segment, which is also the reference segment, the first block element in the phase mapping matrix is the identity 3-by-3 matrix.

In the example feeder used in this thesis it is assumed that the reference segment is located next to the substation. However, the methodology reported in the thesis can be readily generalised to the cases where other segments are considered to be reference segment. In the case of radial network for which the reference segment is not the first but j^{th} segment away from the substation, the corresponding phase mapping matrix is given as:

$$\boldsymbol{M} = [\boldsymbol{0}^{3 \times 3(j-1)} \quad \boldsymbol{I}^{3 \times 3} \quad \boldsymbol{X}_j \quad \boldsymbol{X}_j \cdot \boldsymbol{X}_{j+1} \quad \dots \quad \prod_{i=j}^{n_s+1} \boldsymbol{X}_i] \tag{73}$$

Where n_s+1 is the number of segments, note that the first $j-1$ block elements of the phase mapping matrix are equal to zero to reflect the fact that the realisations of

the PSs located upstream from the reference segment do not affect the phase currents in the reference segment.

The phase currents in the reference segment are then given by:

$$\boldsymbol{i}_P = \boldsymbol{M}\ \boldsymbol{p} \tag{74}$$

Where:

$$\boldsymbol{i}_P = \begin{bmatrix} I_A & I_B & I_C \end{bmatrix} \tag{75}$$

The total phase current is calculated by adding individual phase currents:

$$I_A + I_B + I_C = \sum \boldsymbol{M}\ \boldsymbol{p} \tag{76}$$

In order to simplify the calculation of the neutral current only the magnitudes of the phase currents are considered. Hence, it is implicitly assumed that the mutual phase shift of the three currents is equal to 120 degrees. Under such assumption the calculation of the square of the neutral current can be phrased as simple matrix multiplication.

Firstly, it can be shown in straight forward manner by expanding the expression in that:

$$I_N = \sqrt{I_A^2 + I_B^2 + I_C^2 - I_A I_B - I_A I_C - I_B I_C} \tag{77}$$

It can also be shown that:

$$\frac{(I_A - I_B)^2 + (I_A - I_C)^2 + (I_B - I_C)^2}{2} = I_A^2 + I_B^2 + I_C^2 - I_A I_B - I_A I_C - I_B I_C \tag{78}$$

Therefore:

$$I_N = \sqrt{\frac{(I_A - I_B)^2 + (I_A - I_C)^2 + (I_B - I_C)^2}{2}} \tag{79}$$

This expression for neutral current can be represented using the following quadratic matrix form:

$$I_N^2 = \boldsymbol{i}_P^T \boldsymbol{R} \boldsymbol{i}_P \tag{80}$$

Where:

$$\boldsymbol{R} = \begin{bmatrix} 1 & -0.5 & -0.5 \\ -0.5 & 1 & -0.5 \\ -0.5 & -0.5 & 1 \end{bmatrix} \tag{81}$$

Since $\boldsymbol{i}_p = \boldsymbol{M} \boldsymbol{p}$, neutral current can be expressed as:

$$I_N^2 = \boldsymbol{p}^T \boldsymbol{M}^T \boldsymbol{R} \boldsymbol{M} \boldsymbol{p} \tag{82}$$

Which can be written as:

$$I_N^2 = \boldsymbol{p}^T \boldsymbol{M}^T \boldsymbol{R} \boldsymbol{M} \boldsymbol{p} \tag{83}$$

Where

$$\boldsymbol{Q} = \boldsymbol{M}^T \boldsymbol{R} \boldsymbol{M} \tag{84}$$

Note that for every possible feeder switch position there is a corresponding realisation of $\boldsymbol{M}$ and, therefore the $\boldsymbol{Q}$ matrix as well. However, these different realisations can be computed offline and stored so that during the real-time implementation and only the vector $\boldsymbol{p}$ needs to be computed and then used in the following equation to calculate the total current in the reference segment:

$$I_T = \sum \boldsymbol{M} \cdot \boldsymbol{p} + \sqrt{\boldsymbol{p}^T \boldsymbol{Q} \boldsymbol{p}} \tag{85}$$

This equation contrasts those provided in (55), (58), (60) and (62) and can be computed readily.

The optimisation problem associated with the proposed simple model-based controller is given as follows:

$$\check{X}_k = \arg \min_{\{X_i\}_{i=1}^{x_f}} mean_{5m} \left(I_{T,i|k-1 \to k} \right) \tag{86}$$

Subject to:

$$I_{T,i|k \to k+1} = \sum \boldsymbol{M}_i \cdot \boldsymbol{p}_{k-1 \to k} + \sqrt{\boldsymbol{p}_{k-1 \to k}^T \boldsymbol{Q}_i \, \boldsymbol{p}_{k-1 \to k}} \qquad for \quad i = 1, 2, \dots, x_f \tag{87}$$

Similarly to $_{5m}ICC_k$, the optimal feeder switch position at time k is determined using network measurements of the past time instant at $k-1$ which is implemented

at time k. This point is represented in the right hand side of equation (87) where $k-1 \rightarrow k$ is stated for relevant variables. Hence, the optimal feeder switch position is determined from the network's operation over the previous 5 minutes.

By employing a very simple network model that requires low bandwidth communication between PSs and feeding transformer(s) to determine the optimum feeder switch position, the proposed controller is thought to be economically feasible today for real-time implementation. Clearly, the accuracy of the model is necessarily sacrificed as a consequence of simplification. However, as the results in Section 6.2 indicate, such reduction in model accuracy appeared to have minimal impact on the controller's performance when evaluated using the example feeder.

6 Unlocking cable current Through Phase Reconfiguration - Results

This section details power flow simulations that reveal the cable current PSs can unlock when the control algorithms detailed in chapter 5 are employed. The simulations show specific weekday and weekend scenarios for each month of the year when dwellings are considered as loads without DG. The performance of PSs is shown by comparing results with those obtained from the networks straight through configuration.

6.1 Scheduled Current and Losses Control Algorithms - Results

6.1.1 Weekday: Scheduled Ideal Current Control Algorithms Versus Straight Through

Simulation results for the example feeder are shown in Fig. 24 for a weekday in every month of the year. They show the trends of total current in the feeder's hot spot when the straight through configuration is applied and by visual inspection it can be observed that the highest total current occurs in the winter months at peak time.
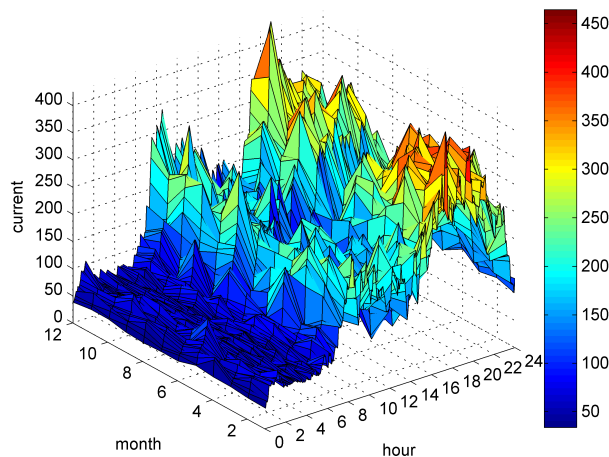
Fig. 24 Daily weekday current flow in the hot spot - straight through configuration

The results shown in Fig. 25 display the trends of total current in the hot spot for all months of the year using PSs and employing the scheduled peak time ideal current

control algorithm. Note that the optimal feeder switch positions were calculated for every month of the year, although it was found that for 9 out of 12 months it was the same feeder switch position that was found.
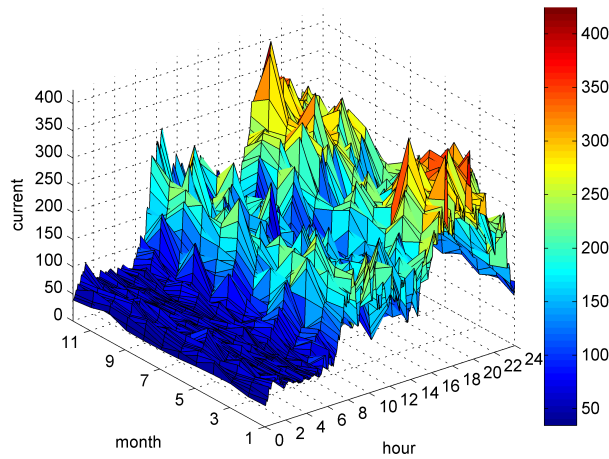
*Fig. 25 Daily weekday current flow result in the hot spot -
scheduled peak time ideal current control algorithm*

Identical power flow simulations were also conducted for the scheduled 24 hour ideal current control algorithm. The feeder switch positions that were found for the both the peak time and 24 Hour ideal current control algorithms are provided in the following table:

Month	Scheduled peak time ideal current control algorithm $_{PT}ICC_{k+1}$	Scheduled 24 hour ideal current control algorithm $_{24h}ICC_{k+1}$
January	$X_4 = X(C_B, C_A)$	$X_4 = X(C_B, C_A)$
February	$X_4 = X(C_B, C_A)$	$X_4 = X(C_B, C_A)$
March	$X_4 = X(C_B, C_A)$	$X_4 = X(C_B, C_A)$
April	$X_2 = X(C_A, C_B)$	$X_4 = X(C_B, C_A)$
May	$X_4 = X(C_B, C_A)$	$X_4 = X(C_B, C_A)$
June	$X_4 = X(C_B, C_A)$	$X_4 = X(C_B, C_A)$
July	$X_4 = X(C_B, C_A)$	$X_2 = X(C_A, C_B)$
August	$X_4 = X(C_B, C_A)$	$X_4 = X(C_B, C_A)$
September	$X_4 = X(C_B, C_A)$	$X_4 = X(C_B, C_A)$
October	$X_9 = X(C_C, C_C)$	$X_9 = X(C_C, C_C)$
November	$X_4 = X(C_B, C_A)$	$X_4 = X(C_B, C_A)$
December	$X_9 = X(C_C, C_C)$	$X_2 = X(C_A, C_B)$

Table 9 *Switch positions found for the scheduled peak time and 24 hour ideal current control algorithms for each month of the year*

Table 9 highlights three favoured feeder switch positions and X_4 as the most favoured for nine months of the year, in the three other months, feeder switch positions X_2 and X_9 were found. The most significant result that can be observed from the table is that there are only three months where the feeder switch position incorperates a PS that is not set to C_A, which suggests that one PS is required in the example feeder to achieve the optimum result found by the scheduled ideal current control algorithms.

In order to focus on the benefits realised using the scheduled peak time ideal current control algorithm the current trends plotted in Fig. 25 are differenced from those obtained using straight through configuration in Fig. 24 and the result is plotted in the following figure:
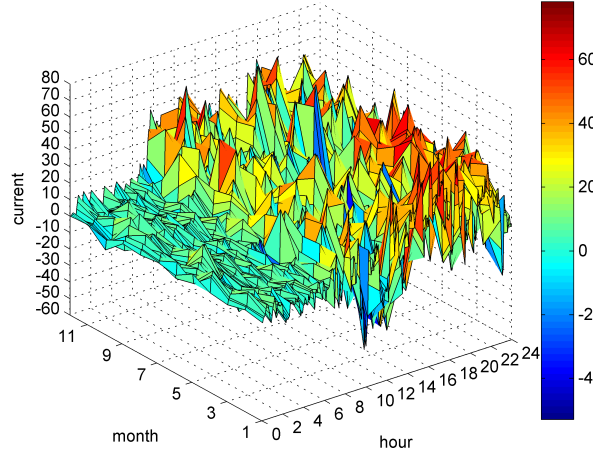
Fig. 26 Daily Weekday current flow result in the hot spot – difference between straight through and the scheduled peak time control algorithm.

Fig. 26 shows quite clearly that the trends shown have both positive and negative values which indicates that the scheduled ideal current control algorithm does not deliver reduced total current when compared to straight through configuration at every sampling instant, this may be viewed as slightly surprising. However, it should be noted that the algorithms focus on the daily or peak time mean imbalance of the individual phases rather than on improving the phase balance at every sampling instant in time. Therefore, it is expected that there will be temporal periods during a given day when the profiles of individual loads cause greater phase imbalance than the straight through configuration, thereby motivating the introduction of dynamic phase reconfiguration which will be considered in Section 6.2. The benefit of the peak time scheduled ideal current control algorithm is more clearly highlighted when the difference in the mean at peak time is examined as shown in Fig. 27 below.
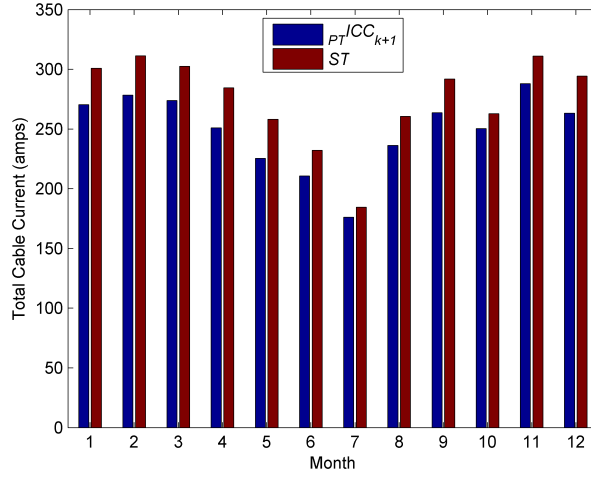
*Fig. 27 Mean peak time hot spot current for straight through
and the scheduled peak time ideal current control algorithm*

The histogram in Fig. 27 shows that a benefit is realised in every month at Peak time when the peak time scheduled ideal current control algorithm is employed. The algorithm consistently offers a reduction in mean peak time current for every month of the year. In order to more closely inspect the benefit of using PSs Fig. 28 is provided that displays for each month the percentage reduction in the total hot spot current. This reduction, relative to straight through, ranges from 4.6% in July to 12.7% in May. Also, for five months in the year the peak time scheduled ideal current control algorithm reduces the total current by more than 10% and the average across 12 months in a year was found to be 9.2%.
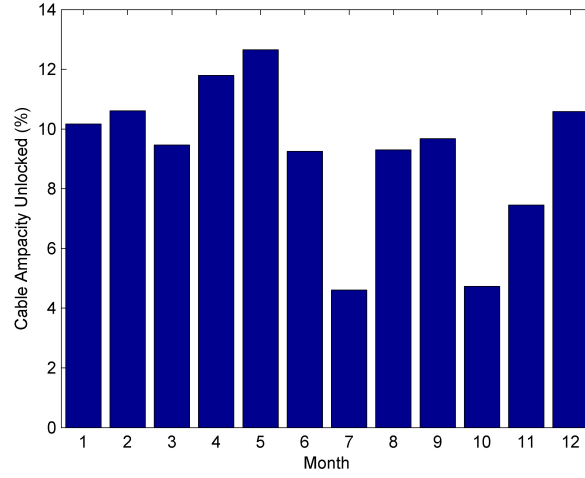
Fig. 28 Percentage reduction in the total hot spot current than would otherwise be experienced for straight through when the scheduled peak time ideal current control algorithm is employed.

The hot spot currents obtained from the example feeder when the Daily ideal current control algorithm was simulated are plotted in Fig. 29. In a similar way to Fig. 27, this figure demonstrates a consistent reduction in hot spot current which is represented as a percentage current that the algorithm unlocks in Fig. 30. This percentage reduction ranges from 5.6% in July to 10% in September. The average benefit of using scheduled phase reconfiguration calculated across all 12 months in a year was found to be 8.3%.
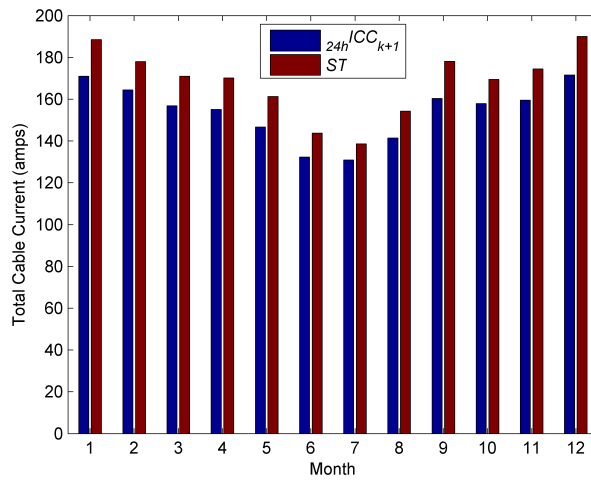
Fig. 29 Mean peak time hot spot current for straight through and the scheduled daily ideal current control algorithm
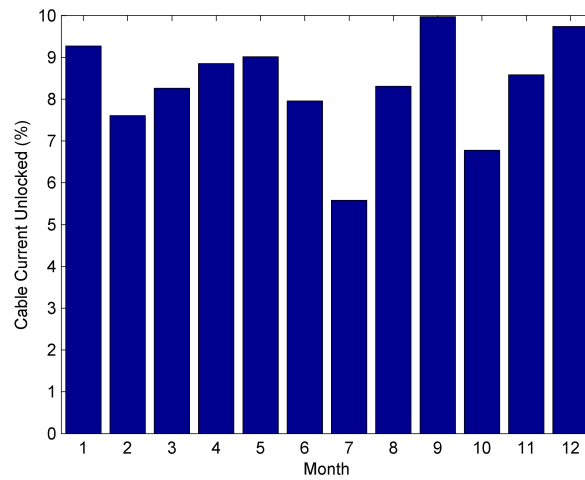
Fig. 30Percentage reduction in the total hot spot current than experienced for Straight Through when the Daily ideal current control algorithm is employed.

It is notable that the results show the peak time ideal current control algorithm to unlock more current than the Daily ideal current control algorithm. This result can be explained, because at peak time mean currents are greater than when averaged over a day, but the unbalanced connection of loads to phases for both periods is the same. Therefore, it is quite intuitive to understand that re-balancing phase currents would unlock more current at peak time just due to the higher phase currents experienced at that time. This is also the time that the greatest thermal strain is placed on network assets meaning that it presents a better indication of the impact of PS when network stresses are greatest.

The full impact on hot spot currents when PSs are deployed on the example feeder and the peak time ideal current control algorithm is employed is shown for all months of the year in Fig. 31 through to Fig. 34. The trends of phase currents are sub-divided into seasons with the figures corresponding to the winter, spring, summer and autumn months shown in Fig. 31, Fig. 32, Fig. 33 and Fig. 34 respectively. The left sub-plot in each of the figures shows the trends of the phase currents obtained when straight through configuration is adopted whereas the right sub-plots refer to the case where

The daily ideal current control algorithm was employed. Also, in each of the plots the mean daily currents are shown with dashed lines.

Fig. 31 Winter: Weekday phase and neutral hot spot currents. Plots on the left show the straight through configuration and those on the right show the resultant currents when the daily ideal current control algorithm controlled PSs. Mean daily currents are represented by dashed lines.
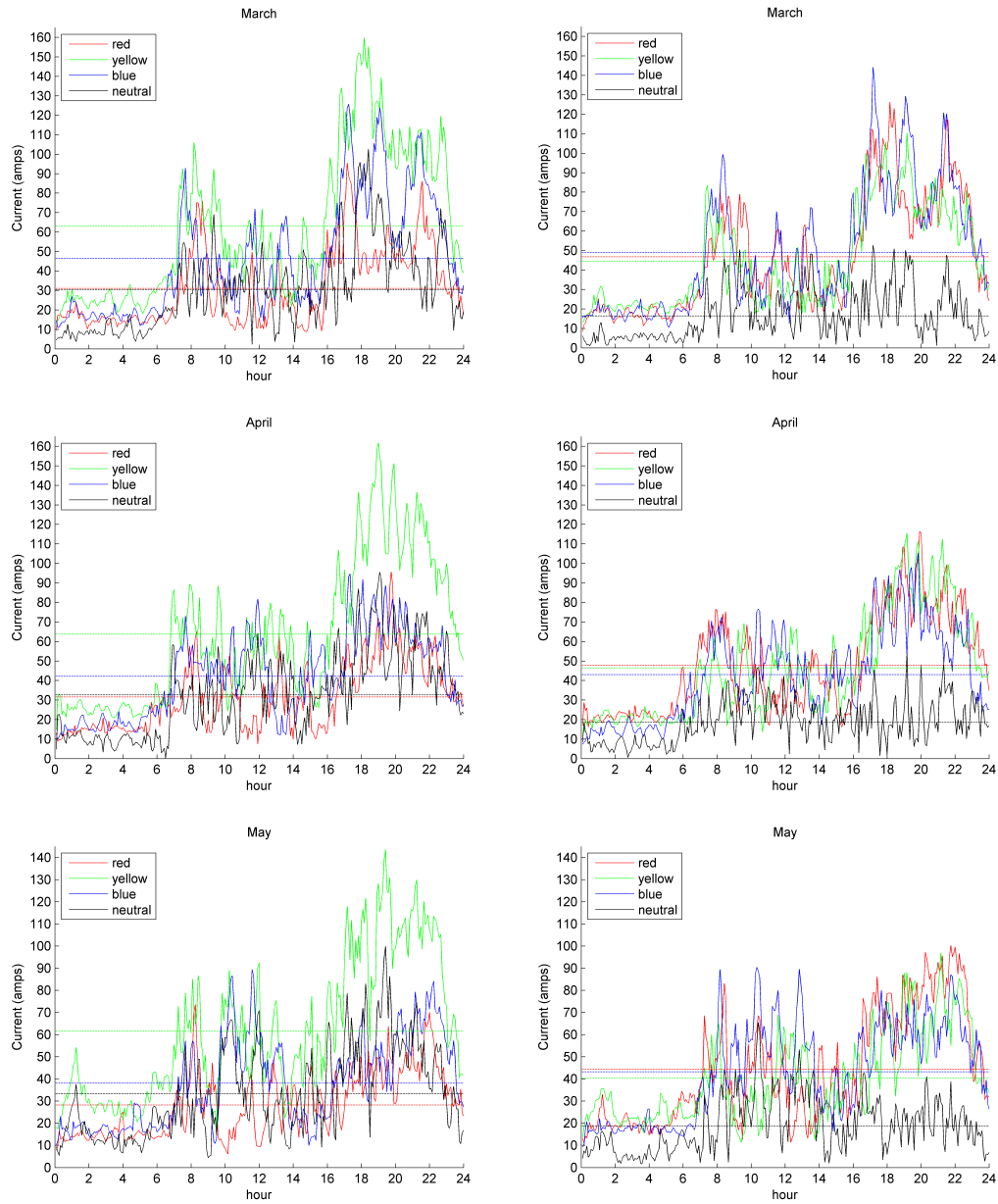
Fig. 32 Spring: Weekday phase and neutral hot spot currents. Plots on the left show the straight through configuration and those on the right show the resultant currents when the daily ideal current control algorithm controlled PSs. Mean daily currents are represented by dashed lines.
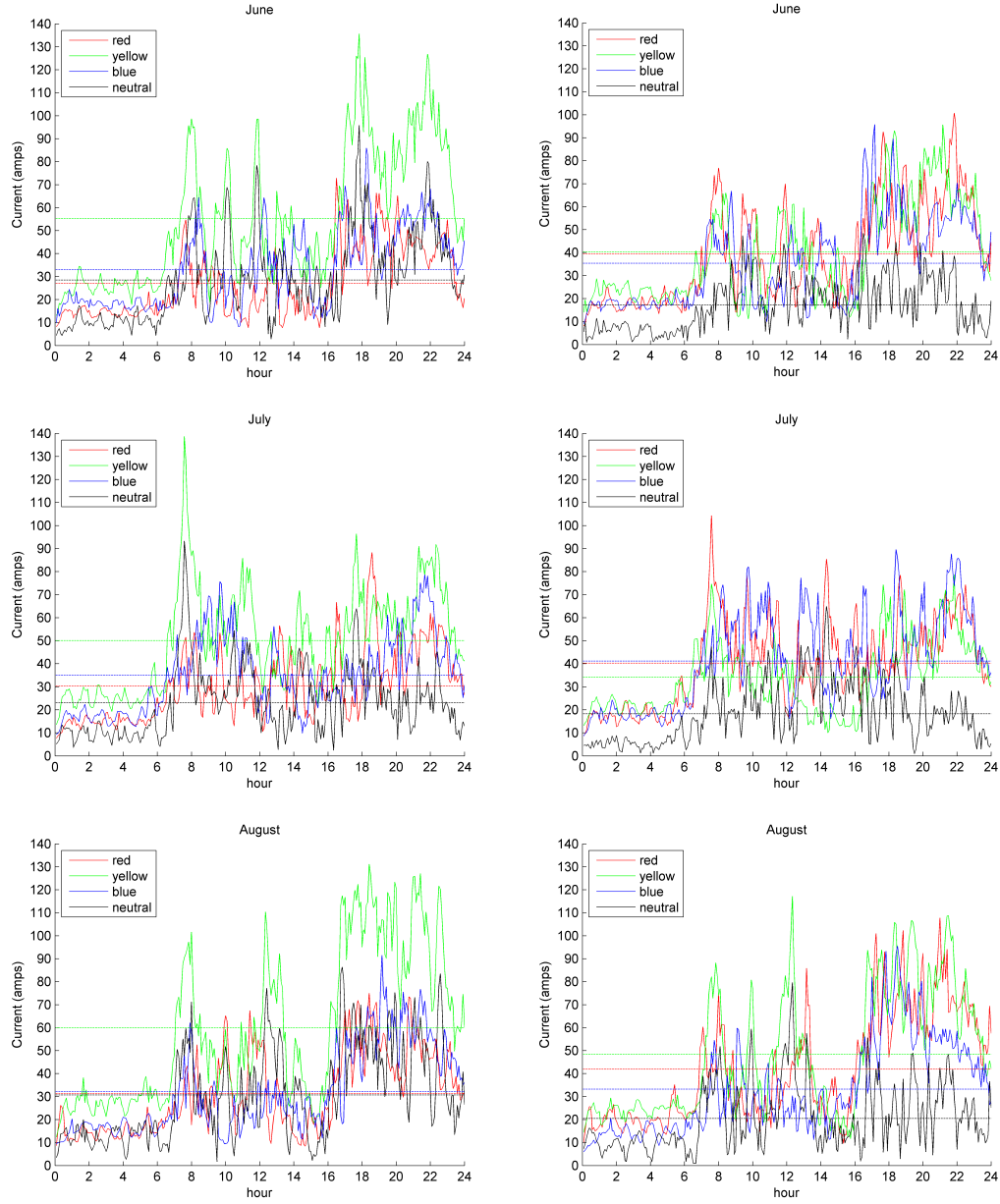
Fig. 33 Summer: Weekday phase and neutral hot spot currents. Plots on the left show the straight through configuration and those on the right show the resultant currents when the daily ideal current control algorithm controlled PSs. Mean daily currents are represented by dashed lines.
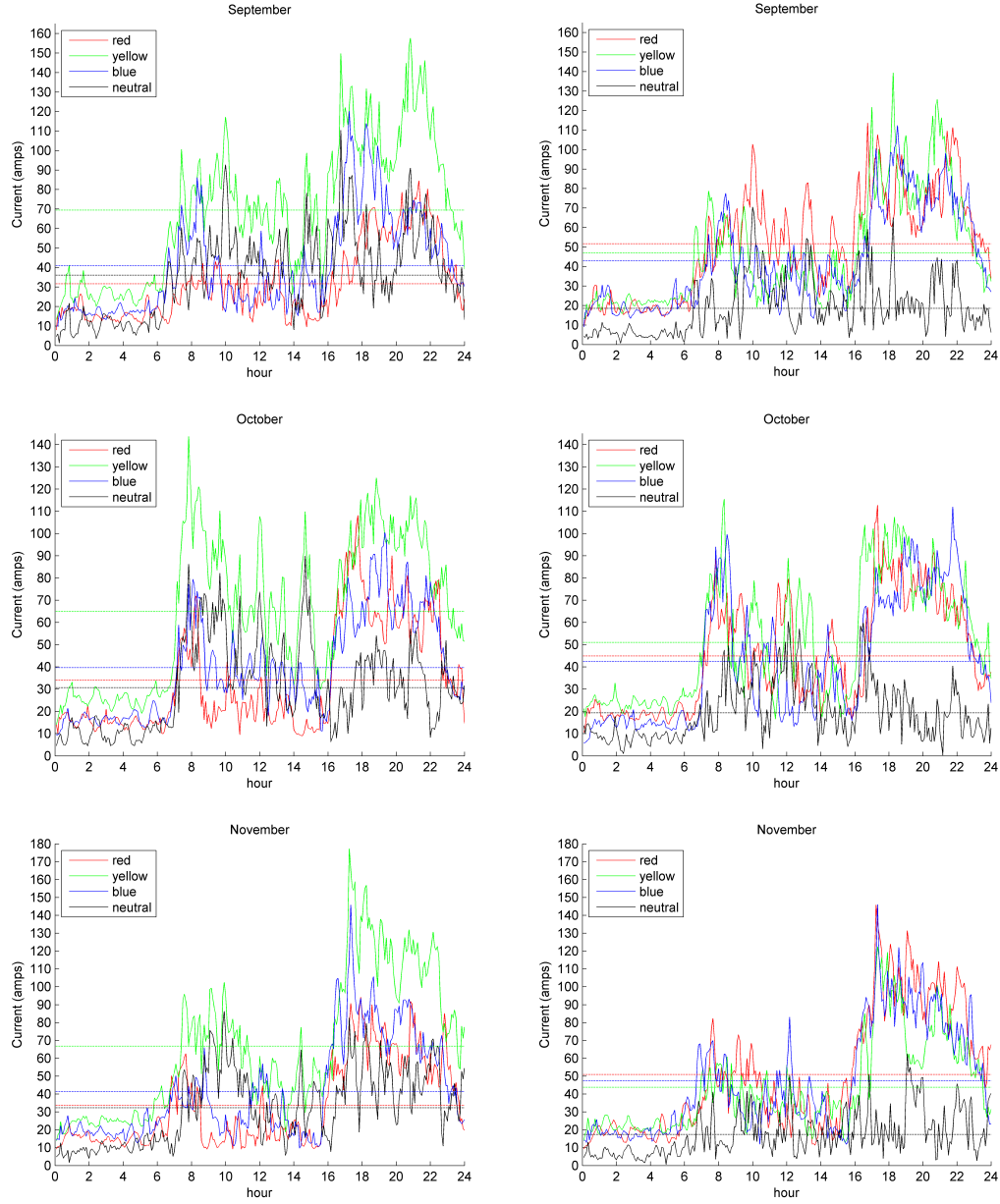
Fig. 34 Autumn: Weekday phase and neutral hot spot currents. Plots on the left show the straight through configuration and those on the right show the resultant currents when the daily ideal current control algorithm controlled PSs. Mean daily currents are represented by dashed lines.

It is observed in Fig. 31 to Fig. 34 that for every month of the year the individual phase currents when the network is in the straight through configuration are unbalanced. In particular, the green phase current appears to be clearly greater in magnitude when compared to the other two phase currents. As a result of this imbalance, neutral current is observed to be of considerable magnitude in all the left hand side sub-plots. Conversely, the sub-plots on the right hand side of each of the figures that correspond to current trends obtained using the peak time ideal current control algorithm show a clear improvement in terms of the phase balance. More specifically, green phase current is evidently reduced in magnitude and all three phase currents exhibit similar trends. This is also confirmed by observing that the neutral current in each of the right sub-plots is consistently lower when compared to that shown in the corresponding left-hand plot. Therefore, these figures provide additional confirmation and demonstration of the benefits attained when utilising PSs in scheduled phase reconfiguration mode.

6.1.2 Weekday: Scheduled Cable Losses Control Algorithms Versus Straight Through and Ideal Current Control Algorithms

Losses are inevitably present in any electrical power network. They represent the power that is actually produced but then lost during its transmission to the end user. The majority of the losses in underground cables manifest themselves as heat which is the main factor considered when their cable current ratings are calculated. Therefore, in the absence of external heating sources, losses effectively limit the a feeders load capacity and lowering them effectively unlocks existing capacity. Reducing the total losses of a feeder would also realise economic benefits by lowering the energy generation requirement, which would lead to savings in energy costs, and by reducing the thermal stresses on cables, the DNO would make maintenance savings. This section focuses on the quatifying the impact that PSs have on losses in the example feeder, the losses control algorithms are used as a bench mark for comparison with the Current Control Algorithms, whilst the straight through configuration is used to show what losses are incurred when no PSs are deployed. Due to the fact that, as shown in previous sections, appropriate application of PSs can reduce the total current in the feeder, it is expected it will also have a positive impact on the total losses incurred in the network.

The optimal positions of PSs that minimise the total losses in the example feeder were obtained by running the daily load flow simulation of the network for each month of the year and for each permissible feeder switch position. The total daily mean losses was minimised using the daily losses control algorithm.

Fig. 35 shows the daily mean losses in the example feeder obtained when it was simulated using the daily ideal current control algorithm, the Daily Losses Control Algorithm and the straight through configuration. As somewhat expected, the straight through configuration results in the greatest daily mean losses for every month of the year. On the other hand, the daily ideal current control algorithm that minimises the total current in the hot spot also reduces the total losses for each of the 12 months when compared to the straight through configuration. A Further reduction is observed when the Daily Losses Control Algorithm is employed which specifically focused on minimising the total losses in the cable. However, it can also be observed in Fig. 35 that during August and October the daily ideal current control algorithm, and the daily losses control algorithm both find the optimal solution that minimises total losses. Therefore, minimisation of the total current in the network hot spot also minimised the total losses in the network for two of the months. This conclusion can be extrapolated more generally using the results displayed in Fig. 35, which show the reduction in cable losses attained using two alternative algorithms to be very similar though not necessarily identical. The implication of this finding is that a PSs configuration which aims to minimise the total current in the feeder hot spot will also result in considerable reduction of the total losses in the entire network and may even in some cases deliver optimal reduction of losses.
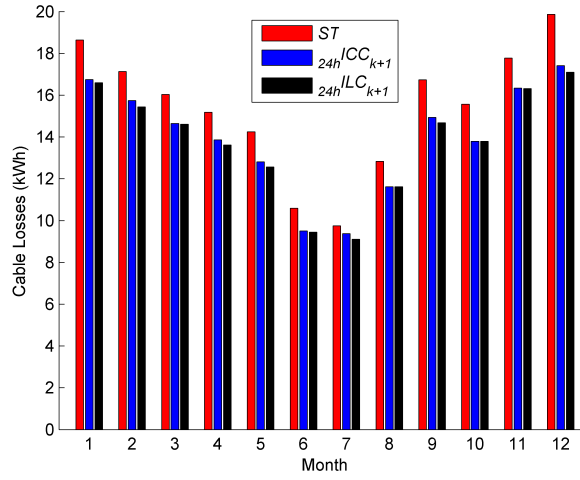
Fig. 35 The Daily Mean Total Cable Losses in the example feeder on a Weekday for the straight through configuration, daily ideal current control algorithm and the Daily Losses Control Algorithm.

The reduction in losses that can be achieved using PSs employing the daily ideal current control algorithm differenced from the straight through configuration which is shown in Fig. 36. The figure shows the real power savings for each of the algorithms which clearly reinforces the points made previously concerning the similar impact on losses that they have.
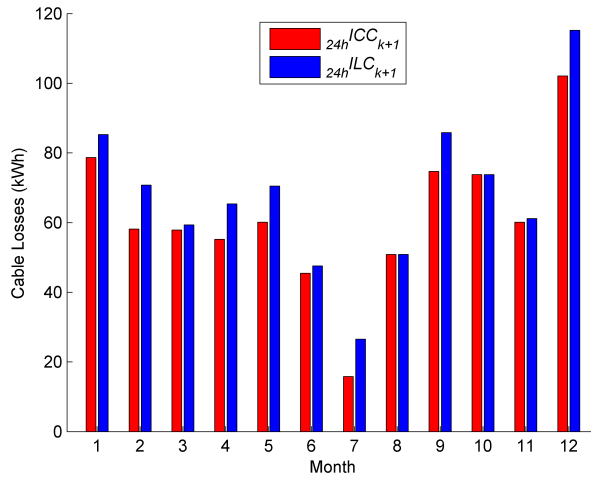
Fig. 36 The difference in losses found between: the daily ideal current control algorithm and the Daily Losses Control Algorithm.

Table 10 shows the switch positions that were found by the Daily ideal current control algorithm and the daily cable losses control algorithm. The table shows that only

three of the nine feeder switch positions are chosen by the algorithms and that the feeder position $\mathbf{X}(C_C, C_C)$ is favoured by the Daily Losses Current Control Algorithm rather than $\mathbf{X}(C_A, C_B)$ which is favoured by the Daily ideal current control algorithm.

Month	Daily ideal current control algorithm $_{24h}ICC_{k+1}$	Daily losses current control algorithm $_{24h}ILC_{k+1}$
January	$X_4 = X(C_B, C_A)$	$X_9 = X(C_C, C_C)$
February	$X_4 = X(C_B, C_A)$	$X_9 = X(C_C, C_C)$
March	$X_4 = X(C_B, C_A)$	$X_9 = X(C_C, C_C)$
April	$X_2 = X(C_A, C_B)$	$X_4 = X(C_B, C_A)$
May	$X_4 = X(C_B, C_A)$	$X_9 = X(C_C, C_C)$
June	$X_4 = X(C_B, C_A)$	$X_9 = X(C_C, C_C)$
July	$X_4 = X(C_B, C_A)$	$X_9 = X(C_C, C_C)$
August	$X_4 = X(C_B, C_A)$	$X_4 = X(C_B, C_A)$
September	$X_4 = X(C_B, C_A)$	$X_9 = X(C_C, C_C)$
October	$X_9 = X(C_C, C_C)$	$X_9 = X(C_C, C_C)$
November	$X_4 = X(C_B, C_A)$	$X_9 = X(C_C, C_C)$
December	$X_9 = X(C_C, C_C)$	$X_2 = X(C_A, C_B)$

Table 10 *Switch Positions found for the Daily ideal current control algorithm and the daily cable losses control algorithm for each month of the year*

6.1.3 Weekend: Scheduled ideal current control algorithms Versus Straight Through

Simulation results for the example feeder are shown in Fig. 37 for a weekend in every month of the year. They show the trends of total current in the feeder's hot spot when the straight through configuration is applied and by visual inspection it can be observed that the highest total current occurs in the winter months at peak time.
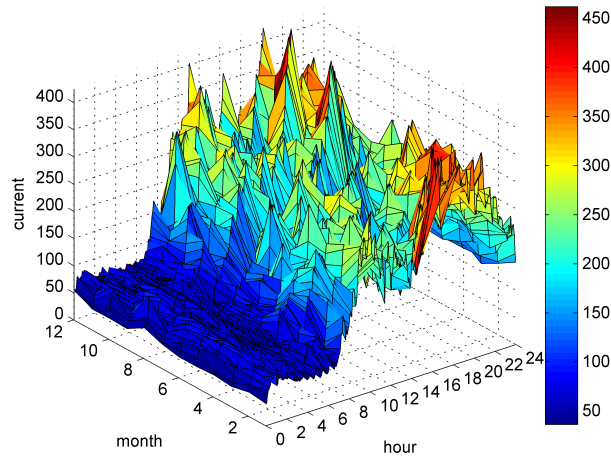
Fig. 37 Daily Weekend Current flow in the hot spot - straight through configuration

The Results shown in Fig. 38 display the trends of total current in the hot spot for all months of the year using PSs and employing the peak time ideal current control algorithm. Note that the optimal feeder switch positions were calculated for every month of the year and it was found that for 9 out of 12 months the same feeder switch position was found, providing consolidation of the corresponding weekday result.
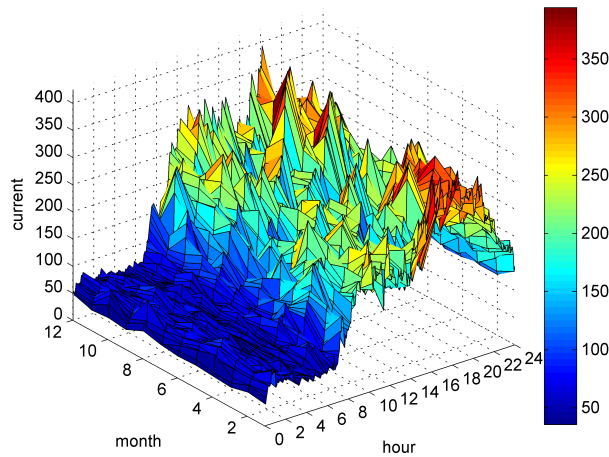
Fig. 38 Daily weekday current flow result in the hot spot - scheduled peak time ideal current control algorithm.

The feeder switch positions that were found for the peak time ideal current control algorithm is provided in the following table:

Month	Scheduled peak time ideal current control algorithm $_{PT}ICC_{k+1}$
January	$X_4 = X(\boldsymbol{C}_B, \boldsymbol{C}_A)$
February	$X_4 = X(\boldsymbol{C}_B, \boldsymbol{C}_A)$
March	$X_4 = X(\boldsymbol{C}_B, \boldsymbol{C}_A)$
April	$X_2 = X(\boldsymbol{C}_A, \boldsymbol{C}_B)$
May	$X_9 = X(\boldsymbol{C}_C, \boldsymbol{C}_C)$
June	$X_4 = X(\boldsymbol{C}_B, \boldsymbol{C}_A)$
July	$X_4 = X(\boldsymbol{C}_B, \boldsymbol{C}_A)$
August	$X_4 = X(\boldsymbol{C}_B, \boldsymbol{C}_A)$
September	$X_4 = X(\boldsymbol{C}_B, \boldsymbol{C}_A)$
October	$X_9 = X(\boldsymbol{C}_C, \boldsymbol{C}_C)$
November	$X_4 = X(\boldsymbol{C}_B, \boldsymbol{C}_A)$
December	$X_4 = X(\boldsymbol{C}_B, \boldsymbol{C}_A)$

Table 11 *Weekend: Switch positions found for the scheduled peak time and 24 hour ideal current control algorithms for each month of the year*

Table 11 highlights the same three favoured feeder switch positions as was found on weekdays. X_4 is again the most favoured for nine months of the year, in the three other months, feeder switch positions X_2 and X_9 were found. Again, as found on weekdays, there are only three months where the feeder switch position incorperates a PS that is not set to $\boldsymbol{C}_A$, which shows that one PS is required in the example feeder to achieve the optimum result found by the scheduled ideal current control algorithms.

The benefit of the peak time scheduled ideal current control algorithm is more clearly highlighted when the difference in the mean at peak time is examined as shown in Fig. 39 below.
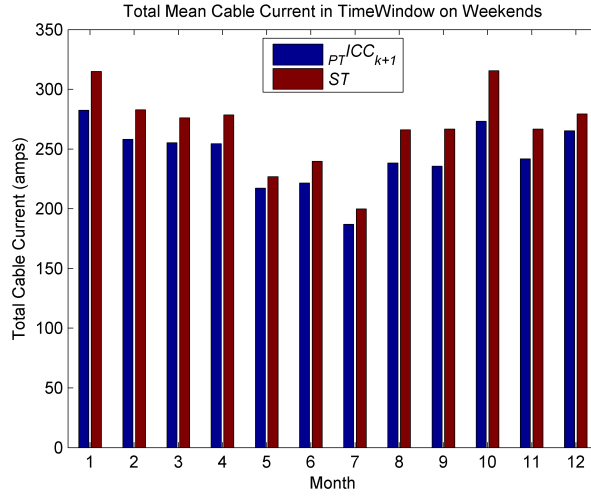
*Fig. 39 Peak time mean cable current at weekend in the hot
spot for straight through and the peak time control algorithm.*

The histogram in Fig. 39 shows that a benefit is realised in every month when the peak time scheduled ideal current control algorithm is employed. The algorithm consistently offers a reduction in mean peak time current for every month of the year. In order to more closely inspect the benefit of using PSs, Fig. 40 is provided displays for each month the percentage reduction in the total hot spot current. This reduction, relative to straight through, ranges from 4.3% in May to 13.4% in October. Also, for four months in the year the total current is reduced by more than 10% and the average across 12 months in a year was found to be 8.6%.
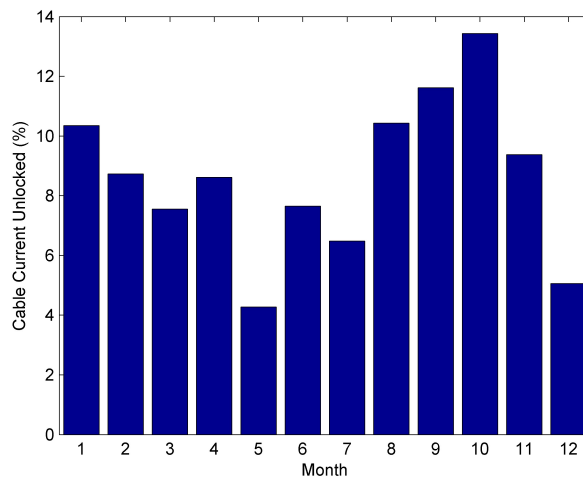
*Fig. 40 Hot spot cable current unlocked at peak time on a
weekend as a percentage of Straight Through hot spot current.*

The full impact on hot spot currents when PSs are deployed on the example feeder when the peak time ideal current control algorithm is employed is shown for all

months of the year in Fig. 41 through to Fig. 44. The trends of phase currents are sub-divided into seasons with the figures corresponding to the winter, spring, summer and autumn months shown in Fig. 41, Fig. 42, Fig. 43 and Fig. 44 respectively. The left sub-plot in each of the figures shows the trends of the phase currents obtained when straight through configuration is adopted, whereas the right sub-plots refer to the case where The daily ideal current control algorithm was employed. Also, in each of the plots the mean daily currents are shown with dashed lines.

Fig. 41 Winter: Weekend phase and neutral hot spot currents. Plots on the left show the straight through configuration and those on the right show the resultant currents when the daily ideal current control algorithm controlled PSs. Mean daily currents are represented by dashed lines.
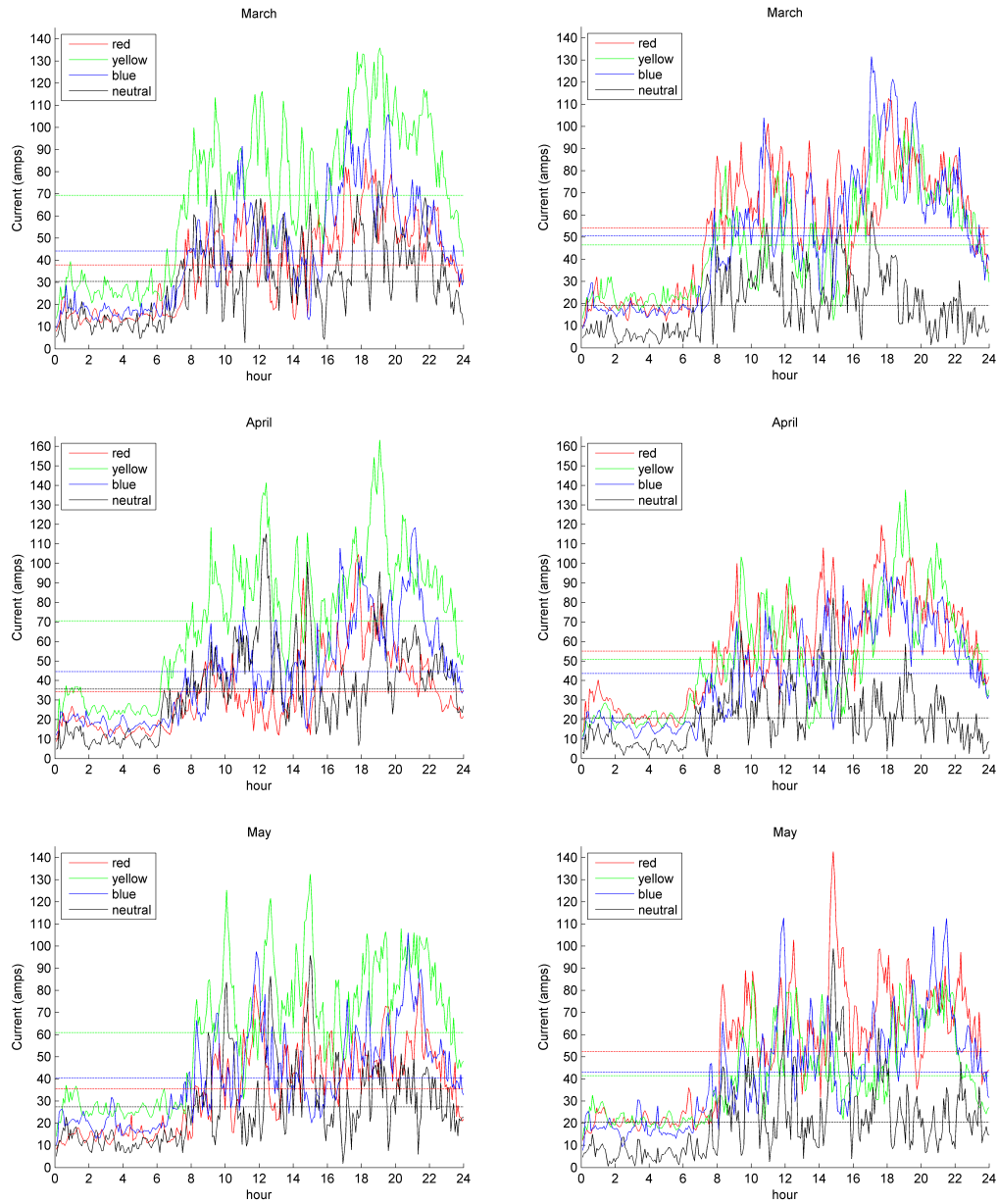
Fig. 42 Spring: Weekend phase and neutral hot spot currents. Plots on the left show the straight through configuration and those on the right show the resultant currents when the daily ideal current control algorithm controlled PSs. Mean daily currents are represented by dashed lines.
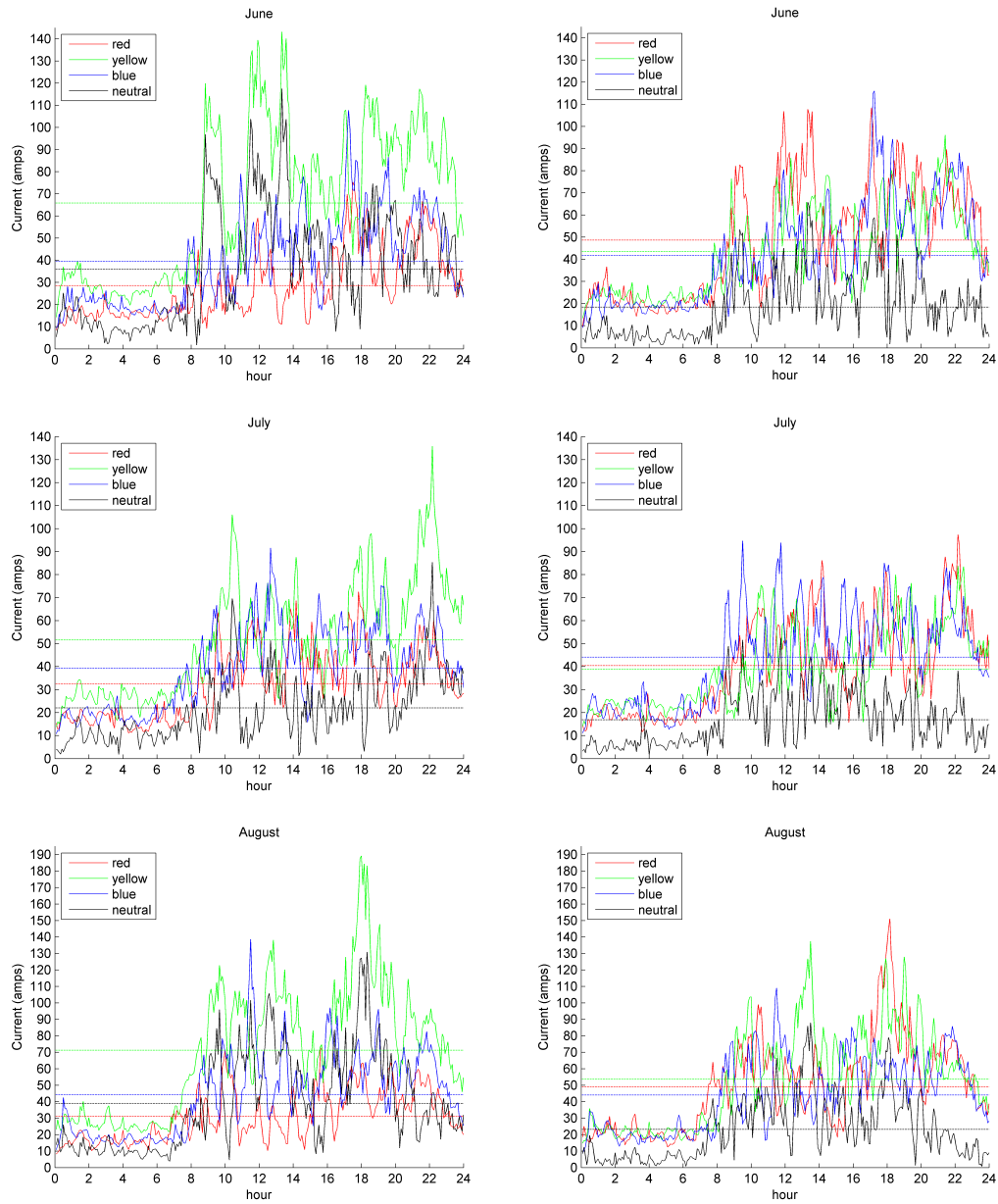
Fig. 43 Summer: Weekend phase and neutral hot spot currents. Plots on the left show the straight through configuration and those on the right show the resultant currents when the daily ideal current control algorithm controlled PSs. Mean daily currents are represented by dashed lines.
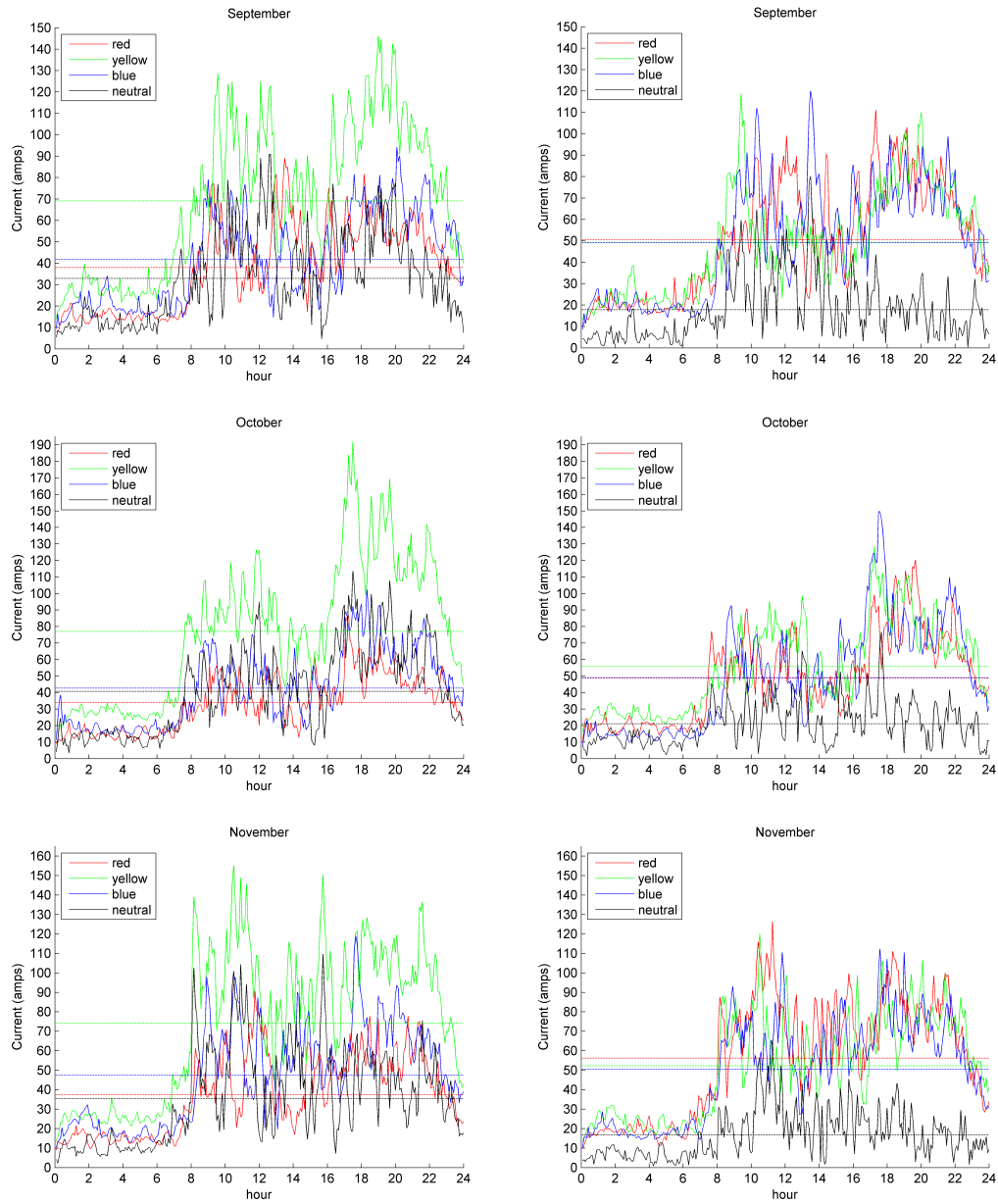
Fig. 44 Autumn: Weekend phase and neutral hot spot currents. Plots on the left show the straight through configuration and those on the right show the resultant currents when the daily ideal current control algorithm controlled PSs. Mean daily currents are represented by dashed lines.

Generally, the observations made about the phase current trends made in the week-day analysis are consolidated in Fig. 41 to Fig. 44. Most importantly, the sub-plots on the right hand side of each of the figures that correspond to current trends obtained using the peak time ideal current control algorithm show a clear improvement in terms of the phase balance that for every month of the year. As observed in the weekday analysis the neutral current in each of the sub-plots on the right is consistently lower when compared to that shown in the plots on the left. The notable difference between the weekday and weekend results is the general load profile shape where at weekends the load is more evenly spread across the day. More specifically, the difference between peak time currents and those during general day time hours is observed as being less than that shown in the weekdays plots of Fig. 31 through to Fig. 34.

6.1.4 Weekend: Losses Control Algorithms Versus Straight Through and Current Control Algorithms

The optimal positions of PSs that minimise the total losses in the example feeder were obtained by running the daily load flow simulation of the network for each month of the year and for each permissible feeder switch position. The total peak time mean losses were minimised using the peak time losses control algorithm.

Fig. 45 shows the daily mean losses in the example feeder obtained when it was simulated in the straight through configuration and using the Daily Current and Losses Control Algorithms. As somewhat expected and in line with the weekday histograms, the straight through configuration results in the greatest daily mean losses for every month of the year. On the other hand, the daily ideal current control algorithm that minimises the total current in the hot spot also achieves a reduction the daily total losses for each of the 12 months when compared to the straight through configuration. A Further reduction is observed in 3 of the 12 months shown in Fig. 45 when the Daily Losses Control Algorithm is employed which specifically focused on minimising the total losses in the cable. However, for the other 9 months of the year the daily ideal current control algorithm finds the optimal solution that minimises total losses at weekend which is an improvement on the 3 found on a weekday. Therefore, minimisation of the total current in the network hot spot at weekends also minimised the total

losses in the network for 9 months of the year. This conclusion can be extrapolated more generally using the results displayed in Fig. 45, which show the reduction in cable losses attained using two alternative algorithms to be very similar in 9 out of 12 cases. The implication of this finding provides some consolidation to that found on weekdays where it was surmised that PSs configured with an algorithm to minimise the total current in the feeder hot spot will also result in considerable reduction of the total losses in the entire feeder and may even in some cases deliver optimal reduction of losses.
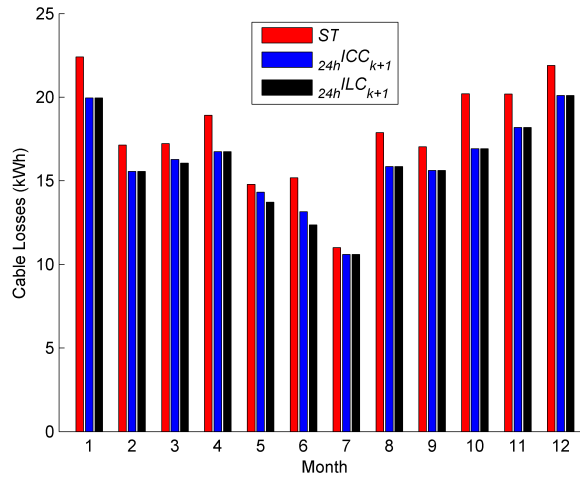
Fig. 45 Weekend: Daily mean total cable losses for Straight Through, Daily Scheduled Current Control and Daily Scheduled Losses Control Algorithms.

The reduction in losses that can be achieved using PSs employing the daily ideal current control algorithm when compared to the straight through configuration is shown in Fig. 46. The figure shows clearly that the Daily Losses and Current Control Algorithms both achieve equal maximum and minimum reductions of total losses in October and July of 3.29kWh and 0.40kWh respectively, and a similar mean across 12 months of approximately 1.75kWh. Generally, Fig. 46 shows the savings that the Daily Current and Losses Control Algorithms achieve, clearly reinforcing the findings on weekdays where some results were equivalent and that the daily ideal current control algorithm is inferred as generally causing a consistent reduction in losses.
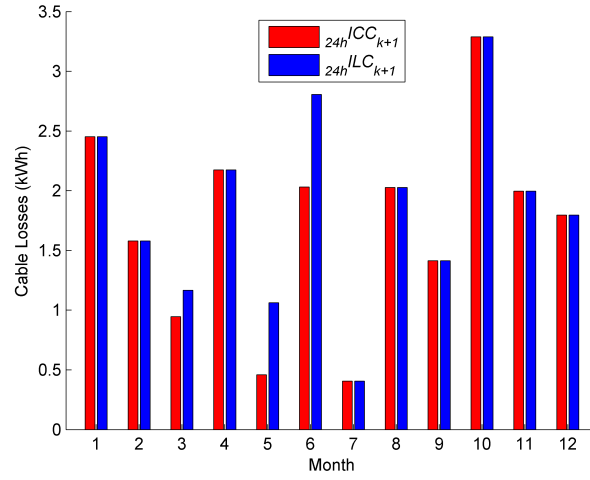
Fig. 46 Weekend: The difference in losses found between Straight Through and Daily Scheduled Current Control and Daily Scheduled Losses Control Algorithms.

Table 12 shows the switch positions that were found by the Daily ideal current control algorithm and the daily cable losses control algorithm at weekend. The table shows that the same three of the nine feeder switch positions are chosen by the algorithms as during the weekday analysis and that the feeder position $\mathrm{X}(C_B, C_A)$ is favoured by both.

Month	Daily ideal current control algorithm $_{24h}ICC_{k+1}$	Daily losses control lgorithm $_{24h}ILC_{k+1}$
January	$X_4 = X(\boldsymbol{C}_B, \boldsymbol{C}_A)$	$X_4 = X(\boldsymbol{C}_B, \boldsymbol{C}_A)$
February	$X_4 = X(\boldsymbol{C}_B, \boldsymbol{C}_A)$	$X_4 = X(\boldsymbol{C}_B, \boldsymbol{C}_A)$
March	$X_4 = X(\boldsymbol{C}_B, \boldsymbol{C}_A)$	$X_9 = X(\boldsymbol{C}_C, \boldsymbol{C}_C)$
April	$X_2 = X(\boldsymbol{C}_A, \boldsymbol{C}_B)$	$X_2 = X(\boldsymbol{C}_A, \boldsymbol{C}_B)$
May	$X_9 = X(\boldsymbol{C}_C, \boldsymbol{C}_C)$	$X_4 = X(\boldsymbol{C}_B, \boldsymbol{C}_A)$
June	$X_4 = X(\boldsymbol{C}_B, \boldsymbol{C}_A)$	$X_9 = X(\boldsymbol{C}_C, \boldsymbol{C}_C)$
July	$X_4 = X(\boldsymbol{C}_B, \boldsymbol{C}_A)$	$X_4 = X(\boldsymbol{C}_B, \boldsymbol{C}_A)$
August	$X_4 = X(\boldsymbol{C}_B, \boldsymbol{C}_A)$	$X_4 = X(\boldsymbol{C}_B, \boldsymbol{C}_A)$
September	$X_4 = X(\boldsymbol{C}_B, \boldsymbol{C}_A)$	$X_4 = X(\boldsymbol{C}_B, \boldsymbol{C}_A)$
October	$X_9 = X(\boldsymbol{C}_C, \boldsymbol{C}_C)$	$X_9 = X(\boldsymbol{C}_C, \boldsymbol{C}_C)$
November	$X_4 = X(\boldsymbol{C}_B, \boldsymbol{C}_A)$	$X_4 = X(\boldsymbol{C}_B, \boldsymbol{C}_A)$
December	$X_4 = X(\boldsymbol{C}_B, \boldsymbol{C}_A)$	$X_4 = X(\boldsymbol{C}_B, \boldsymbol{C}_A)$

Table 12 *Switch Positions found for the Daily ideal current control algorithm and the daily cable losses control algorithm for each month of the year*

6.2   Dynamic Current and Losses Control Algorithms - Results

In order to ensure that the short-term imbalances caused by temporal load variations are dealt with it is necessary to employ dynamic reconfiguration of the network. Dynamic network reconfiguration requires continuous monitoring of the currents flowing in the network and then the evaluation of each feeder switch position in order to determine the one that minimises the total current in the hot spot.   By repetitively executing the control algorithm, it is expected that the short-term imbalances can be addressed much more adequately when compared to scheduled phase reconfiguration, which focuses on addressing the average phase imbalance.

Dynamic reconfiguration requires repetitive calculation of the optimal feeder switch positions which may for some time periods and situations be unnecessary, especially during light loading conditions and when the neutral current is low. Hence, the rate of control algorithm execution can be readily modified according to the load conditions and the magnitude of neutral current. The possibility of using an adaptive sampling rate for the controller is facilitated by the fact that model of the network is described by algebraic rather than differential equations. Hence, time-dependent relationships are ignored by the model used within control algorithm. However, to explore the impact as thoroughly as possible within this thesis, the sampling rate of the controller equals that of the simulation for all the results that are documented.

6.2.1 *Weekday: Dynamic Current Control Algorithms Versus Straight Through*

The simulation results shown in Fig. 47 display the trends of total current in the feeder's hot spot for all months of the year on a weekday when PSs are employed using the simple model based, non-causal ideal current, and causal ideal current algorithms. Also, to provide direct comparison the current trend for the straight through configuration plot is provided. The Straight Through current plot is located to the top left of Fig. 47 and is observed as being generally greater in magnitude than that shown in the plots representing the algorithms, this is particularly evident during the winter months. However, when the algorithms are compared with each other no significant difference can be reported which suggests that the simple model based controller algorithm is comparable to the high fidelity Non-Causal and causal ideal current controller algorithms that use the OpenDSS model in conjunction with measurements from every connected load.
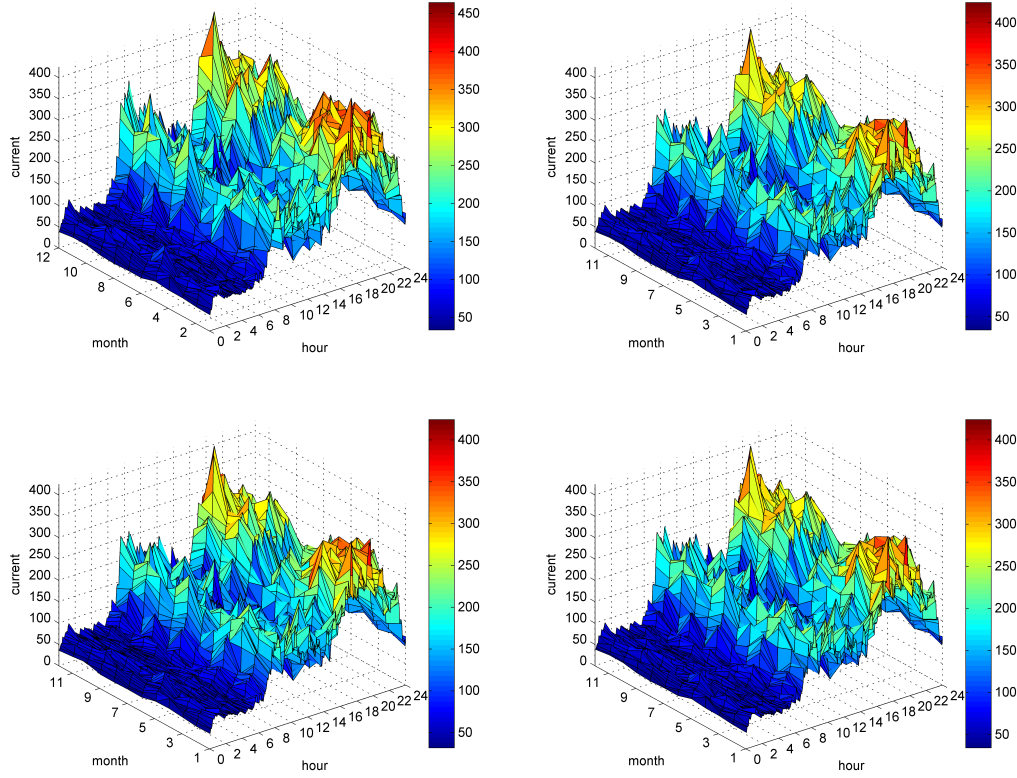
Fig. 47: Daily Weekday Current flow Result in the hot spot

Top Left: *Straight through configuration*

Top Right: *Simple model based controller algorithm -* $_{5m}SMCC_k$

Bottom Left: *Non-causal ideal current controller algorithm -* $_{5m}ICC_{k+1}$

Bottom Right:*Causal ideal current controller Algorithm -* $_{5m}ICC_k$

The histogram provided in Fig. 48 highlights the peak time values for total hot spot current when the straight through configuration was adopted and also when peak time scheduled current control algorithm and each of the 3 dynamic control algorithms were used to select the feeder switch position. The figure clearly shows that for every month of the year all the dynamic control algorithms reduce the total peak time hot spot current when compared to the straight through configuration. The figure also shows an additional benefit in 11 of the 12 months when the dynamic control algorithms are employed rather than the peak time Scheduled ideal current control algorithm. The exception to this case occurs in the month of April where the peak time Scheduled ideal current control algorithm achieves a greater benefit than the causal dynamic control algorithms. This exception suggests that temporal imbalances caused by

the loads are sometimes shorter than the causal algorithms 5min period. However, it is evident that the non-causal ideal current controller algorithm always achieves the greatest benefit of all in all the 12 months considered. The non-causal ideal current controller algorithms show the scope for an additional benefit to be realised either by employing an algorithm that predicts changes in load and/or by speeding up the sampling period or switching frequency.
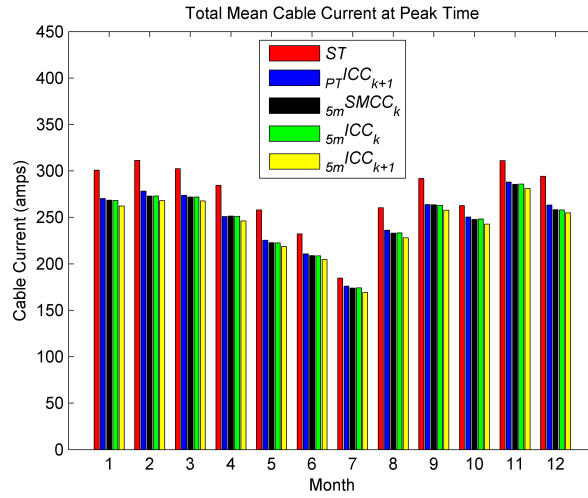
Fig. 48 Weekday: Mean hot spot peak time cable current for straight through, peak time scheduled current control algorithm, simple model based controller and causal Ideal current controller and non causal ideal current controller algorithms.

Fig. 49 shows the amount of total cable current that each of the control algorithms unlock in amps and as a percentage of total current when the straight through configuration is adopted. Comparison of the simple model based controller algorithm and the causal ideal current controller algorithm shows that the former unlocked less current in 8 months, but more current in 4 months. Although, the mean annual peak time current unlocked by the simple model based controller algorithm was 10.08% (28.02amps) of the total cable current, whilst the causal ideal current controller Algorithm unlocked 10.09% (28.09amps) of the total cable current. Therefore, the simple model based controller algorithm unlocked virtually the same current as the causal ideal current controller algorithm model which is significant because it proves that a simple causal

model that uses only a few inputs is virtually as effective as a high-fidelity OpenDSS model that requires inputs from every load on the feeder.
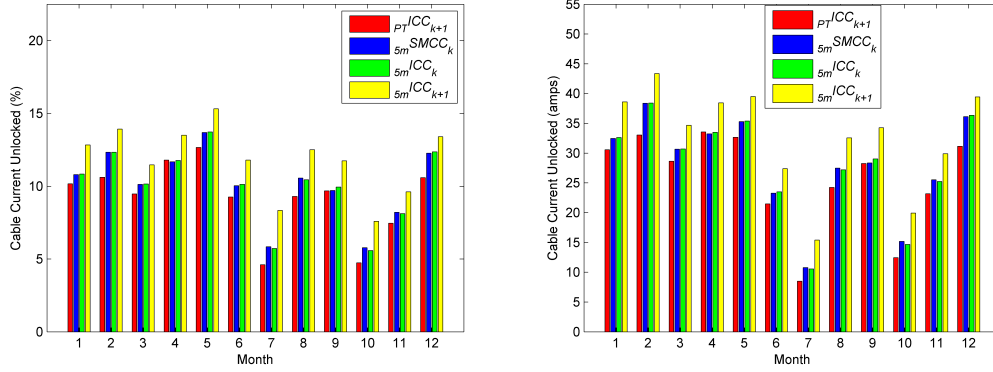
Fig. 49: Hot spot mean peak time cable current unlocked by the peak time scheduled current control algorithm, simple model based controller and causal ideal current controller and non causal ideal current controller algorithms: **Left:** *As a percentage of potal cable current* **Right:** *In amps.*

The plots in Fig. 50 through to Fig. 53 show the phase and neutral conductor currents in the feeder hot spot for the: straight through configuration, simple model based controller algorithm, non-causal ideal current controller algorithm and causal ideal current controller for all seasons and months on a weekday. Simple visual inspection of the trends uncover little difference in terms of the phase and neutral current profiles for the 2 causal algorithms. Hence, as previously noted the simple model based controller algorithm delivers comparable performance to the causal ideal current controller algorithm even though it uses a considerably more complicated OpenDSS model. This is a significant finding due to the fact that the causal ideal current controller algorithm is costly and difficult to implement due to its high fidelity OpenDSS model requiring measurements from every dwelling on the feeder as inputs. Whereas, the simple model based controller algorithm relies only on phase current measurements taken at the transformer(s) and PSs for inputs, which it is thought to be economically feasible today when compared to reinforcement or replacement.

The traces from the non-causal ideal current controller algorithm in Fig. 50 through to Fig. 53 show a reduction in neutral current and better phase current balance than all

106

the others. However, the non causal nature of this algorithm effectively assumes knowledge of the state of the network one sampling period ahead of time at $k+1$ where k is the discrete sampling instant. This assumption means that the algorithm is useful in providing the benchmark result for a given PS scheme where the number of PS and the sampling period is set.
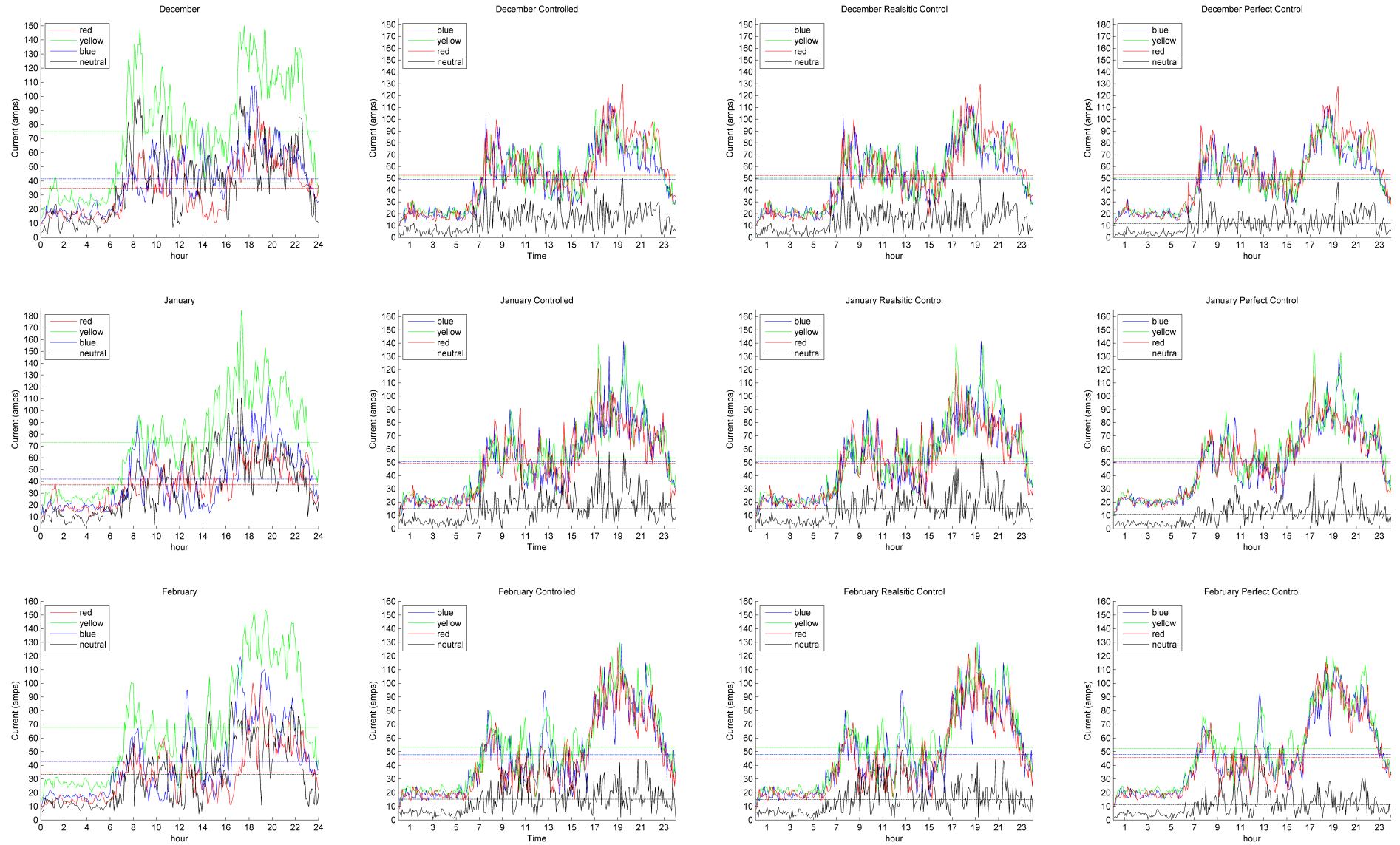
Fig. 50 Winter: Weekday phase and neutral currents of the example feeder's hot spot (from left to right the plots show switch positions determined by the following Control Algorithms: straight through configuration, $_{5m}SMCC_k$, $_{5m}ICC_k$ and $_{5m}ICC_{k+1}$ respectively. Dotted lines indicate 24 hour mean values.)
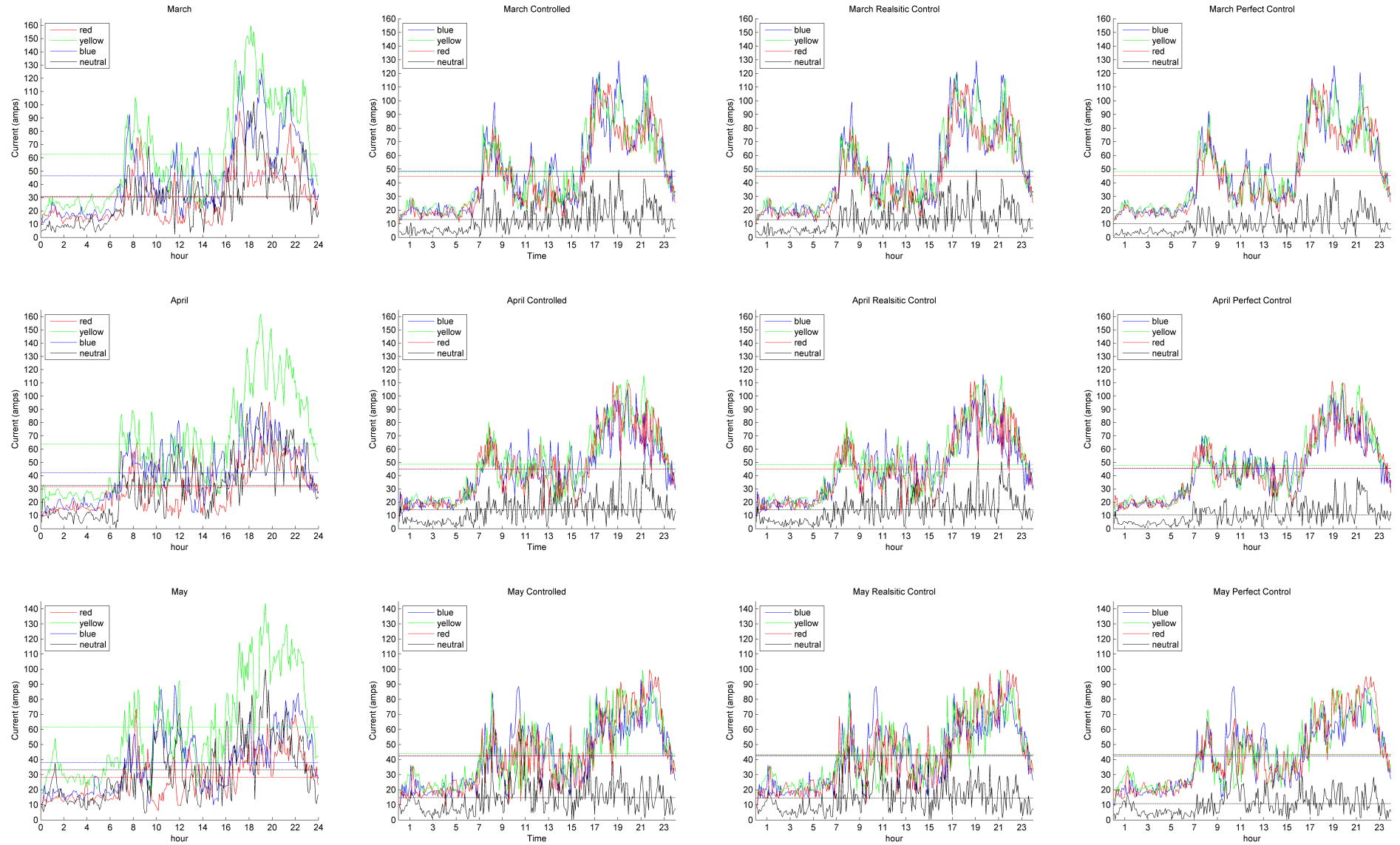
Fig. 51 Spring: Weekday phase and neutral currents of the example feeder's hot spot (from left to right the plots show switch positions determined by the following Control Algorithms: straight through configuration, $_{5m}SMCC_k$, $_{5m}ICC_k$ and $_{5m}ICC_{k+1}$ respectively. Dotted lines indicate 24 hour mean values.)
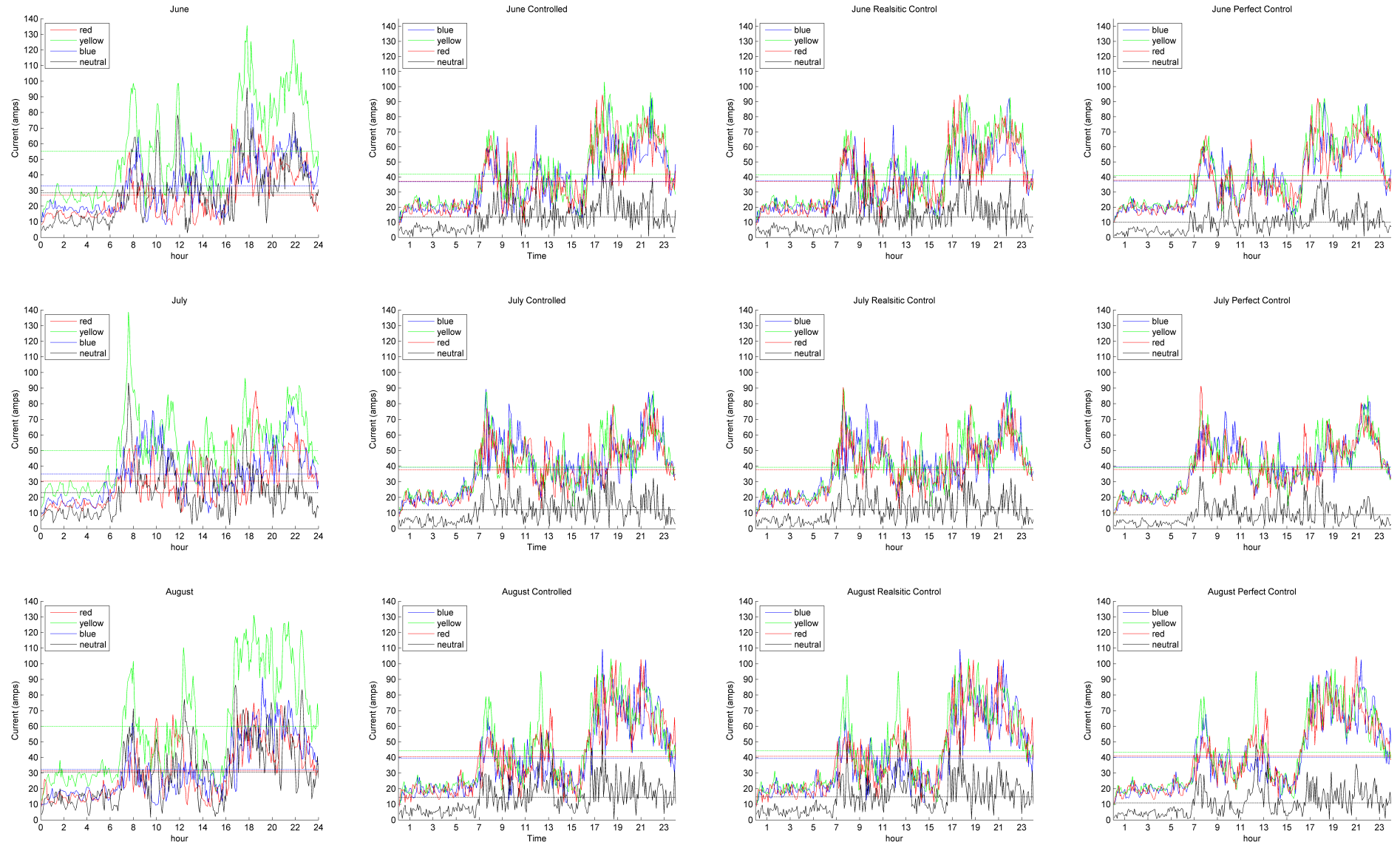
Fig. 52 Summer: Weekday phase and neutral currents of the example feeder's hot spot (from left to right the plots show switch positions determined by the following Control Algorithms: straight through configuration, $_{5m}SMCC_k$, $_{5m}ICC_k$ and $_{5m}ICC_{k+1}$ respectively. Dotted lines indicate 24 hour mean values.)
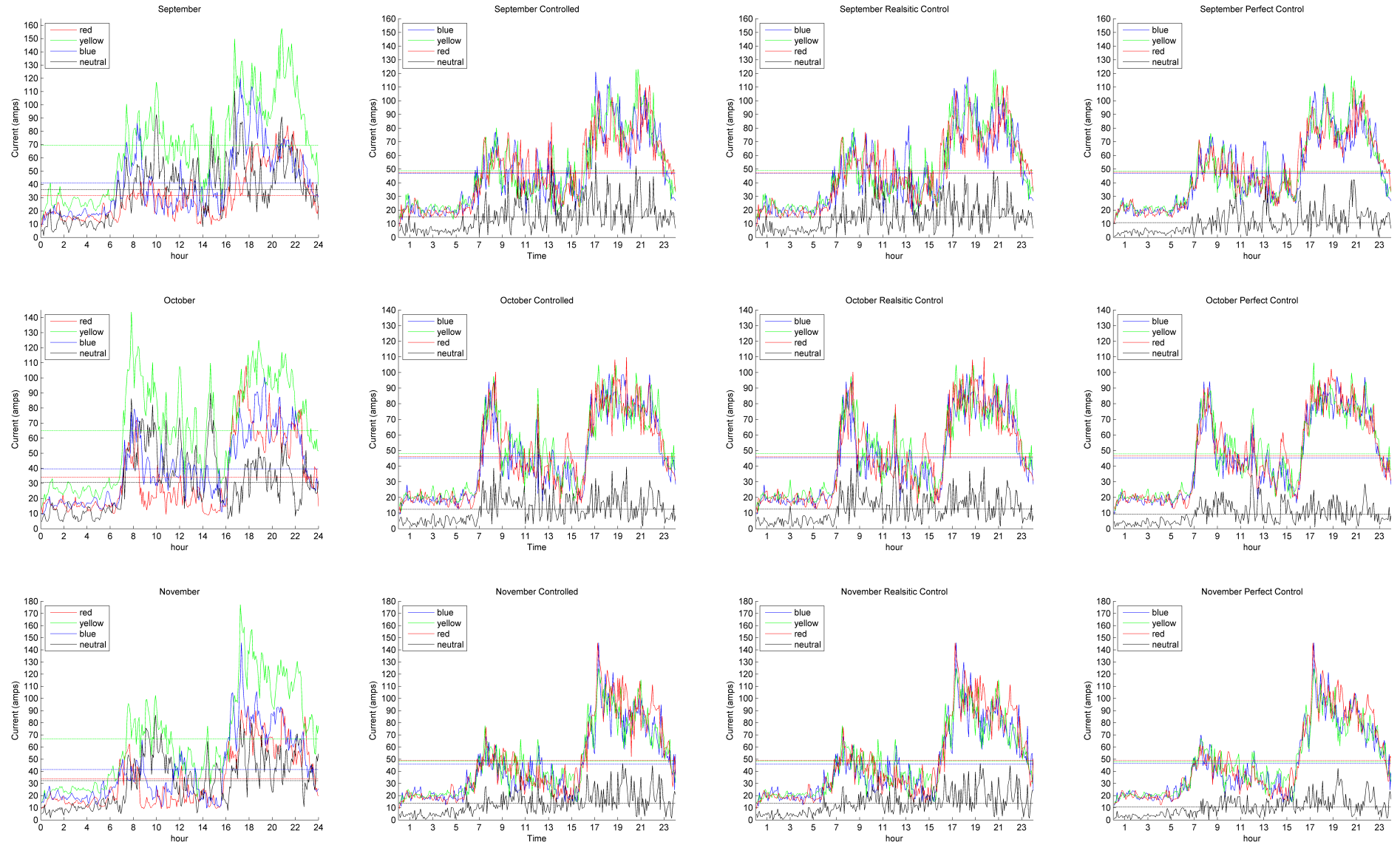
Fig. 53 Autumn: Weekday phase and neutral currents of the example feeder's hot spot (from left to right the plots show switch positions determined by the following Control Algorithms: straight through configuration, $_{5m}SMCC_k$, $_{5m}ICC_k$ and $_{5m}ICC_{k+1}$ respectively. Dotted lines indicate 24 hour mean values.)

6.2.2 Weekday: The impact of Current Control Algorithms on Losses

This section details the weekday results that show the effect on total cable losses that PSs have when the are set using the straight through configuration, scheduled ideal current controller algorithm, simple model based controller algorithm, non-causal ideal current controller algorithm and causal ideal current controller Algorithm.

The histograms provided in Fig. 54 highlight the total cable losses of the feeder for each of the considered control algorithms. The chart to the left in the figure shows the straight through configuration which incurs greater losses than all the other control algorithms. Whilst, that that on the right of Fig. 54 shows the difference from the straight through configuration for each of the control algorithms. Observation of the histogram to the right clearly shows the reduction in losses that the algorithms facilitate when they control PSs. The scheduled ideal current controller algorithm was found to cause higher total cable losses than the other algorithms in 9 of the 12 months with the 3 exceptions occurring in October, March and April. It may seem surprising that there are a few results where the scheduled ideal current controller algorithm achieved a greater benefit than the ideal dynamic current control algorithm. These 3 exceptions suggest that for cases where the objective is to minimise losses rather than unlock capacity, a dynamic losses based algorithm should be specifically developed. Also, that optimising hot spot current using a 5min frequency does not always optimise the total losses of a feeder.

As shown in the right hand histogram in Fig. 54, the scheduled ideal current controller algorithm, simple model based controller algorithm, causal ideal current controller Algorithm and non-causal ideal current controller algorithm achieved annual peak time reductions in losses of 0.8016kWh, 0.9518kWh, 0.9514kWh and 1.05kWh respectively. Therefore, on average over 12 months the algorithms performed exactly as would be expected because the non-causal current controller algorithm is the best at minimising total losses, the causal ideal current controller and simple model based controller were found to be very similar and 2nd best whilst, the scheduled ideal current controller algorithm is the least effective at minimising total losses.
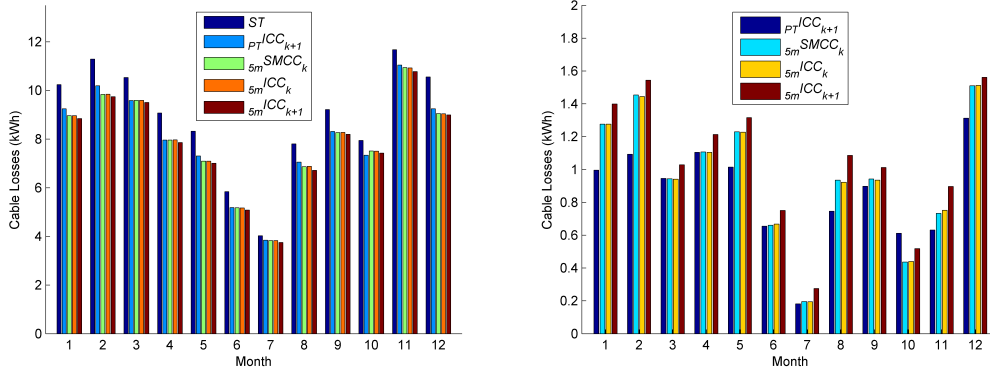
*Fig. 54: Weekdays **Left:** Real total cable Losses for example feeder at peak time **Right:** Difference in mean peak time real cable losses from straight through*

6.2.3 Weekend: Dynamic Current Control Algorithms Versus Straight Through

6.2.3.1 Annual Plots

The simulation results in Fig. 55 display the trends of total current in the feeder's hot spot for all months of the year on a weekend when PSs are employed using the simple model based, non-causal ideal current, and causal ideal current algorithms. The plots in Fig. 55 show the load to be more evenly spread across the day when compared to corresponding weekday plots shown in Fig. 47, but the observations are the same as those for weekdays contained in section 6.2.1.
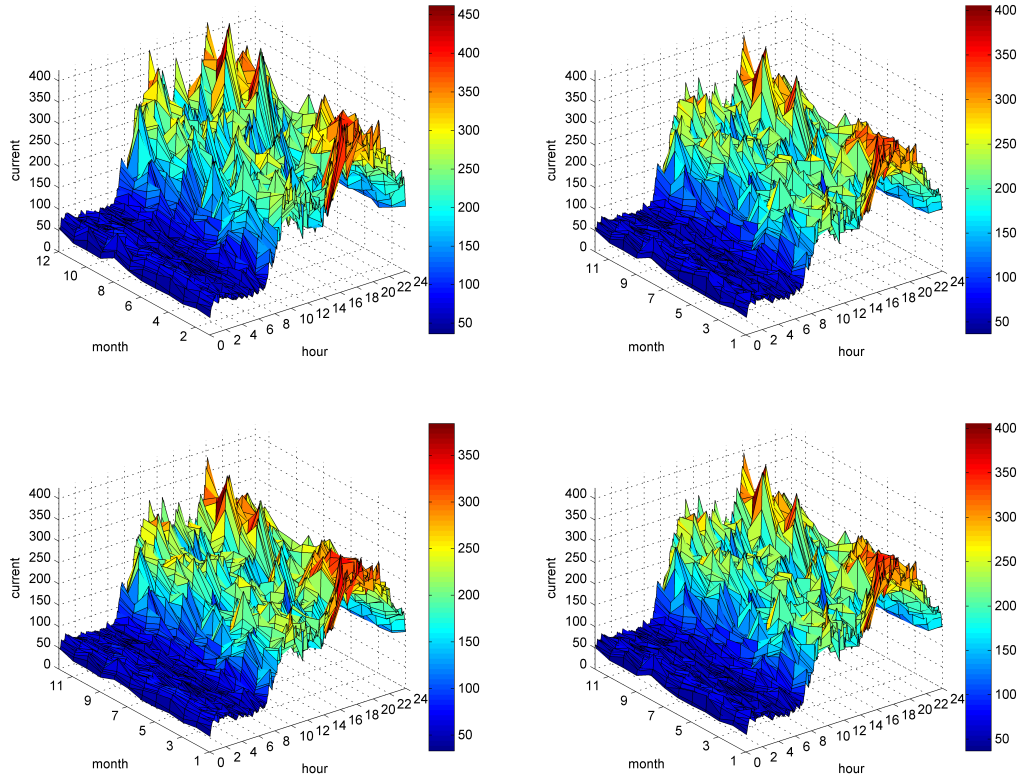
Fig. 55: Daily Weekday Current flow Result in the hot spot

Top Left: *straight through configuration -* $\quad X = X_I$

Top Right: *simple model based controller algorithm -* $\quad _{5m}SMCC_k$ - $\quad X = \check{X}$

Bottom Left: *non-causal ideal current controller algorithm -* $\quad _{5m}ICC_{k+1}$ - $\quad X = \dot{X}$

Bottom Right:*causal ideal current controller Algorithm -* $\quad _{5m}ICC_k$ - $\quad X = \bar{X}$

The histogram provided in Fig. 56 shows the peak time mean hot spot cable current at a weekend. The figure clearly shows that for every month of the year all the algorithms reduce the total peak time hot spot current when compared to the straight through configuration. The figure also shows an additional benefit in 10 of the 12 months when the dynamic control algorithms are employed rather than the peak time scheduled ideal current control algorithm. Therefore, for the weekend case, 2 months were found that the peak time scheduled ideal current control algorithm achieved a greater peak time reduction in hot spot current which is an additional month to that found on weekdays. Although they are sparse, the cases where the scheduled algorithm outperform the dynamic algorithm show that the 1 month exception found for a weekday was not an anomaly. The cause may be that the sampling frequency is insufficient to for the number of loads on this particular feeder but further work is required to establish its specific nature. Another likely contributing factor is the number of dwellings on a feeder which is expected to have an impact on the algorithms sampling time, feeders with greater numbers of loads may will have smoother aggregated current and perhaps require lower frequency sampling.
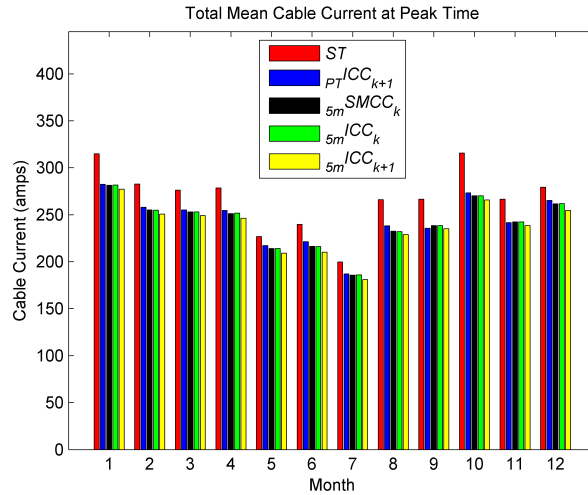
Fig. 56 Mean cable current at peak time in hot spot.

Fig. 57 shows the amount of total cable current that each of the control algorithms unlock both in amps and as a percentage of total current when the straight through configuration is adopted. As found for weekdays in Fig. 49, comparison of the simple model based controller algorithm and the causal ideal current controller Algorithm shows that the former unlocked less current in 8 months, but more current in 4 months.

Although the mean annual peak time current unlocked by the simple model based controller algorithm was 9.45% (25.9amps) of the total cable current, the causal ideal current controller Algorithm unlocked 10.09% (28.09amps) of the total cable current. Therefore, the simple model based controller algorithm unlocks virtually the same current as the causal ideal current controller algorithm model which consolidates the finding that a simple causal model using only a few inputs is virtually as effective as a high-fidelity OpenDSS model that requires inputs from every load on the feeder.
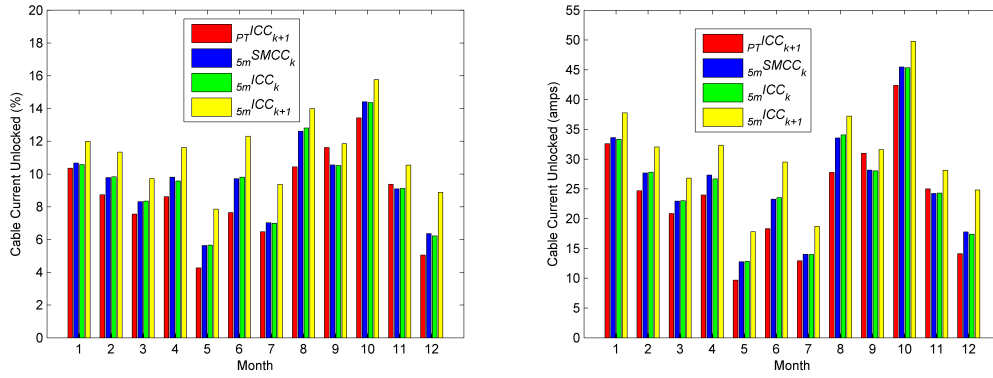
*Fig. 57: Hot spot mean cable current unlocked at peak time **Left:** As a Percentage of Total Cable Current **Right:** In amps*

The plots in Fig. 58 through to Fig. 61 show the phase and neutral conductor currents in the feeder hot spot for the: straight through configuration, simple model based controller algorithm, non-causal ideal current controller algorithm and causal ideal current controller Algorithm, for all seasons and months on a weekend. These weekend plots show the load to be more evenly spread over the day when compared to corresponding weekday plots in Fig. 50 through to Fig. 53. The similarity in the weekday traces of the non-causal ideal current controller algorithm and the simple model based controller algorithm are reflected in the weekend result shown in Fig. 58 through to Fig. 61. This provides further evidence that the simple causal model that uses only a few inputs is virtually as effective as a high-fidelity OpenDSS model which requires inputs from every load on the feeder and would therefore be considerably more expensive. Aside from the general spread of the load, the other observations made of the plots are the same as those for weekdays contained in section 6.2.1.
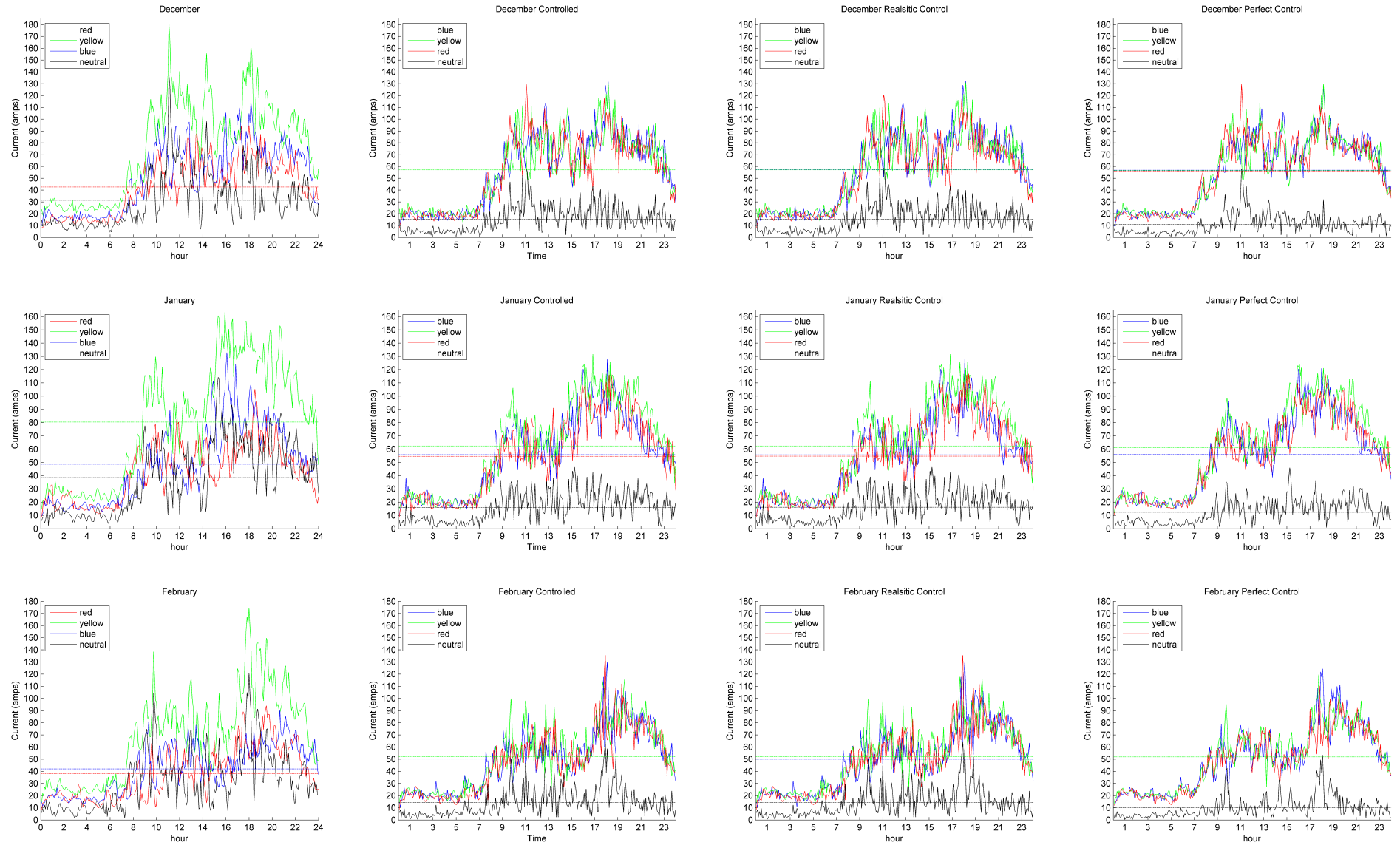
Fig. 58 Winter: Weekend phase and neutral currents of the example feeder's hot spot (from left to right the plots show switch positions determined by the following Control Algorithms: straight through configuration, $_{5m}SMCC_k$, $_{5m}ICC_k$ and $_{5m}ICC_{k+1}$ respectively. Dotted lines indicate 24 hour mean values.)
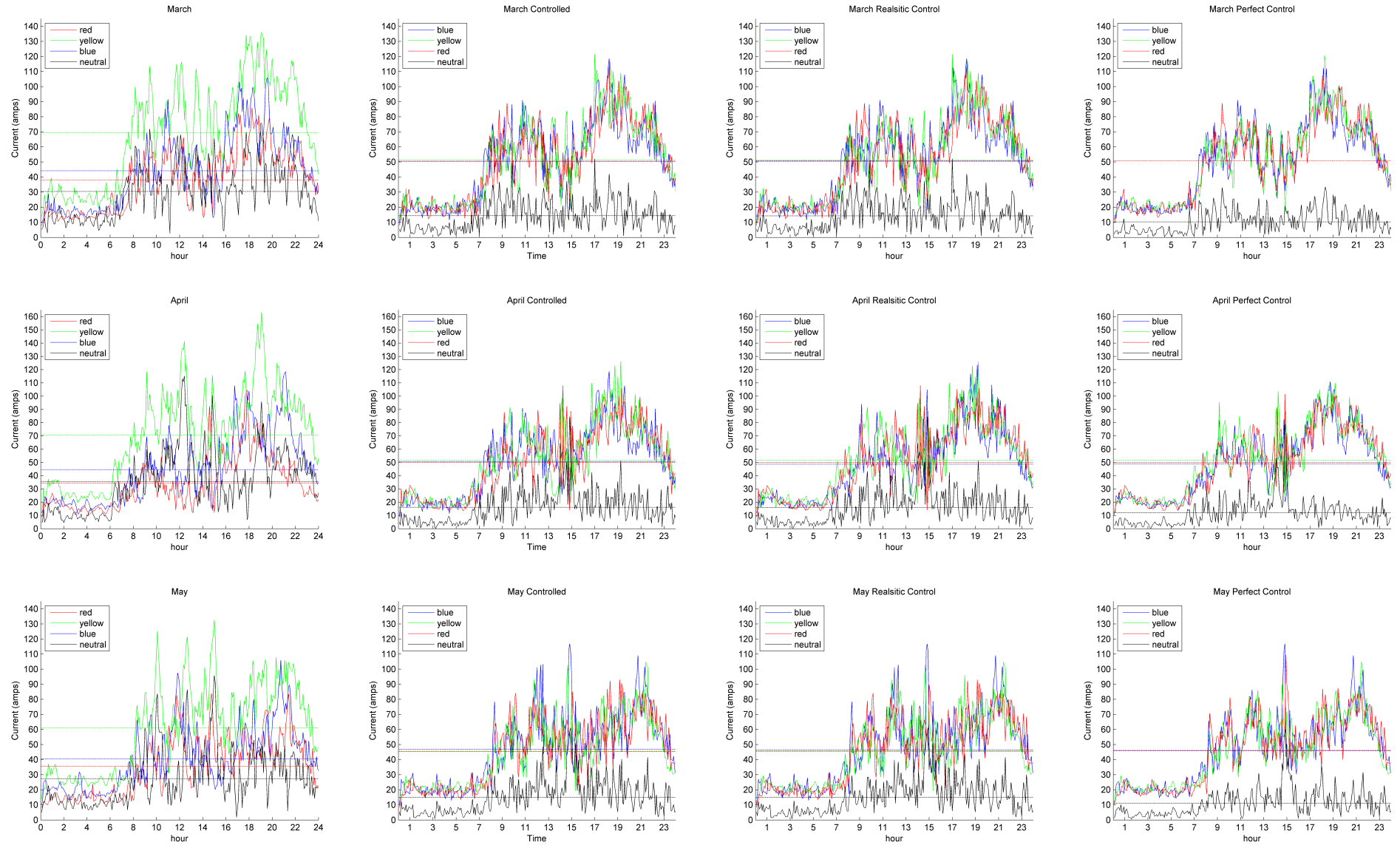
Fig. 59 Spring: Weekend phase and neutral currents of the example feeder's hot spot (from left to right the plots show switch positions determined by the following Control Algorithms: straight through configuration, $_{5m}SMCC_k$, $_{5m}ICC_k$ and $_{5m}ICC_{k+1}$ respectively. Dotted lines indicate 24 hour mean values.)
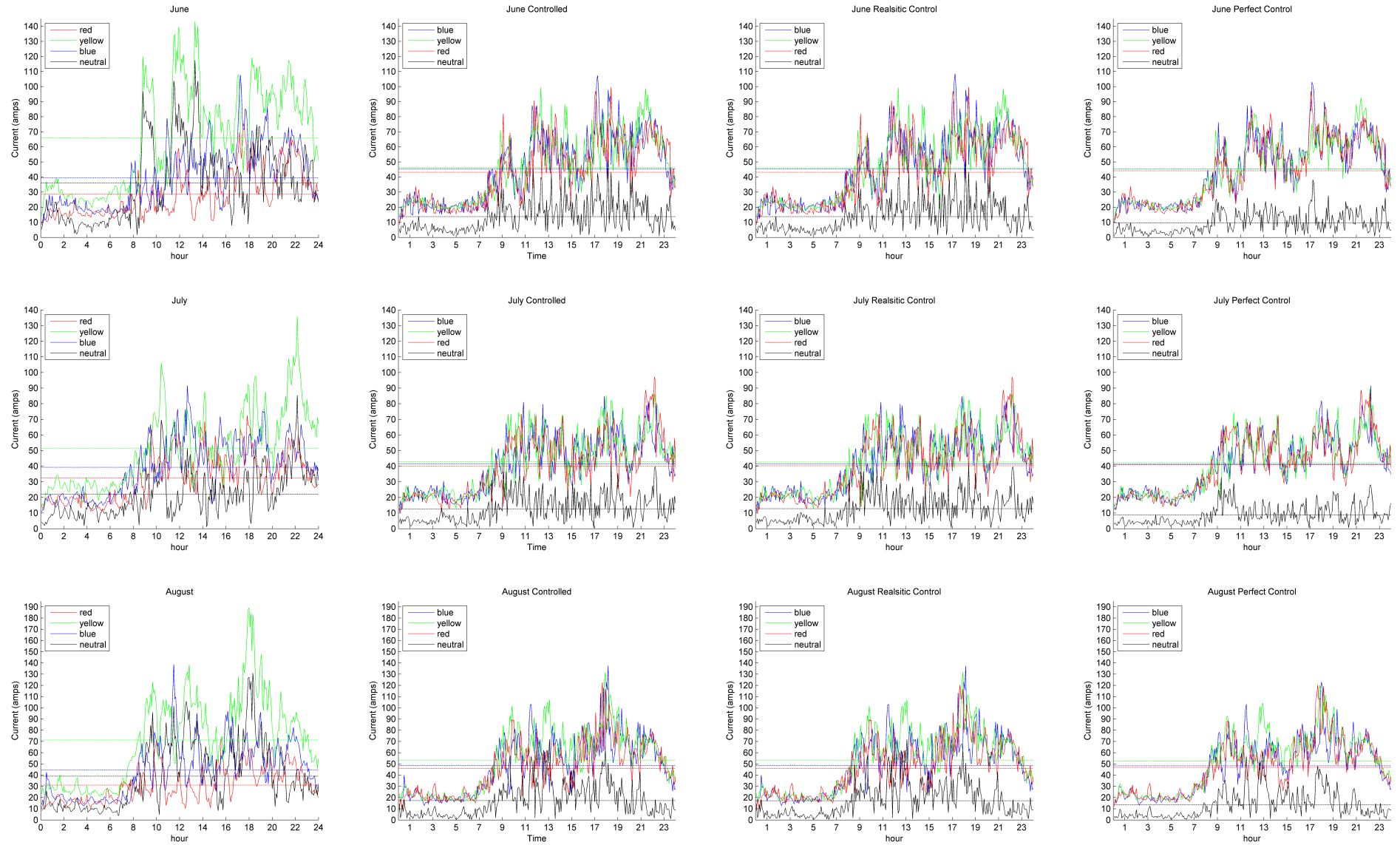
Fig. 60 Summer: Weekend phase and neutral currents of the example feeder's hot spot (from left to right the plots show switch positions determined by the following Control Algorithms: straight through configuration, $_{5m}SMCC_k$, $_{5m}ICC_k$ and $_{5m}ICC_{k+1}$ respectively. Dotted lines indicate 24 hour mean values.)
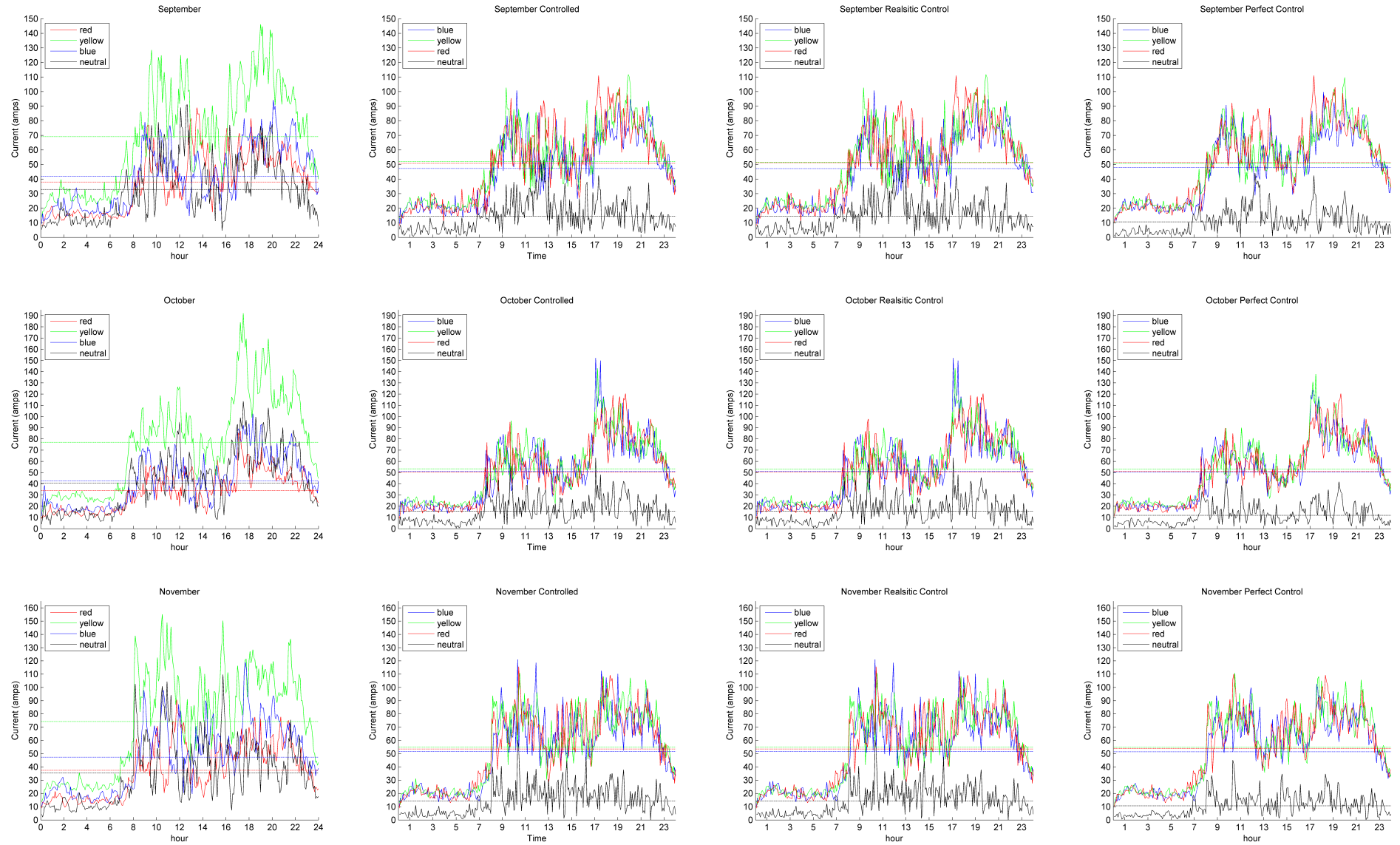
Fig. 61 Autumn: Weekend phase and neutral currents of the example feeder's hot spot (from left to right the plots show switch positions determined by the following Control Algorithms: straight through configuration, $_{5m}SMCC_k$, $_{5m}ICC_k$ and $_{5m}ICC_{k+1}$ respectively. Dotted lines indicate 24 hour mean values.)

6.2.4 Weekend: The impact of Current Control Algorithms on Losses

This section details the weekend results that show the effect on total cable losses when PSs are set using the straight through configuration, scheduled ideal current controller algorithm, simple model based controller algorithm, non-causal ideal current controller algorithm and causal ideal current controller Algorithm.

The total cable losses of the feeder are shown in Fig. 62, where the left hand histogram highlights the straight through configuration as incurring greater losses than all all the control algorithms. Whilst, the right-hand histogram in Fig. 62 is provided to show the difference between each of the algorithms and the straight through configuration. Both plots clearly show the reduction in losses that the algorithms facilitate when they control PSs. The scheduled ideal current controller algorithm was found to cause higher total cable losses than the other algorithms in 6 of the 12 months which is a result that shows it to be as effective on weekends as the dynamic algorithms for reducing total cable losses. Therefore, this weekend result shows that the dynamic current controller algorithms that specifically focus on unlocking hot spot current do not also always provide as good a result in terms of total feeder cable losses as the scheduled ideal current controller algorithm. The reason for this result is likely to be that although the dynamic current controller algorithms do unlock hot spot current, they ignore unbalances in the feeder cables that lie between dwellings.
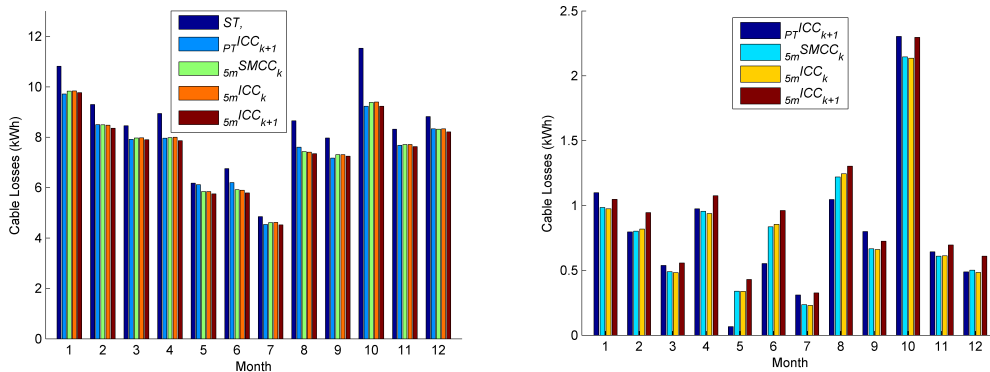
*Fig. 62: Weekends **Left:** Real cable losses for the example feeder at peak time **Right:** Difference in mean peak time Real Cable Losses from straight through*

6.2.5 Reduced Generating Capacity Estimate

The results in section 6.2.2 and 6.2.4 show that PSs effectively curtail the generation requirement by reducing cable losses. An estimate for the size of reduction in UK generating capacity when PSs are controlled by the the simple model based controller algorithm nationally is provided for each month of the year in Fig. 63. The values shown assume the example feeder is average for the UK and were calculated by constructing a mean week for every month of the year using the real losses results documented section 6.2.2 and 6.2.4. The figure shows that the maximum reduction to be 75MW which occurs in the winter months and the minimum of 12.4MW to occur in the summer. The annual mean reduction in generating capacity obtained is 54.6MW which roughly equates to half a wind farm like Burbo Bank which is Located at the mouth of the river Mersey and comprises of 25 3.6MW wind turbines.
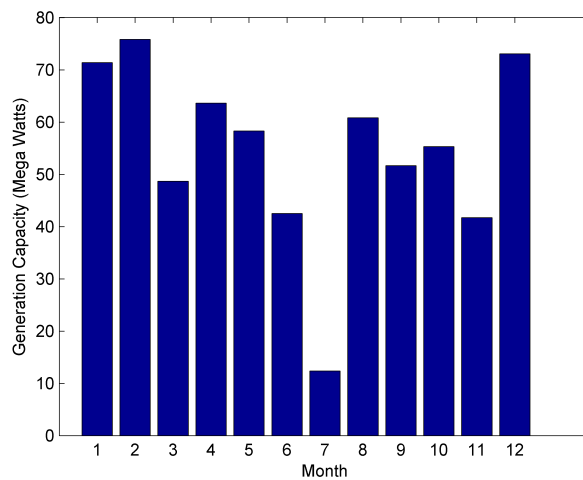
Fig. 63 Estimate of the daily UK reduction in generating capacity that may be achieved if PSs were applied nationally employed by the simple model based controller algorithm.

7 PV Penetration on LV Feeders

This chapter documents assessment methodologies that can be used to establish a feeder's susceptibility to OV induced by PV. Also, it details what impact PSs have on the example feeder when they are scheduled to create voltage headroom for the case where they are placed: at the fixed locations identified in section 5.3.4, and explicitly to maximise voltage headroom. The fundamental assumptions that are used in this chapter are outlined in advance and the chapter is structured as follows. The assessment methods are documented that search for PV penetration scenarios upon dwellings that cause OV, where the smallest and largest number of dwellings allocated PV are considered as the worst and best case scenarios respectively. Next, using the example feeder, the impact of PSs on the results achieved by the assessments is documented. Finally, random scenarios are generated where PV is allocated to a proportion of dwellings on the example feeder, and the impact that two PSs have when they are and are not explicitly placed is shown.

In order to reduce computational complexity whilst also considering the worst-case impact of PV on OV in a given network, it is assumed that the loads are inactive and that PV is active and rated at 4kW. The PV rating of 4kW was chosen because 86% of all DG installations in the UK are of this rating as noted in chapter 1. Such assumptions allow a snapshot evaluation of the impact that PV installations have on the feeder voltage profile. Also, by removing the impact of the loads, which act as counterbalance to the distributed generation in the context of voltage fluctuation, the worst case scenario in terms of the voltage rise is considered.

In this chapter, it is assumed that the P_b matrix, initially introduced in Chapter 3, which contains elements that represent the number of dwellings that are connected to a particular bus and phase only. Also, it is assumed that PV can only be allocated to dwellings, such a constraint is imposed by constructing a matrix, denoted as P_b^{max}, that specifies the permissible locations for PV installation. An example of P_b^{max} is given as follows:

$$\boldsymbol{P}_b^{max} = \begin{bmatrix} 0 & 0 & 0 & 0 & 1 \\ 1 & 1 & 0 & 0 & 0 \\ 0 & 0 & 1 & 0 & 0 \end{bmatrix} \tag{88}$$

Note that the maximum number of possible PV installations is the sum of the elements that make up $\boldsymbol{P}_b^{max}$. The feeder that is represented by $\boldsymbol{P}_b^{max}$ in (88) is given in Fig. 64 below.
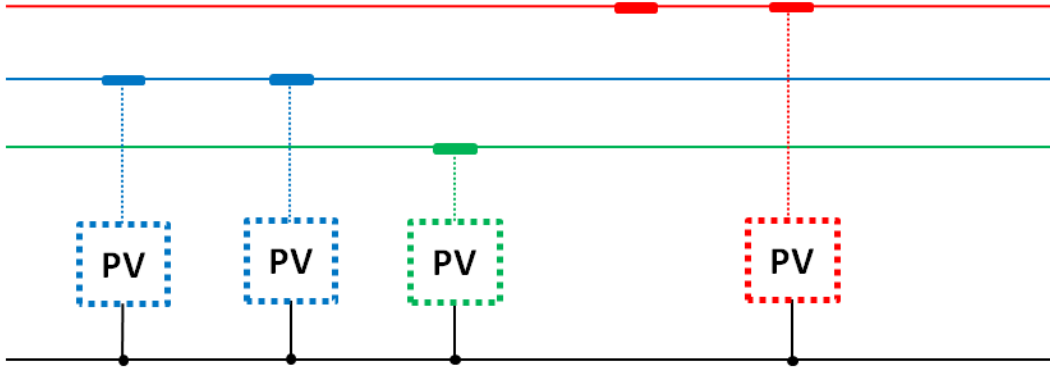
Fig. 64 $\boldsymbol{P}_b^{max}$ *example network*

In this particular example there are 4 dwellings and therefore 4 possible locations for PV installation. The dashed lines link to buses that could accommodate PV installations and the buses that do not have dashed lines attached cannot host PV connections.

When allocating PV installations, the following element-wise constraint must to be satisfied:

$$\boldsymbol{P}_b \leq \boldsymbol{P}_b^{max} \tag{89}$$

$\boldsymbol{P}_b$ contains the information regarding the phase connection of the individual PV installations. Note that each entry in this matrix is equal to either 0 or an integer that reflects the number of connected active PV installations to a particular bus and phase. The number of PV installations for a given realisation of $\boldsymbol{P}_b$ is represented with the variable n_{pv} which is defined as follows:

$$n_{pv} = \sum_{i,j} \boldsymbol{P}_{b,[i,j]} \tag{90}$$

Given a particular realisation of $\boldsymbol{P}_b$ that satisfies the element-wise constraint (89), feeder bus voltages can be computed and stored in a row vector, denoted as $\boldsymbol{v}$, that has as many elements as there are buses in the network. This vector is obtained from a power flow analysis that is a function of $\boldsymbol{P}_b$ which can be mathematically presented as:

$$\boldsymbol{v} = g_v(\boldsymbol{P}_b) \tag{91}$$

Note that the voltage profile is purely dependent on the particular realisation of $\boldsymbol{P}_b$ matrix.

Once $\boldsymbol{v}$ is obtained using (91) it is then possible to find its element with the maximum value, which is termed maximum feeder bus voltage and is denoted as v^*:

$$v^* = \max_i v_{[i]} \tag{92}$$

The matrix $\boldsymbol{P}_b$ can be generated as many times as the particular method outlined in this section dictates, but the core process described above is the same and relevant to them all.

7.1   The Assessment of LV Feeders

This section outlines the Uniform Random Assessment, Impedance Assessment and Incremental PV Allocation Through Simulation Assessment methods. The methods are then simulated on the example feeder model that incorporates PSs placed at the fixed locations used in chapter 6. A discussion is provided that compares results from the different assessment methodologies and the impact that feeder switch position has on scores is summarised.

7.1.1 The Uniform Random Assessment Method

This method assumes equal (uniform) probability of PV installation for each dwelling on a given network. It then randomly allocates n_{pv} PV installations so that:

$$\sum_{i,j} \boldsymbol{P}_{b,[i,j]} = n_{pv} \tag{93}$$

Whilst satisfying the following constraint:

$$\boldsymbol{P}_b \leq \boldsymbol{P}_b^{max} \tag{94}$$

The PV is now allocated, next all the feeder's bus voltages are calculated using a power flow analyser:

$$\boldsymbol{v} = g_v(\boldsymbol{P}_b) \tag{95}$$

Then, the maximum bus voltage is found:

$$v^* = \max_i (\boldsymbol{v}_{[i]}) \tag{96}$$

The steps outlined in (93) through to (96) are then iterated N times whilst keeping n_{pv} constant and for each iteration, the maximum feeder voltage v^* is stored in the vector $\boldsymbol{v}_{n_{pv}}$ which contains N elements as follows:

$$\boldsymbol{v}_{n_{pv},[j]} = v^* \tag{97}$$

Where j is the iteration integer.

Steps (93) through to (97) are then executed over range of PV penetration levels n_{pv} for which the feeder is to be assessed.

To identify the best case and the worst case voltages for a particular level of PV penetration n_{pv}, the following two calculations are performed:

$$\check{\beta} = \min_N (\boldsymbol{v}_{n_{pv}}) \tag{98}$$

$$\hat{\beta} = \max_N (\boldsymbol{v}_{n_{pv}}) \tag{99}$$

Hence for any specific n_{pv}, $\check{\beta}$ denotes the minimum of the maximum feeder bus voltages and, therefore, describes the best case scenario. Conversely, $\hat{\beta}$ is equal to the maximum of the maximum feeder bus voltage and depicts the worst case scenario.

The Particular allocation of PV that either maximises or minimises the maximum feeder voltage is denoted as:

$$\check{P}_b = arg \min_{N} \left(v_{n_{pv}} \right) \tag{100}$$

$$\hat{P}_b = arg \max_{N} \left(v_{n_{pv}} \right) \tag{101}$$

An example result of uniform random assessment performed on the example feeder is provided in the error bar plot shown in Fig. 65. It shows the results obtained when the iteration level was set to 100 for each of the 71 unique PV penetration levels which are identified from the x-axis. Each error bar shows the maximum and minimum voltages found by the method through the execution of steps (93) to (97) for a specific PV penetration level. Whilst, the green and red dotted lines show the worst and best cases that the method found overall to be 9.45% to 46% of PV penetration respectively.
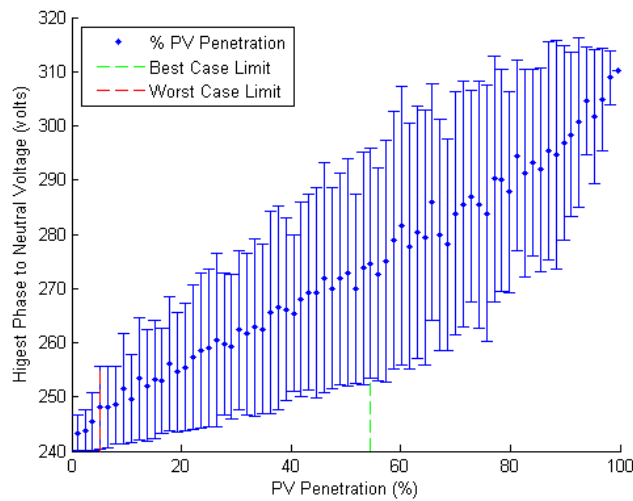
Fig. 65: Maximum feeder bus voltage against the percentage PV penetration range obtained from 100 iterations when loads are considered to be 0W and PV 4kW

7.1.2 The Impedance Method

This method is based on the fundamental property of electrical circuits which is the fact that the voltage across a given cable for a given current flowing through the cable is directly proportional to the impedance of the cable. Hence, for a given current the cable with higher impedance will result in higher voltage change.

If the current is flowing downstream from the secondary substation towards the loads, which is the conventional power flow assumption, then the radial network will experience voltage drop. Conversely, if the distributed generation output installed on the network exceeds the load demand then it will cause reversal of current direction and result in the voltage rise. The amount by which the voltage will rise or drop for a given value of feeder current is determined by the impedance of the cable.

This method is based on the impedance of the cable connecting dwellings to the secondary substation. This information is then used to identify the locations of PV that will result in worst case (maximum voltage rise) and best case (minimum voltage rise) for a given network. The main benefit of this method is that it is simple and requires the analysis of only one variable to find a solution.

To find the worst case result the phase impedance of each dwellings' phase connection is evaluated and the maximum is found. That dwelling is then allocated with a PV and $\boldsymbol{P}_b$ is constructed.

A power flow analysis executed:

$$\boldsymbol{v} = g_v(\boldsymbol{P}_b) \tag{102}$$

The maximum bus voltage is next found:

$$v^* = \max_i v_{[i]} \tag{103}$$

Then, the following condition is evaluated:

$$v^* \le v_{th} \tag{104}$$

Where v_{th} is the threshold voltage which is the maximum acceptable bus voltage.

If the condition (104) is true, the dwelling with the next greatest impedance is allocated PV and the $\boldsymbol{P}_b$ matrix is updated accordingly. Then, steps (102) through to (104) are repeated. Otherwise, the worst case scenario has been found which is defined as:

$$\check{\beta}=\sum_{i,j} \boldsymbol{P}_{b,[i,j]}-1 \tag{105}$$

To find the best case result the phase impedance of each dwellings' phase connection is evaluated and the minimum is found. That dwelling is then allocated with a PV and $\boldsymbol{P}_b$ is constructed.

A power flow analysis executed:

$$\boldsymbol{v}=g_v\left(\boldsymbol{P}_b\right) \tag{106}$$

The maximum bus voltage is next found:

$$v^*=\max_i \boldsymbol{v}_{[i]} \tag{107}$$

Then, the following condition is evaluated:

$$v^* \leq v_{th} \tag{108}$$

Where v_{th} is the threshold voltage which is the maximum acceptable bus voltage.

If the condition (108) is true, the dwelling with the next least impedance is allocated PV and the $\boldsymbol{P}_b$ matrix is updated accordingly. Then, steps (106) through to (108) are repeated. Otherwise, the best case scenario has been found which is defined as:

$$\hat{\beta}=\sum_{i,j} \boldsymbol{P}_{b,[i,j]}-1 \tag{109}$$

7.1.3 The Incremental PV Allocation through Simulation Assessment Method

An exhaustive assessment of the example feeder would take 2.54×10^{13} years if each snapshot solution took just 0.17s to evaluate because there are 2^{72} possible permutations of PV allocation. Therefore, even for a modest feeder the search space is enormous, the Incremental PV Allocation Through Simulation (ITS) method is presented below as an effective alternative to exhaustive feeder assessment.

This method utilises a detailed model of a feeder to identify dwellings for PV allocation to find its best and worst case PV penetration levels. Individual PV installations are allocated one at a time. For each individual PV installation the algorithm is executed N times which is as follows:

$$N = (N_{pv} - n_{pv}) \qquad (110)$$

Where N_{pv} is the total number of possible PV installations, which is equal to the number of dwellings in the network, and n_{pv} is the number of PV installations that have already been allocated.

For every algorithm execution, the maximum bus voltage is obtained for the entire feeder. Once all possible locations of the PV installation are evaluated, the placement of the single PV installation that results in maximum voltage rise (worst case) and also minimum voltage rise (best case) can be identified. The process is then repeated where the n_{pv} integer is incremented by 1.

P_b is modified by including an additional PV installation at each of the N possible locations, the resulting P_b matrix is then used to calculate the maximum feeder voltage for each possible location which is stored in the vector v_{np}. Then, once the maximum feeder voltage is obtained for each possible location, the following two calculations are performed in order to identify the best and the worst case PV allocation:

$$\check{P}_b = arg\, \min_N (v_{np}) \qquad (111)$$

$$\hat{P}_b = arg \max_N (v_{np})$$ (112)

The flow charts for coding the ITS algorithm for the worst and best cases is provided in Fig. 66 and Fig. 67 respectively and all the variables used within them are defined below.

$\check{q}_i^*$ and $\hat{q}_i^*$ are the PV allocation vectors for the worst and best case analysis respectively, j is a counter, k is the total number of dwellings on the feeder, q_t is a temporary PV allocation vector, w is the index of the maximum bus voltage, v is a vector of maximum bus voltages, $\tilde{v}$ is the maximum bus voltage vector, V_{th} is the OV threshold voltage, $\hat{\beta}$ and $\check{\beta}$ is the respective best and worst case number of dwellings that can accommodate PV without causing an OV, v_{pf} is a vector of all bus phase to neutral calculated via a voltages from a power flow, i is the number of dwellings that have been allocated PV and P_b is the phase allocation matrix.
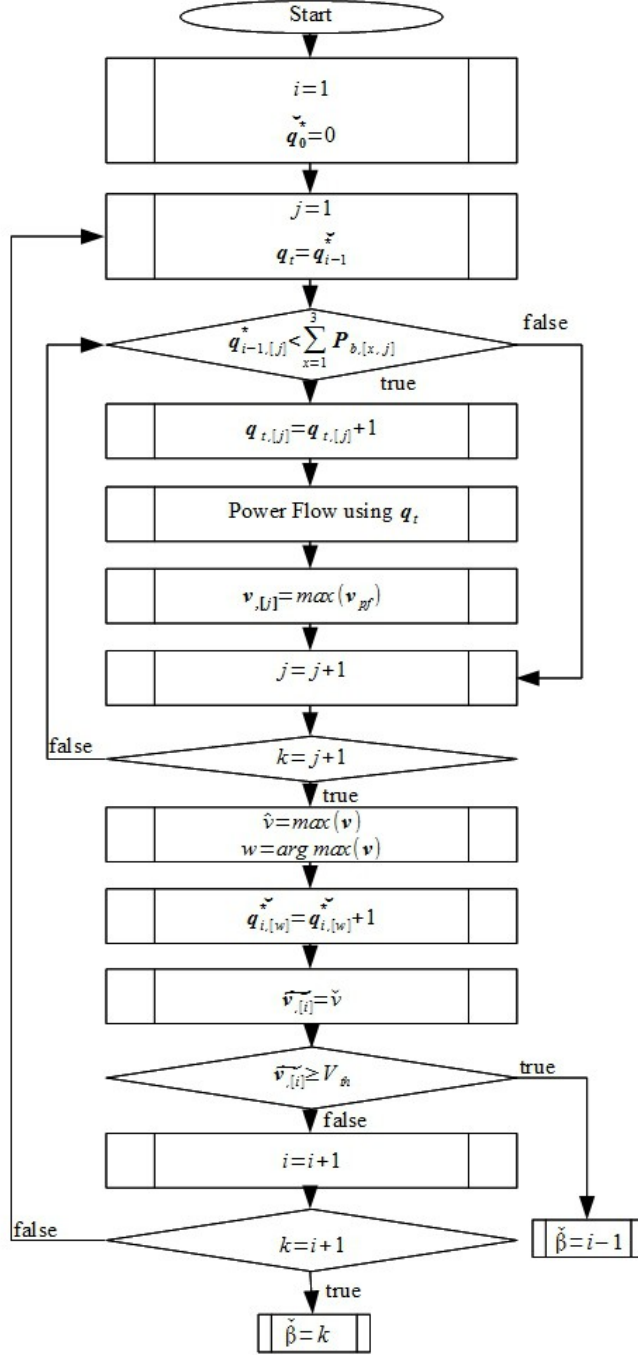
Fig. 66 Worst Case ITS Assessment Flow Chart
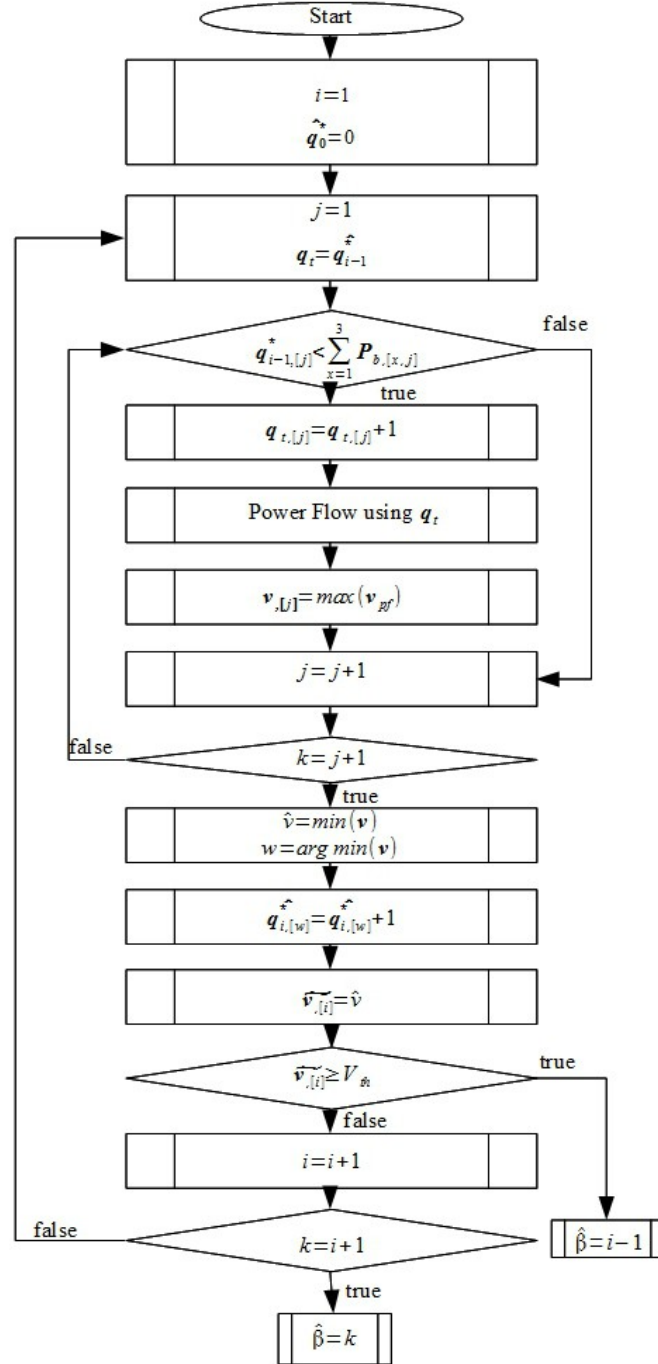
Fig. 67 Best Case ITS Assessment Flow Chart

One useful potential application of the ITS method is, given the initial allocation of PV, identifying locations of additional PV installations that would result in either best case or worst case scenario. For example, assume that the network has 50 dwellings that could be populated with PV, i.e. $N_{pv}=50$, and also assume that there are already 10 PV installations implemented. The task then is to find the locations of additional 10 dwellings denoted by x_{pv} that would result in a minimum or maximum voltage rise. The number of iterations that would be required to solve this problem is equal to:

$$2.\left[x_{pv}.\left(N_{pv}-n_{pv} \right)-\sum_{i=1}^{x_{pv}-1} i \right]=2.\left(400-45 \right)=710 \tag{113}$$

This is contrasted by the exhaustive search which would require the following number of network model evaluations:

$$\frac{\left(N_{pv}-n_{pv} \right)!}{x_{pv}!.\left(N_{pv}-n_{pv}-x_{pv} \right)}=847{,}660{,}528 \tag{114}$$

Hence, there is a clear benefit in terms of the computational burden with the number of evaluations in this particular case reduced by a factor of more than 1 million.

7.1.4 Results

This section compares the results obtained when the example feeder was assessed in using the Uniform Randomised (UR), the Impedance (IMP) and the Incremental PV Allocation Through Simulation (ITS) methods. Also, it highlights the impact that that PSs have on the results for each method by showing assessments for every feeder switch position when PSs are placed the locations shown in Fig. 22. The UR method was the only method used to assess the feeder twice, where 10 (UR10) and 100 (UR100) iterations were used respectively.

The plot in Fig. 68 shows the results from each of the methods for each of the 9 feeder switch positions, which it should be noted is similar to evaluating 9 unique example feeders. The figure shows that if the actual installed PV penetration level percentage is between any of the two points for any particular assessment methodology, the method has found that there is a risk of an OV condition. All the methods produce

variable results across feeder switch positions apart from ITS which finds consistent best and worst case results for all 9 feeder switch positions. Also, the figure clearly identifies ITS as the method to always finds the most extreme PV penetration scenarios for both the best and worst cases. Although, the exception to this was when feeder switch position 1 was simulated and ITS was matched by UR100 for the best case scenario. Therefore, for eight of the nine feeder switch positions ITS found more extreme best cases and for all nine found the most extreme worst cases. This is a useful because it indicates a robustness in the ITS algorithm when compared to the others as they are shown to underestimate the worst and best case scenarios (excluding the aforementioned UR100 best case exception). On average, the ITS, UR100, UR10 and IMP methods found best scenarios of 54.93%, 44.91%, 23.44% and 30.99% PV penetration and worst case scenarios of 1.41%, 6.41%, 6.56%, 4.23% PV penetration respectively.
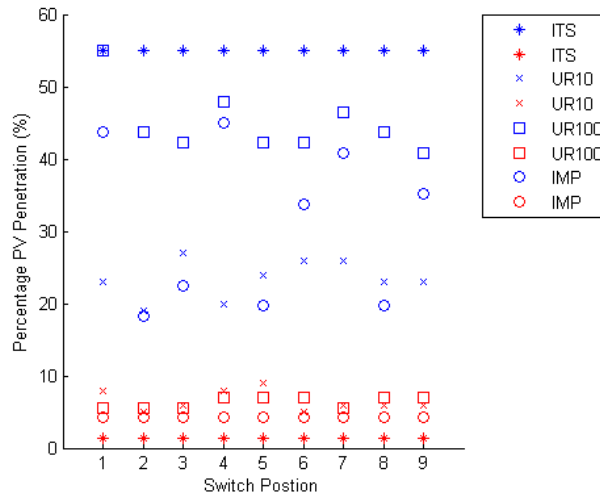
Fig. 68: Comparison of Assessment Methodologies

The time it took for the IMP, UR10, ITS and UR100 method to execute was 1.4mins, 15mins, 40mins and 2.5hours respectively. The impact of the number of iterations on simulation time is significant as increasing from 10 to 100 iterations took an an additional 2.25hours, the additional time did however improve accuracy as UR100 is clearly shown to achieve better results in Fig. 68. The main point to note is that the ITS method could be used by DNOs as a tool to identify if there is any risk of an OV condition on a given feeder. Although, what the ITS method does not do should be

fully understood, it doesn't assess how likely it is that there will be an OV condition for a particular PV penetration level! Rather, the ITS method outlines if the risk of OV exists for a given PV penetration level quickly when using PCs widely in use today.

7.2 Using PSs to Maximise PV Penetration

For a given allocation of PV it is possible to utilise PSs in order to minimise the maximum feeder voltage and therefore, mitigate the OV condition. Optimal feeder switch positions are calculated offline, assuming that the PV allocation is known in advance and then in line with other methods presented in this chapter, it is assumed that the loads are inactive in a given network.

In summary, for a given PV allocation and PS quantity, this algorithm determines the maximum bus voltage across all the buses on the feeder for every possible PS placement and feeder switch position. It then identifies the feeder switch position and placement combination that minimises that maximum voltage.

Given an allocation of PV installations, encoded in matrix $\boldsymbol{P}_b$, the network model is evaluated by an unbalanced power flow solver denoted as g_v for each permissible feeder switch position, denoted by X_j, to determine the feeder voltage profile:

$$\boldsymbol{v}_j = g_v(\mathrm{X}_j, \boldsymbol{P}_b) \tag{115}$$

Where j is an integer over the range $1 \le j \le (x_f \times c)$, x_f is the number of feeder switch positions given by (26) and c is the number of PS placement possibilities given by (44).

Then the maximum feeder bus voltage for each possible feeder switch position is obtained:

$$\hat{v}_j = \max_i (\boldsymbol{v}_{j,[i]}) \tag{116}$$

Once this maximisation routine is performed $x_f \times c$ times every possible PS placement in every possible feeder switch position has been evaluated. Therefore, the

optimum result of PS placement and feeder switch position denoted by X^* can be found by minimising the maximum feeder voltages $\hat{v}_j$ as follows:

$$X^* = arg\ \min_{\{X_j\}_{j=1}^{x_f \times c}} \hat{v}_j(X_j)$$

(117)

Note that $\hat{v}_j$ is a function of X_j which represents every possible PS placement in every possible feeder switch position.

The least optimum result may also be of interest and can be found by maximising and finding the argument of the same equation as follows:

$$X^{*^{-1}} = arg\ \max_{\{X_j\}_{j=1}^{x_f \times c}} \hat{v}_j(X_j)$$

(118)

Therefore, X^* represents the PS placement and feeder switch position for a given number of PSs and a particular allocation of PV. Note that the optimisation problem can also be formulated for the more trivial problem of when the placement of PSs is fixed, therefore not required. This is simply achieved by finding X^F which involves limiting the evaluations to capture only the number of possible feeder switch positions. Therefore, for steps (115) and (116) j is valid over the significantly reduced range of $1 \le j \le x_f$, and instead of invoking (117), the following equation is applied:

$$X^F = arg\ \min_{\{X_j\}_{j=1}^{x_f}} \hat{v}_j(X_j)$$

(119)

And the least optimum result can be found by maximising in the same equation as follows:

$$X^{F^{-1}} = arg\ \max_{\{X_j\}_{j=1}^{x_f}} \hat{v}_j(X_j)$$

(120)

7.2.1 Results

Fig. 69 shows the maximum feeder voltage for 6 random and unique PV penetration allocations on the example feeder, and for each of the cases the placement of PSs was fixed at the locations shown in Fig. 22. The legend in the plot refers to a high result, low result and straight through result which correspond with the feeder realisations of

$X^{F^{-1}}$, X^F and X^I respectively. Also, the red and green dotted lines in the plot show grid and inverter OV thresholds respectively.
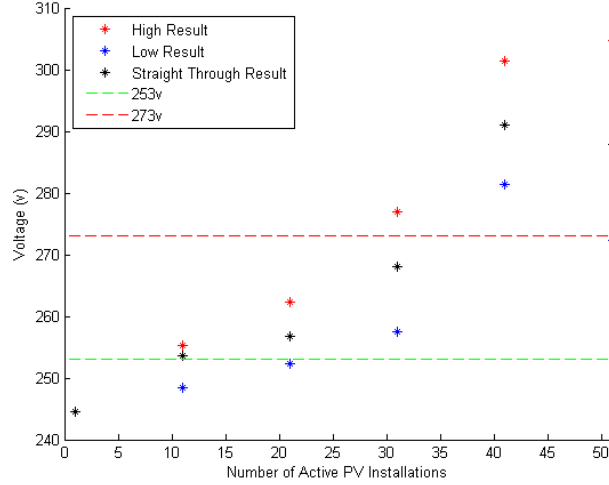
Fig. 69 Maximum feeder bus voltage for fixed PSs -
$X^{F^{-1}}$, X^F and X^I

The Low Result in Fig. 69 shows that PSs are effective at reducing the maximum bus voltage when compared to the other results for each of the 6 unique PV allocations considered. The impact that PSs have on the maximum bus voltages is best expressed by comparing the difference between the High and Low result, where for PV allocations levels of 1%, 15%, 30%, 43% and 58% a difference of 7V, 10V, 19V, 20V and 32V was found. Therefore, it has been found on the example feeder that even when PSs are not explicitly placed to reduce bus voltages for a particular PV allocation a significant voltage drop is still achieved.

The same random PV allocations that obtained the results shown in Fig. 69 were used to test the impact of (118) that specifically places PSs for a particular PV allocation. Fig. 70 shows how the algorithm performed, the high result, low result and straight through result correspond in this figure with the feeder realisations of $X^{F^{-1}}$, X^* and X^I respectively. The low result where X^* is applied achieves lower voltages than all realisations, but achieves a particularly impressive 31V and 25V drops when compared to the straight through configuration for the 41 and 51 dwelling PV allocations.
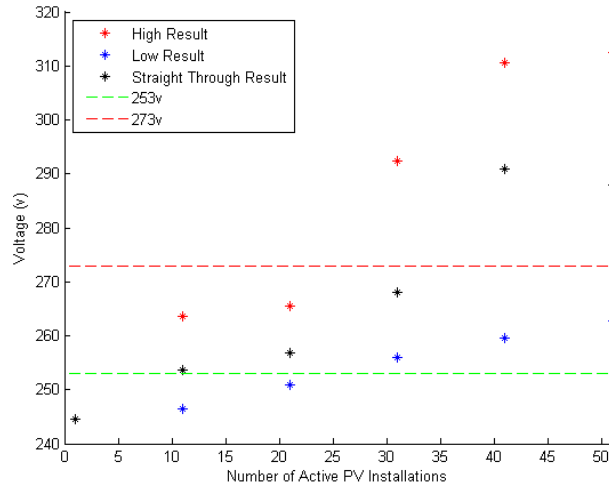
Fig. 70 Maximum feeder voltage for placed PSs -
$X^{F^{-1}}, X^*$ *and* X^I

A significant result is exposed in the trend of the low result in Fig. 70 which almost form a straight line, this can be fully appreciated in the line plot provided in Fig. 71. The straight line shows not only that a significant amount of voltage headroom can be created by placing PSs, but also that the amount created can be predicted by establishing the gradient of the low results' line. The inputs that are required to the power flow simulation to make this prediction is the rating of PV installations already installed and predictions of what rating of PV installations will be connected in the future. This method could be a very useful tool to DNOs because it enables feeders to be assessed, therefore highlighting those that are at or nearing PV saturation whilst also predicting what headroom PSs or phase rejointing would unlock.

The placement of PSs on the example feeder was found to achieve a significantly better reduction on maximum feeder bus voltages than that found when the placement was fixed. This result is significant and could even be applied and implemented by permanent reconfiguration of a feeders' phase connections to a specific PV installation today.
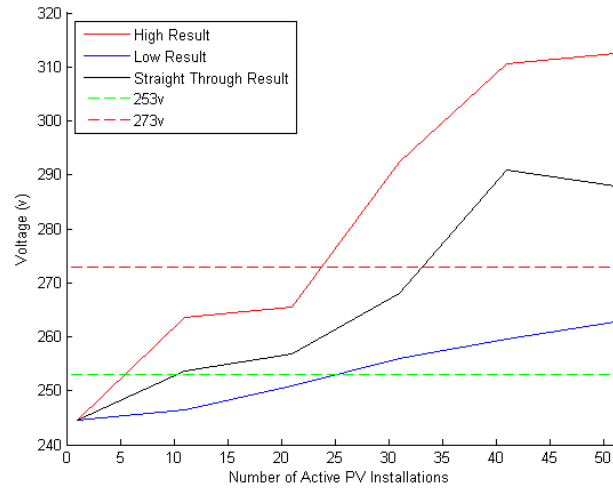
Fig. 71 Maximum feeder voltage for placed PSs -
$X^{F^{-1}}$, X^* and X^I *(Note: PV penetrations levels of 1%, 15%, 30%, 43% and 58% only are represented)*

8 Conclusions

This section details the key conclusions drawn from the research documented in thesis and identifies some avenues for further research.

8.1 The Phase Switcher

A potentially cost effective scheme for the novel PS device has been introduced with an accompanying new general mathematical framework that defines a method for expressing device phase connections and their subsequent calculation when manipulated by PSs. The framework was generalised so that it can can be applied to any radial or interconnected LV feeder where PSs are considered for deployment to resolve either breeches in the thermal or voltage constraints of cables. Therefore, objective 1. and 3. which were defined as objectives in section 1.4 have been fully addressed.

8.2 Unlocking Cable Current

In order to calculate the optimum state of balance that a PS scheme allows, the high fidelity OpenDSS model that interoperates PSs in simulations was established which is detailed in chapter 4 and that satisfies objective 2., see section 1.4. This enabled objective 4. to be addressed by evaluating actual optimum states of balance through the use in simulation of non-causal and causal, scheduled and dynamic control algorithms documented in chapter 5 and the results from it are discussed in detail in chapter 6. This section highlights the key conclusions that were determined from the simulation of all the control algorithms documented in chapter 6.

Initially, in chapter 4 it was shown through the simulation of present day dwelling loads that when the number of them on a feeder that are connected to phases is unbalanced, a corresponding current unbalance is induced. Later, in chapter 6, it was demonstrated on the example feeder that two PSs can be placed at fixed locations on the feeder and employed to improve such a current balance and unlock current headroom. Scheduled and dynamic control algorithms were tested and were both shown to be effective at unlocking headroom that was determined to be the cable that contituted the thermal hot spot. It was also shown that all the algorithms achieved a reduction in

real cable losses when compared to the straight through configuration. The perceived benefits of employing PSs on LV feeders is summarised below:

- A clear improvement in terms of phase imbalance was found when scheduled and dynamic control algorithms that focus on minimising the total current in the feeder hot spot control PSs. The scheduled peak time ideal current control algorithms were found to unlock the following proportions of cable current flowing through them: a maximum of 13.4%, a minimum of 4.6% and an annual average of 8.9%. Whilst the simple model based control algorithm achieved an annual reduction of 10.08% which amounts to a 28.02amp reduction in total cable current.

- Control algorithms that focus on minimising the total current in the feeder hot spot were shown to achieve a considerable reduction of the total cable losses and in some cases delivered the optimal reduction. Specifically, the scheduled ideal current controller algorithm, simple model based controller algorithm, causal ideal current controller algorithm and non-causal ideal current controller algorithm achieved annual peak time reductions in cable losses of 0.8016kWh, 0.9518kWh, 0.9514kWh and 1.05kWh respectively. To better appreciate the impact of these reductions on the how much the average generation capacity is reduced at peak time, the corresponding power ratings are provided: 130.65W, 146.43W, 146.367W and 161.54W.

- Of the current control algorithms, a significant number of cases (up to 50%) were found where scheduled algorithms achieved greater reductions in total cable losses than the corresponding dynamic algorithms. The reason for this is likely to be that although the dynamic current controller algorithms do unlock hot spot current, they ignore unbalances in other cables that make up the feeder.

- An estimate on the potential reduction of UK cable losses in the LV network if PSs were applied to all networks was calculated as being equivalent to a generating capacity of 54.6MW.

- In the majority of cases, dynamic control algorithms are most effective at reducing the total peak time hot spot current when compared to the straight through configuration, although the difference is modest.

- There were a small number of cases found where the scheduled ideal current control algorithm achieved a greater benefit than the dynamic control algorithms which suggests that dynamic algorithms would be improved if the sampling frequency was increased. Another likely contributing factor is the number of dwellings on a feeder which is expected to have an impact on the algorithms sampling time, feeders with greater numbers of loads will have smoother aggregated phase currents and perhaps require lower frequency sampling.

- The results obtained from the non-causal ideal current controller algorithms indicate that additional benefits would be realised if a predictive controller was to be developed, although these are not anticipated to be significant for the case of the present day network.

- The simple model based controller algorithm unlocks virtually the same current as the causal ideal current controller algorithm. This is a significant finding because the causal ideal current controller algorithm is costly and difficult to implement as it requires communication to and sensing at every dwelling as feedbacks, which today is not economically feasible. In contrast, the simple model based controller algorithm only requires phase current measurements taken at PS and transformer locations, which is thought to be economical today when compared to reinforcement or replacement.

8.3 Maximising PV Penetration

PS were found to create a significant amount of voltage headroom and maximise PV penetration in the example network. The following key conclusions were drawn from the simulations conducted on the example network:

- When the PSs are placed for the specific objective of minimising the maximum bus voltage, the greatest amount of voltage headroom was found to be created. For the specific random scenarios considered where 41 and 51 of 71 dwellings were allocated with PV, an impressive 31V and 25V of voltage headroom was created.

- When PSs were placed to minimise the maximum bus voltage, an almost linear relationship between maximum voltage and PV penetration was found. The

straight line enables the amount of headroom created by PSs or phase conductor rejointing to be predicted when the methodology outlined in 7.2 is followed. This knowledge could be applied by DNOs as a simple rule of thumb to assess a feeder for it's suitability for PSs or phase conductor rejointing to address OV.

- When the placement of PS is fixed, PSs are effective at creating voltage headroom and therefore increasing the levels of PV penetration before an OV condition occurs. For the specific random scenarios considered where 41 and 51 of 71 dwellings were allocated with PV, a substantial 10V and 15V of voltage headroom was created.

8.4 Implementation Remarks Regarding Unlocking Cable Current and Maximising PV Penetration

In light of the conclusions drawn in sections 8.2 and 8.3, it is anticipated that in the present day the economic case for PSs implementation is strongest when they are intended to be controlled by scheduled control algorithms that to unlock hot spot current at peak times and unlock voltage headroom when PV generation is high. Thus, the voltage and thermal constraints would be managed at times when they are causing a network bottleneck. It may also be economically desirable to employ PSs or rejoint phase conductors at key locations for the sole purpose of unlocking voltage headroom on a feeder, because the impact of doing this is significant headroom creation. However, for the present day network it is unlikely that the simple model based controller would be implemented because although it is determined to be effective and robust, the modest benefits that it brings when compared to the scheduled control algorithms are unlikely to be economical as the device is likely to require more maintenance or more expensive hardware due to the faster switching frequency.

8.5 LV Feeder PV Assessments

The ITS method of assessing feeders for extreme PV penetration level scenarios that cause OV was found to find be the most consistent when compared to others, this addressed thesis objective 5. which is outlined in section 1.4. On average, for the 9 feeder switch positions of considered on the example network, which is similar to considering 3 unique feeders, ITS was 10% better than its closest competitor which was

UR100 at finding a best case extreme scenario and 5% better at finding worst case extreme scenarios. Also, the ITS algorithm was found to execute approximately 2 hours faster than UR100. ITS could be used as a tool by DNO's today in order to establish if there is any risk that OVs are occurring on specific feeders through offline analysis by following the methodology outlined in 7.1.3.

8.6 Online and Offline Application

The methods and control algorithms presented for the unlocking of cable current and voltage headroom can be split into the two general categories of online and offline analysis. The causal dynamic control algorithms presented to unlock cable current constitute online analysis because they evaluate the network in real time. Whereas, the non-causal cable current along with all the PV algorithms presented can be are conducted offline just by analysing data collected from the network. It would be possible to implement the offline algorithms today, although accurate phase connection information is required which is a particular requirement for when the aim is to unlock voltage headroom. Implementation of the offline algorithms in the simplest form would involve permanently re-jointing phase conductors at PS placement locations. Although, by permanently re-jointing phase conductors the flexibility of switching between a PV operating mode where either creating voltage headroom or unlocking cable current is the objective could not be realised and this may be desirable on some feeders both today and in the future.

8.7 Further work

The following avenues of further work have been identified:

- Establish conclusively that PV power rating and phase connection are the key feeder characteristics that lead to the linear relationship between maximum feeder voltage and PV penetration level found in section 7.2.1. Find out if the gradient of the line can be generalised to create a very crude rule of thumb with a small margin for error that could be applied to any feeder in order to assess it's suitability to PS or phase rejointing to resolve feeder OV issues.
- Implement phase conductor rejointing on a real feeder with high PV penetration levels to prove the concept of minimising the maximum bus voltage.

- Perform PS frequency analysis simulations on feeders with different numbers of dwellings and network topologies to establish how they impact on sampling frequency. This would inform an understanding of the types of networks where dynamic outperform scheduled algorithms.

- If implemented widely, the impact of balancing the LV network with PSs is expected to have a significant benefits for the whole power system. Evaluating the impact on the losses and temperatures of secondary transformers and MV level components could be the starting point to quantifying this benefit.

- Investigate the impact of the scheduled offline algorithms on the MV network.

9 References

[1] 'Climate Change Act 2008'. [Online]. Available:
     http://www.legislation.gov.uk/ukpga/2008/27/contents. [Accessed: 16-Aug-
     2012].
[2] DFERA, 'UK Climate Change Risk Assessment: Government Report'. UK HM
     Government, 25-Jan-2012.
[3] EU, 'Renewable Energy Directive 2009', *Off. J. Eur. Union 2009*, Apr. 2009.
[4] DECC, 'UK Renewable Energy Roadmap Update 2012'. 27-Dec-2012.
[5] 'Monthly central Feed-in Tariff register statistics - Statistical data sets -
     GOV.UK'. [Online]. Available: https://www.gov.uk/government/statistical-data-
     sets/monthly-central-feed-in-tariff-register-statistics. [Accessed: 17-Sep-2013].
[6] DECC, 'Smart Metering Implementation Programme: response to prospectus
     consultation – overview'. Mar-2011.
[7] 'Written Ministerial Statement by Edward Davey: Smart Metering - Written
     statements to Parliament - GOV.UK'. [Online]. Available:
     https://www.gov.uk/government/speeches/written-ministerial-statement-by-
     edward-davey-smart-metering. [Accessed: 12-Dec-2013].
[8] 'The Electricity Safety, Quality and Continuity Regulations 2002'. [Online].
     Available: http://www.legislation.gov.uk/uksi/2002/2665/made. [Accessed: 29-
     May-2013].
[9] The British Standards Institution, 'BS EN 50160:2010 Voltage characteristics of
     electricity supplied by public electricity networks'. .
[10] 'Energy Trends table 5.6: Feed in Tariff Capacity April 2012'. DECC.
[11] P. Palensky and D. Dietrich, 'Demand Side Management: Demand Response,
     Intelligent Energy Systems, and Smart Loads', *IEEE Trans. Ind. Inform.*, vol. 7,
     no. 3, pp. 381 –388, Aug. 2011.
[12] K. Qian, C. Zhou, M. Allan, and Y. Yuan, 'Modeling of Load Demand Due to EV
     Battery Charging in Distribution Systems', *IEEE Trans. Power Syst.*, vol. 26, no.
     2, pp. 802–810, 2011.
[13] H. L. Willis and L. Philipson, *Understanding Electric Utilities and De-
     Regulation*, 2nd ed. CRC Press, 2005.
[14] B. G. A. Skrotzki, *Electric transmission and distribution.*, 1st ed. New York,:
     McGraw-Hill, 1954.
[15] I. Richardson, M. Thomson, D. Infield, and C. Clifford, 'Domestic electricity use:
     A high-resolution energy demand model', *Energy Build.*, vol. 42, no. 10, pp.
     1878–1887, Oct. 2010.
[16] I. Richardson and M. Thomson, 'Integrated domestic electricity demand and PV
     micro-generation model', 2011. [Online]. Available:
     https://dspace.lboro.ac.uk/dspace-jspui/handle/2134/7773. [Accessed: 01-Jul-
     2013].
[17] A. Keane, L. F. Ochoa, C. L. T. Borges, G. W. Ault, A. D. Alarcon-Rodriguez, R.
     A. F. Currie, F. Pilo, C. Dent, and G. P. Harrison, 'State-of-the-Art Techniques
     and Challenges Ahead for Distributed Generation Planning and Optimization',
     IEEE Trans. Power Syst., vol. 28, no. 2, pp. 1493–1502, 2013.
[18] Energy Networks Association, 'Engineering Recommendation G83'. ENA, Dec-
     2012.

[19] UKPN, 'ENA Smarter Networks Portal - Smart Urban Low Voltage Network'. [Online]. Available: http://www.smarternetworks.org/Project.aspx? ProjectID=404#downloads. [Accessed: 17-Dec-2013].

[20] ENWL, 'ENA Smarter Networks Portal - Low Voltage Network Solutions'. [Online]. Available: http://www.smarternetworks.org/Project.aspx? ProjectID=404#downloads. [Accessed: 17-Dec-2013].

[21] 'First Tier Registration Proforma: UKPNT1004 - Validation of Photovoltaic (PV) connection assessment tool'. [Online]. Available: https://www.ofgem.gov.uk/publications-and-updates/first-tier-registration-proforma-ukpnt1004-validation-photovoltaic-pv-connection-assessment-tool. [Accessed: 27-Aug-2013].

[22] M. Thomson and D. G. Infield, 'Network Power-Flow Analysis for a High Penetration of Distributed Generation', *IEEE Trans. Power Syst.*, vol. 22, no. 3, pp. 1157–1162, 2007.

[23] D. Shirmohammadi, H. W. Hong, A. Semlyen, and G. X. Luo, 'A compensation-based power flow method for weakly meshed distribution and transmission networks', *IEEE Trans. Power Syst.*, vol. 3, no. 2, pp. 753–762, 1988.

[24] W. H. Kersting, *Distribution System Modeling and Analysis, Third Edition*. CRC Press, 2012.

[25]] Navarro, L.F. Ochoa, D. Randles, 'Monte Carlo-based assessment of PV Impacts on real UK low voltage networks', presented at the IEEE/PES General Meeting, 2013, vol. 2013–07 21–25, p. 5.

[26] R. C. Dugan, 'Reference Guide - The Open Distribution System Simulator (OpenDSS) Version 7.4.3'. Electric Power Research Institute, Mar-2012.

[27] J. H. Neher and M. H. Mcgrath, 'The calculation of the temperature rise and load capability of cable systems', *Power Appar. Syst. Part Iii Trans. Am. Inst. Electr. Eng.*, vol. 76, no. 3, pp. 752–764, 1957.

[28] 'IEEE Standard Power Cable Ampacity Tables Amendment 1: Revision to Introduction', *IEEE Std 835a-2012 Amend. IEEE Std 835-1994*, pp. 1–16, 2013.

[29] British/ International Electrotechnical Commission, 'Electric cables — Calculation of the current rating. BS IEC 60287-3-3:2007 part 1 to 3'. BS IEC, 2007.

[30] S. British, 'BS 7870-3.40:2011 - LV and MV polymeric insulated cables for use by distribution and generation utilities'. BS, 2011.

[31] British Standard, 'BS IEC 60287 (2-1:1994+A2:2006, 1-1:2006 and 3.1:1997) Electric cables. Calculation of the current rating. Thermal resistance; Electric cables. Calculation of the current rating. Current rating equations (100% load factor) and calculation of losses; Electric cables. Calculation of the current rating. Sections on operating conditions. Reference operating conditions and selection of cable type.', *BS*, Current.

[32] British Standard, 'BS 7870-2:2011 LV and MV polymeric insulated cables for use by distribution and generation utilities. Methods of test'. BS.

[33] M. Terracciano, S. Purushothaman, F. de Leon, and A. V. Farahani, 'Thermal Analysis of Cables in Unfilled Troughs: Investigation of the IEC Standard and a Methodical Approach for Cable Rating', *IEEE Trans. Power Deliv.*, vol. 27, no. 3, pp. 1423–1431, 2012.

[34] H. Shaker, M. Fotuhi-Firuzabad, and F. Aminifar, 'Fuzzy Dynamic Thermal Rating of Transmission Lines', *IEEE Trans. Power Deliv.*, vol. 27, no. 4, pp. 1885–1892, 2012.

[35] A. Michiorri, P. C. Taylor, S. C. E. Jupe, and C. J. Berry, 'Investigation into the influence of environmental conditions on power system ratings', *Proc. Inst. Mech. Eng. Part J. Power Energy*, vol. 223, no. 7, pp. 743–757, Nov. 2009.

[36] S. C. E. Jupe, D. Kadar, G. Murphy, M. G. Bartlett, and K. T. Jackson, 'Application of a dynamic thermal rating system to a 132kV distribution network', in *2011 2nd IEEE PES International Conference and Exhibition on Innovative Smart Grid Technologies (ISGT Europe)*, 2011, pp. 1 –8.

[37] M. Matus, D. Saez, M. Favley, C. Suazo-Martinez, J. Moya, G. Jimenez-Estevez, R. Palma-Behnke, G. Olguin, and P. Jorquera, 'Identification of Critical Spans for Monitoring Systems in Dynamic Thermal Rating', *IEEE Trans. Power Deliv.*, vol. 27, no. 2, pp. 1002–1009, 2012.

[38] 'Implement three-phase transmission line section with lumped parameters - Simulink - MathWorks United Kingdom'. [Online]. Available: http://uk.mathworks.com/help/physmod/sps/powersys/ref/threephasepisectionline .html. [Accessed: 19-Jan-2015].

[39] D. Geibel, T. Degner, A. Seibel, T. Bolo, C. Tschendel, M. Pfalzgraf, K. Boldt, P. Muller, F. Sutter, and T. Hug, 'Active, intelligent low voltage networks #x2014; Concept, realisation and field test results', in *22nd International Conference and Exhibition on Electricity Distribution (CIRED 2013)*, 2013, pp. 1–4.

[40] UK Power Networks, 'Long Term Development Statement (LTDS) Network Summary 2012'. UK Power Networks, Nov-2012.

[41] A. Navarro, L. F. Ochoa, and P. Mancarella, 'Learning from residential load data: Impacts on LV network planning and operation', in *Transmission and Distribution: Latin America Conference and Exposition (T D-LA), 2012 Sixth IEEE/PES*, 2012, pp. 1–8.

[42] M. J. Lawson, P. C. Taylor, S. Bell, D. Miller, and N. S. Wade, 'An interdisciplinary method to demand side participation for deferring distribution network reinforcement', in *2011 2nd IEEE PES International Conference and Exhibition on Innovative Smart Grid Technologies (ISGT Europe)*, 2011, pp. 1–8.

[43] Y. Zhang, F. Li, Z. Hu, and G. Shaddick, 'Quantification of low voltage network reinforcement costs: A statistical approach', *IEEE Trans. Power Syst.*, vol. 28, no. 2, pp. 810–818, 2013.

[44] N. Zhang, L. F. Ochoa, and D. S. Kirschen, 'Investigating the impact of demand side management on residential customers', in *2011 2nd IEEE PES International Conference and Exhibition on Innovative Smart Grid Technologies (ISGT Europe)*, 2011, pp. 1–6.

[45] P. Ravibabu, A. Praveen, C. V. Chandra, P. R. Reddy, and M. Teja, 'An approach of DSM techniques for domestic load management using fuzzy logic', in *IEEE International Conference on Fuzzy Systems, 2009. FUZZ-IEEE 2009*, 2009, pp. 1303–1307.

[46] S. Koch, D. Meier, M. Zima, M. Wiederkehr, and G. Andersson, 'An active coordination approach for thermal household appliances #x2014; Local communication and calculation tasks in the household', in *PowerTech, 2009 IEEE Bucharest*, 2009, pp. 1–8.

[47] V. Hamidi, F. Li, and F. Robinson, 'Demand response in the UK's domestic sector', *Electr. Power Syst. Res.*, vol. 79, no. 12, pp. 1722–1726, Dec. 2009.

[48] C. Doyle, C.T. Gaunt, R. Herman, 'Using Load Research Data to Assess Demand Side Management Interventions', in *40th International Universities Power Engineering Conference (UPEC)*, Cork, Ireland, 2005.

[49] A. O'Connell, D. Flynn, and A. Keane, 'Rolling Multi-Period Optimization to Control Electric Vehicle Charging in Distribution Networks', *IEEE Trans. Power Syst.*, vol. 29, no. 1, pp. 340–348, 2014.

[50] D. R. R. Penido, L. R. de Araujo, S. Carneiro, J. L. R. Pereira, and P. A. N. Garcia, 'Three-Phase Power Flow Based on Four-Conductor Current Injection Method for Unbalanced Distribution Networks', *IEEE Trans. Power Syst.*, vol. 23, no. 2, pp. 494–503, 2008.

[51] SSEPD, 'ENA Smarter Networks Portal - LV Monitoring Demonstrating the Possibilities'. [Online]. Available: http://www.smarternetworks.org/Project.aspx?ProjectID=404#downloads. [Accessed: 17-Dec-2013].

[52] WPD, 'ENA Smarter Networks Portal - PV Impacts on Suburban Networks'. [Online]. Available: http://www.smarternetworks.org/Project.aspx?ProjectID=404#downloads. [Accessed: 17-Dec-2013].

[53] Jennifer Taylor, 'Load Imbalance', *Milsoft Utility Solutions*. [Online]. Available: http://www.milsoft.com/resources/presentations/load-imbalance. [Accessed: 17-Dec-2013].

[54] M. W. Siti, D. V. Nicolae, A. A. Jimoh, and A. Ukil, 'Reconfiguration and Load Balancing in the LV and MV Distribution Networks for Optimal Performance', *IEEE Trans. Power Deliv.*, vol. 22, no. 4, pp. 2534–2540, 2007.

[55] C. H. Castro, J. B. Bunch, and T. M. Topka, 'Generalized Algorithms for Distribution Feeder Deployment and Sectionalizing', *IEEE Trans. Power Appar. Syst.*, vol. PAS-99, no. 2, pp. 549–557, 1980.

[56] S. Civanlar, J. J. Grainger, H. Yin, and S. S. H. Lee, 'Distribution feeder reconfiguration for loss reduction', *IEEE Trans. Power Deliv.*, vol. 3, no. 3, pp. 1217–1223, 1988.

[57] C.-H. Lin, C.-S. Chen, H.-J. Chuang, M.-Y. Huang, and C.-W. Huang, 'An Expert System for Three-Phase Balancing of Distribution Feeders', *IEEE Trans. Power Syst.*, vol. 23, no. 3, pp. 1488–1496, 2008.

[58] R. A. Hooshmand and S. Soltani, 'Fuzzy Optimal Phase Balancing of Radial and Meshed Distribution Networks Using BF-PSO Algorithm', *IEEE Trans. Power Syst.*, vol. 27, no. 1, pp. 47–57, 2012.

[59] M. W. Siti, A. A. Jimoh, and D. V. Nicolae, 'Feeder's load balancing using an expert system', in *2005 European Conference on Power Electronics and Applications*, 2005, p. 9 pp.–P.9.

[60] W. M. Siti, A. A. Jimoh, and D. V. Nicolae, 'Load balancing in distribution feeder through reconfiguration', in *31st Annual Conference of IEEE Industrial Electronics Society, 2005. IECON 2005*, 2005, p. 6 pp.–.

[61] A. Ukil, M. Siti, and J. Jordaan, 'Feeder load balancing using combinatorial optimization-based heuristic method', in *13th International Conference on Harmonics and Quality of Power, 2008. ICHQP 2008*, 2008, pp. 1–6.

[62] W. M. Siti, D. V. Nicolae, and A. A. Jimoh, 'LV and MV Distribution Networks Reconfiguration for Minimum Losses', in *Power Electronics and Motion Control Conference, 2006. EPE-PEMC 2006. 12th International*, 2006, pp. 1478–1483.

[63] D. V. Nicolae, M. W. Siti, and A. A. Jimoh, 'LV self balancing distribution network reconfiguration for minimum losses', in *PowerTech, 2009 IEEE Bucharest*, 2009, pp. 1–6.

[64] M. W. Siti, A. A. Jimoh, and D. V. Nicolae, 'Phase load balancing in the secondary distribution network using fuzzy logic', in *AFRICON 2007*, 2007, pp. 1–7.

[65] M. Siti, A. Jimoh and D. Nicolae, 'Automatic load balancing in Distribution Feeeder', presented at the IECON 05, Raleigth North Caroline, USA.

[66] A. Raminfard, S. M. Shahrtash, 'A Practical Method for Load Balancing in the LV Distribution Networks Case study: Tabriz Electrical Network'. Worla Academy of Science, Engineering and Technology, 2010.

[67] A. Raminfard, S. M. Shahrtash, 'Extending MOLFOP Method for Balancing the LV Distribution Network Loads with Variable Power Factor'. 2011.

[68] A. Raminfard, S. M. Shahrtash, T. Herizchi, and H. Khoshkhoo, 'Long-term load balancing program in LV distribution networks', in *Power Engineering and Optimization Conference (PEDCO) Melaka, Malaysia, 2012 Ieee International*, 2012, pp. 220–224.

[69] J. A. Snyman, 'The LFOPC leap-frog algorithm for constrained optimization', *Comput. Math. Appl.*, vol. 40, no. 8–9, pp. 1085–1096, Oct. 2000.

[70] 'Low Voltage Network Solutions Project'. .

[71] British/ International Electrotechnical Commission, 'Electric cables — Calculation of the current rating. BS IEC 60287-1-3:2002'. BS IEC, 2007.